BRITISH GEOTECHNICAL ASSOCIATION

SURREY ADVANCED GEOTECHNICAL ENGINEERING
UNIVERSITY OF SURREY

15th BGA Young Geotechnical Engineers' Symposium

Guildford, 2-3 July 2018

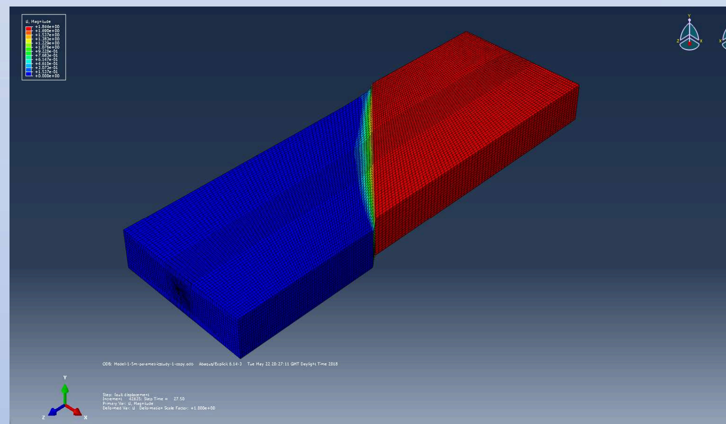

Edited by

L Cui, S Bhattacharya & G Nikitas

PROCEEDINGS OF THE 15th BGA YOUNG GEOTECHNICAL ENGINEERS' SYMPOSIUM,
2-3 JULY 2018, UNIVERSITY OF SURREY, GUILDFORD, UK

15th BGA Young Geotechnical Engineers' Symposium

Edited by

L Cui, S Bhattacharya & G Nikitas
Geomechanics Group, Department of Civil and Environmental Engineering, University of Surrey

Table of Contents

Numerical Modelling

Foreword

The summaries in these proceedings were presented at the 15^{th} British Geotechnical Association Young Geotechnical Engineers' Symposium held at the University of Surrey in July 2018. These BGA symposia offer an excellent opportunity for young students, researchers and practicing engineers working in industry to present latest advances, innovative projects and techniques applied to the field of geotechnical engineering. While each participant delivers a presentation on an aspect of their work, these meetings also provide a forum where information and ideas can be exchanged in an informal, friendly and constructive atmosphere. For some of the youngest participants, these meetings represent their first major conference participation and certainly a significant experience for receiving feedbacks from professionals and building relationships with colleagues from different organisations and sectors.

The presented summaries show the extent of topics and methodologies used in the UK Geotechnical Engineering research and practice today: from laboratory, numerical and analytical analysis to complex small scale testing, including soil-structure interaction problems, via industrial and field investigations. It is certain that many of these contributions will have a significant impact and will successfully contribute to advancing the state of the art and state of practice in geotechnical engineering.

The organising committee is delighted to host the 15^{th} Young Geotechnical Engineers' Symposium and we would like to thank all the delegates for their active and enthusiastic participation in the event. We would like to thank in particular Dr Hugo Wood, Dr Ganga Prakhya and Prof. Dipanjan Basu for delivering keynote lectures. We would also like to thank the Head of Department, Prof Abigail Bristow, for her support.

Liang Cui

Guildford 2-3 July 2018

Organisation

The symposium is organised by the Geomechanics Group in the Department of Civil & Environmental Engineering at the University of Surrey. The team consists of the following six members of staff and eleven PhD students.

Dr. Liang Cui (co-ordinator)
Prof. Subhamoy Bhattacharya
Dr Ignazio Cavarretta
Dr Rao Martand Singh
Dr Rick Woods
Mr Georgios Nikitas

The organising committee would like to thank the following colleagues for kindly accepting to chair the technical sessions:

Prof Dipanjan Basu, University of Waterloo, Canada
Prof. Malcolm Bolton, University of Cambridge
Dr Erdin Ibraim, University of Bristol
Dr Susana Lopez-Querol, University College London
Dr George Marketos, Tony Gee and Partners LLP
Prof. Catherine O'Sullivan, Imperial College London
Dr Brian Simpson, Arup
Dr. Rick Woods, University of Surrey

We would like also to acknowledge the BGA team for their continuous support throughout the preparation of the event.

Experimental Testing

Stability of working platforms for tracked plant

G. Tanghetti[1]

Correspondence: greta.tanghetti@city.ac.uk

[1]*City, University of London, London, UK*

Abstract

The aim of this research is to investigate the factors which might influence the stability of working platforms in order to define a better design approach able to guarantee safety of the platform once ready to operate. Based on bearing capacity theory, the stability of platforms mostly depends on their thickness (Skinner, 2004) which need to be defined according to the characteristics of the platform material and of the subgrade. Among these factors, of most influence on the thickness is the design angle of friction of the platform. The easiest way to derive this value is the use of the direct shear test. However, the literature indicates the presence of scale effects associated with the size of the shear box and use of downscaled samples. These effects might lead to incorrect estimations of the angle of friction and consequently to an inefficient platform design. The proposed solution to the problem is the design of a large apparatus able to test the material at full scale and guarantee more reliable results.

Introduction

Nowadays a wide range of recycled and secondary aggregates (RSA) are adopted in the UK construction industry. Their use is also advantageous in working platforms thanks to the reduction of costs of granular material extraction/transportation and of potential incidents during quarrying operations/lorry movements. Problems associated with recycled materials are the large variability of components and particle size distribution (Highways Agency, 2004), factors which can determine different material behaviour. Testing should be carried out in order to study the change in behaviour due to change of these factors. The problem associated with testing is the large particle size of the material which makes standard test apparatus unsuitable for obtaining representative results.

Methodology

After a literature review concerning scale effects associated with shear box tests it was found that the main factors influencing the test results are: the use of too small an apparatus in relation to the maximum particle size of the samples (Fu *et al.,* 2015) and the use of downscaled samples when the size of particles is too large to conduct full scale tests (Nakao and Fityus, 2008). In order to evaluate the influence of these factors it would be useful to compare the results obtained from testing the same sample at small and full scale. Here presented is the first series of tests carried out at small scale on a sample of crushed Devonian limestone. The material was sieved and combined in the correct proportions in order to recreate a grading distribution corresponding to a downscaled version of real platform material. The sample was firstly used for centrifuge model plate bearing capacity tests, conducted with the use of different plate sizes to verify the effect of changing the plate to maximum particle size ratio. Secondly, the same sample was used in standard shear box tests. Both the tests allowed the calculation of the angle of friction of the sample and results from shear tests were used for the development of a large shear box apparatus.

Results and Discussion

From the series of bearing capacity tests (Figure 1) it was possible to observe a decrease of bearing capacity with the reduction of plate diameter to maximum particle size ratio. The results confirm the validity of the BS1377 Part 9 (1990), which impose for plate tests on soils a plate diameter to nominal particle size exceeding five. Another observation is related to the boundary effect which was found when testing the sample with the largest plate diameter. This phenomenon was observed for a test characterized by a boundary distance to plate diameter ratio equal to 5.3, very close to the lower value of 5 presented as a limit by Ullah et al. (2016).

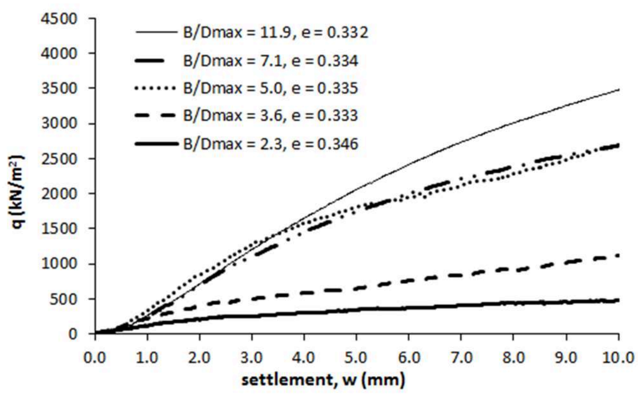

Figure 1. Bearing stress (q) – settlement (w) variation obtained from testing the same granular soil with different plate diameter to maximum particle size ratios (B/D_{max}).

A back calculation of the angle of friction of the soil was conducted using a simple bearing capacity formulation for a circular footing (Das, 2010). It was found that once the plate diameter exceeds five times the maximum particle size the angle of friction is relatively constant at around 51.5°, while smaller values are obtained for lower values of this ratio confirming again the importance of adopting a proper ratio.

From a series of standard shear test it was possible to derive the angle of friction at peak (ϕ_{pk}'=52.7°) and at critical state (ϕ_{cr}'=47°). Furthermore, the test results showed a percentage of maximum volumetric strain equal to 2.3% and maximum shear strain equal to 42%. On the basis of these initial data and the decisions made based upon the literature a draft design for the large apparatus was created. The structure consists of a large box (1.5m x 1.5m x 1m) made of steel I-beams.

Conclusions and Future Work

It is proposed that the following working plan will concentrate on testing different kinds of platform material at full scale using the large shear box apparatus with the intent to verify, not only the variation of results which might be obtained from testing at larger scale, but also the effect produced by testing material with different characteristics (such as grading, stress level, density and particle properties). Another possible objective could be to investigate the magnitude of particle crushing and the effect deriving from the consequent increase of fine content by reconfiguring the large shear apparatus as an oedometer. Finally, numerical analysis could be possibly carried out in order to investigate a wider range of geometries and material behaviour.

Acknowledgements

I would like to express my gratitude to Dr R.J. Goodey and Dr A.M. McNamara, my research supervisors, for their guidance and useful critiques of this research. My thanks are extended to all the members of the Geotechnical Engineering Research Group for their valuable support and constructive suggestions.

References

British Standards Institution (1990b) BS 1377-9:1990. *Methods of Test for Soils for Civil Engineering Purposes- Part 9: In-situ tests.* London, BSI.

Das, B.M. (2007) *Principles of foundation engineering.* 6th edition. London, Thomson Learning Publishing.

Fu, X., Zheng, X., Lei, X. & Deng, J. (2015) Using a modified direct shear apparatus to explore gap and size effects on shear resistance of coarse grained soil. *Particuology.* 23, 82–89.

Highways Agency (2004) MCHW: 2004. *Manual of Contract Documents for Highway Works-Volume 1.* London, The Stationary Office.

Nakao, T. & Fityus, S. (2008) Direct Shear Testing of a Marginal Material Using a Large Shear Box. *Geotechnical Testing Journal.* 31 (5), 393-403.

Skinner, H. (2004) *Working platforms for tracked plant.* Garston (UK), IHE BRE Press.

Ullah, S.N., Hu, Y., Stanier, S. & White, D. (2016). Lateral boundary effects in centrifuge foundation tests. *International Journal of Physical Modelling in Geotechnics.* 17(3), 144-160.

Study of thermal performance enhancement in geothermal energy pile

I.O. Olawoore*[1], R.M Singh[1], and S.Bhattacharya[1]

*Correspondence: i.olawoore@surrey.ac.uk, olawooreolaniyi@gmail.com

[1] *University of Surrey, Dept. of Civil & Env Eng., Guildford, GU2 7XH, UK*

Abstract

Geothermal energy piles (GEPs) are dual purpose structural deep foundation that harnesses the constant ground temperature below our feet for space heating / cooling. GEP recently became popular to provide space conditioning to building due to their easy installation and low cost. GEP is installed at shallow depth 10–50 m, where the ground temperature is around 10°C to 15°C in most European countries. Limited heat capacity, shorter length of the piles are some of GEP limitations. This study aimed at investigating a sustainable and environmental friendly way of enhancing the thermal performance of GEP.

Introduction

Residential and, commercial heating/cooling needs are increasing day by day as the world population rises. A significant part of the total energy consumption of a building consists of heating/cooling and hot water. Heating and cooling demand is currently being taken care of worldwide using conventional methods such as gas boilers and electrically powered air conditioning which are (a fossil fuel based technologies and cause carbon emission). On the usage of energy in the UK, Eames et al. (2014) reported that over half (63%) of total energy consumption in a residential house in the UK is currently used for space heating purposes (Figure 1). Space heating and hot water consumes more than ¾ (77%) of total energy of a household with approximately 80% derived from fossil fuels (Eames et al. 2014). This has negative impact on the climate due to high carbon footprint of fossil fuels. To meet the increasing energy demand for space heating/cooling, it is imperative to provide sustainable space conditioning that are eco-efficient and renewable. A good example of this sustainable source of energy for space heating/cooling is geothermal energy available at shallow depth (< 100 m) which utilises stable and constant ground temperature. This will reduce the demand for the usage of fossil fuel.

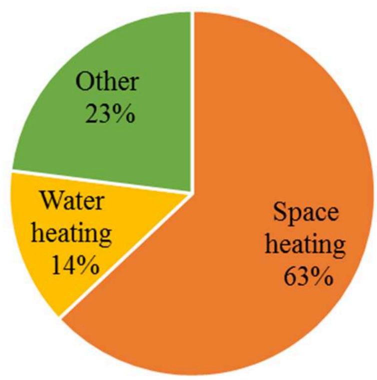

Figure 1. UK heat use by purpose (adapted from Eames et al. 2014)

Geothermal energy pile

Utilisation of shallow geothermal energy in providing thermal needs of a building is already common. Geothermal energy piles (GEPs) recently became popular to provide space conditioning to building due to their easy installation and low cost. GEP is installed at shallow depth 10–50 m, where the ground temperature is around 10°C to 15°C in most European countries (Adam and Markiewicz, 2009). Energy pile is a closed loop system (Fig. 2) where closed-coil absorber pipes are attached to reinforcement cage and placed into borehole vertically and later concrete is poured. A heat carrier medium is circulated through absorber pipes to transport heat from the ground via concrete pile to the heat pump.

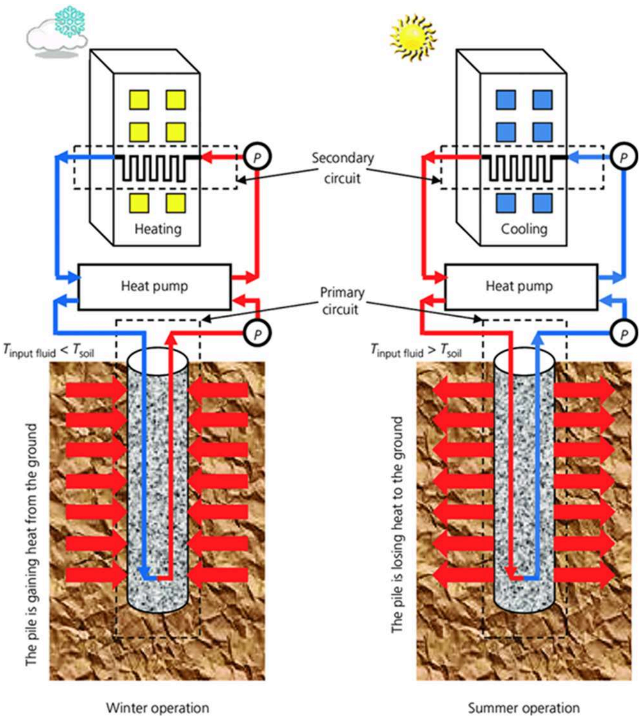

Figure 2. Typical geothermal energy pile system (adapted from Abuel-Naga et al. 2015)

Limitations of geothermal energy pile

The challenges associated with geothermal energy piles include limited heat capacity, low ground thermal conductivity, shorter length of the piles etc. Many research has been conducted on means of increasing thermal performance of energy pile via an increase in the energy pile diameter, loops (Brandl, 2006) but the issue of the limited heat capacity associated with it is yet to be extensively researched.

Aim of the study

The aim of the study is to come up with a sustainable and environmental friendly way of enhancing the thermal performance of energy pile.

Methodology

In order to increase the thermal performance of the energy pile, a smart and advanced material is being proposed to be incorporated with the concrete in order to enhance the thermal storage capacity of the energy pile.

This research is an experimental based study. Here, a rigorous controlled laboratory setup will be designed to simulate the field condition of energy pile and the effects of thermal cycling will be investigated.

Conclusion

Geothermal energy pile is a dual purpose structural element that harnesses the constant ground temperature below our feet for space heating and cooling. Limited heat capacity, low ground thermal conductivity, shorter length of the piles are some of the limitations associated with energy pile.

Acknowledgements

The first author has been fully funded by the Federal Government of Nigeria through Petroleum Technology Development Fund (PTDF) Nigeria, for his PhD.

References

Abuel-Naga, H., Raouf, A.M.I., Raouf, M.I.N., Nasser, A.G., 2015. Energy piles: current state of knowledge and design challenges. Environ. Geotech. 2, 195–210.

Adam, D., Markiewicz, R., 2009. Energy from earth-coupled structures, foundations, tunnels and sewers. Géotechnique 59, 229–236.

Brandl, H., 2006. Energy foundations and other thermo-active ground structures. Géotechnique 56, 81–122.

Eames, Philip; Dennis, Loveday; Victoria, Haines; Romanos, P., 2014. The Future Role of Thermal Energy Storage in the UK Energy System : An Assessment of the Technical Feasibility and Factors Influencing Adoption Research Report The Future Role of Thermal Energy Storage in the UK Energy System : An assessment of the Techni. Res. Rep. (UKERC London).

Early detection of seepage-induced internal erosion using acoustic emission monitoring

T. Biller*[1], A. Smith[1] and N. Dixon[1]

*Correspondence: t.biller@lboro.ac.uk

[1] *School of Architecture, Building and Civil Engineering, Loughborough University, LE11 3TU, UK*

Abstract

Techniques for monitoring water-retaining earth structures are currently limited in their capacity to detect seepage-induced internal erosion (e.g. suffusion) in its early stages, or before serious damage has occurred. Acoustic emission (AE) is widely used in many industries for non-destructive assessment of materials and systems, but despite its advantages it is seldom used in geotechnical engineering as the AE generated by particulate materials is highly complex and difficult to measure and interpret. This project aims to develop the interpretation of AE generated by seepage-induced internal instability phenomena. A continuous, real-time AE early warning system for detecting seepage erosion mechanisms and processes will enable safety-critical decisions to be made. Laboratory testing with a large permeameter apparatus is being used to characterise and quantify the AE generated by the hydromechanical behaviour of a range of internally unstable soils. Initial results show that key processes such as the internal movement of particles can be measured and interpreted using AE.

Introduction

A long-standing problem with the longevity of water-retaining earth structures is their vulnerability to seepage-induced internal erosion – in the United Kingdom alone millions of people rely on ca. 2200 large embankment dams and 7500km of levees for flood protection, clean water supply and renewable energy (ICOLD, 2014), with internal erosion and piping being their main cause of failure (Fell and Fry, 2007). Current monitoring techniques have technological or financial limitations for the deployment of reliable early warning systems. Acoustic Emissions (AE) are high-frequency stress waves (>10kHz) generated by mechanisms and processes occurring inside a material. AE from particulate materials is highly complex and difficult to measure and interpret, thus being seldom used in geotechnical engineering. However, a body of research has demonstrated its significant potential for use in the monitoring of soil behaviour (Koerner et al., 1981; Smith et al., 2017; Smith and Dixon, 2014). This project aims to develop methodologies to interpret the AE generated by seepage-induced internal instability, the basis for a real-time early warning system enabling safety-critical decisions to be made (e.g. evacuation of vulnerable people, timely and targeted interventions).

Methodology

Element testing with a large permeameter apparatus (Figure 2) is being used to analyse the AE generated from internally unstable soils subjected to a range of hydraulic regimes. Parameters of AE are being quantified in both time and frequency domains for comparison with measurements of hydromechanical behaviour. This paper presents results from testing the material in Figure 3, which was homogenized and subjected to horizontal water flow.

Results and Discussion

Migration of finer particles through voids in the soil skeleton was observed in the direction of seepage flow throughout the test. Figure 4 shows the amplitude ratio frequency spectrum for this test, showing significant AE in the 20-45kHz range. Seepage erosion generates AE through several mechanisms, including particle collisions and frictional interactions (Koerner et al., 1981; Ferdos et al., 2018).

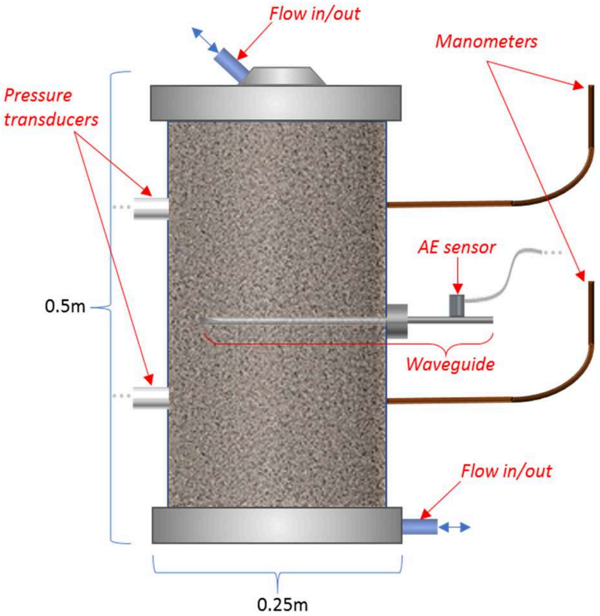

Figure 2. Permeameter schematic.

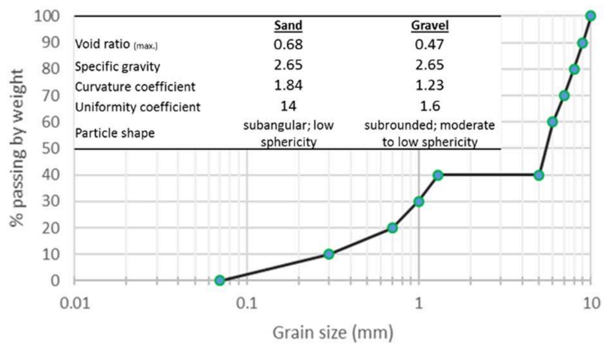

Figure 3. Grain size distribution and properties of the tested specimen.

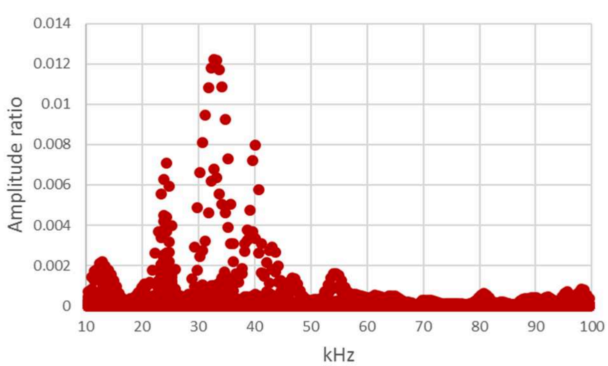

Figure 4. Scatter plot of amplitude ratio and AE frequency from experiment.

Conclusions and Future Work

This paper has introduced the use of AE to detect and interpret seepage-induced internal instability, which was demonstrated by preliminary results from permeameter tests. An ongoing experimental programme aims to characterise the AE signatures generated by different mechanisms and behaviours in internally unstable soils under varied hydraulic regimes, aiming to develop methodologies to interpret the AE for early detection of seepage erosion. A new permeameter is in development to enable control of effective stress and measurement of volume change. Field trials are also planned to assess performance of the approach in the field environment.

Acknowledgements

The authors acknowledge the excellent technical assistance provided by Mr Lewis Darwin. Tiago Biller gratefully acknowledges the support of a Loughborough University School of Architecture, Building and Civil Engineering studentship for his doctoral work, and Alister Smith gratefully acknowledges the support of an EPSRC Fellowship (EP/P012493/1)

References

Fell, R. and Fry, J.J. (2007) *Internal erosion of dams and their foundations*. Taylor & Francis.

Ferdos, F., Dargahi, B. and Solari, L. (2018) Mechanism of Suffusion Erosion Phenomenon In Porous Media. *J Geol Geosci*, 2 (1): 2018–1.

ICOLD (2016) Internal erosion of existing dams, levees and dikes, and their foundations, Volume 2: Case histories, investigations, testing, remediation and surveillance. In *International Commission on Large Dams, Paris*. 2016.

Koerner, R.M., McCabe, W.M. and Lord Jr, A.E. (1981) Acoustic Emission Behavior and Monitoring of Soils. *Acoustic Emissions in GeotechnicalEngineering Practice*, pp. 93–141.

Smith, A. and Dixon, N. (2014) Quantification of landslide velocity from active waveguide-generated acoustic emission. *Canadian Geotechnical Journal*, 52 (4): 413–425. doi:10.1139/cgj-2014-0226.

Smith, A., Dixon, N. and Fowmes, G.J. (2017) Early detection of first-time slope failures using acoustic emission measurements: large-scale physical modelling. *Géotechnique*, 67 (2): 138–152. doi:10.1680/jgeot.15.P.200.

Evolution of stiffness in artificially cemented sands for geotechnical centrifuge modelling.

J.A. Mendoza Ulloa[1], D. Lombardi[1]

*Correspondence: jorge.mendoza@postgrad.manchester.ac.uk

[1]*University of Manchester, Oxford Road M139PL, UK*

Abstract

A method for monitoring the effect of cementation on the stiffness properties of artificially cemented sand is presented. Fast-setting Portland Cement was used as cementing agents to create samples cured under confining pressure of 200 kPa. Evolution of stiffness was monitored by measuring shear wave velocities using bender elements at different curing times.

Introduction

In the attempt of replicate natural cementation under laboratory conditions Consoli, Rotta, and Prietto (2002) studied the effect of confining stress in the curing of artificially cemented sands prepared with (you may include the percentage by weight used or its range) Portland cement. Consoli (2009) studied the fundamental parameters controlling the stiffness and strength of artificially cemented sand used bender elements through shear wave velocities measurements.

In the design of geotechnical centrifuge models, the simulation of cemented soil is often required. A method for monitoring the evolution of stiffness during curing of artificially cemented samples is here employed as a technique to prepare samples aimed to be used in the W.H. Craig 6G-Tonne geotechnical centrifuge at the University of Manchester, UK

Methodology

Samples were prepared used 3% of fast-setting cement by dry weight and a 0.66 void ratio. Samples of 75mm diameter and 150 mm height were cured under confining pressure inside the triaxial. Full details in procedure can be found in Dalla Rosa, Consoli, and Baudet (2008).

The frequency (f) of the s-wave was set in the range defined by **Error! Reference source not found.**, where the lower limit ensure the reduction of so-called near-field effect due to the arrival of P-waves, and the upper limit limits potential overshooting effect owing to higher modes of vibration of the bender elements. (Lee & Santamarina, 2005),

$$2 \leq f\Delta t = \frac{L}{\lambda} \leq 8$$

Equation 1

Where:
Δt= travel time,
L= travel distance, and
λ= wavelength

A wave frequency and amplitude of 16.6 kHz 10V, respectively, were used in the present study .the cross-correlation method was used to determine the arrival time was obtained based on the local of absolute maximum of the cross correlation function (eg, see Figure 3) GDSBES software was used to acquire the shear wave measurements from samples subjected to an isotropic confining pressure.. The evolution of the stiffness was computed by determining the arrival time of shear wave every hour.

Results and Discussion

At an early stage of cementation, shear wave velocity was similar for both cemented and uncemented samples. Figure 5 shows the increase of shear wave velocity after 12 hours of curing (a) compared with the initial test (b).

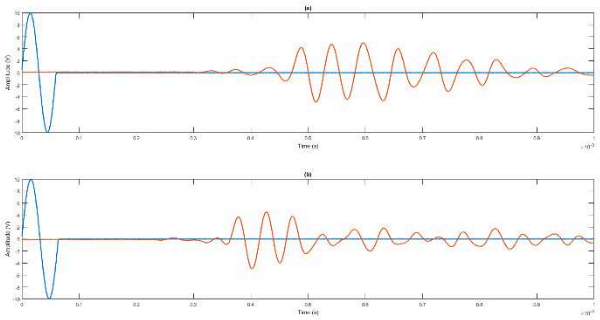

Figure 5 Source and received S-waves in cemented sample. Figure (a) is the initial response of the cemented sample under a confining pressure of 200 kPa. Figure (b) shows the response after curing of 12 hours after.

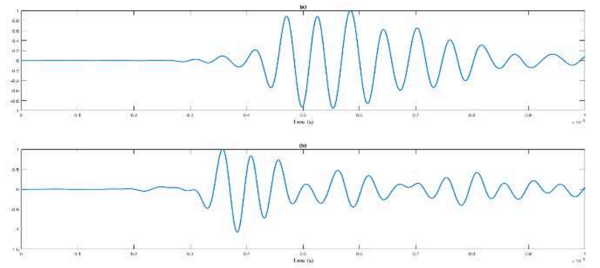

Figure 6 Normalised cross-correlation for cemented sample. (a) Cross-correlation at initial condition under 200 of confining pressure. (b) Cross-correlation after 12 hours of curing.

Travel times were obtained from the first peak in the cross-correlation functions shwon in Figure 6. Travel times and computed G_{max} are summarised in Table 1.

Results show G_{max} increased significantly in the first 7 hours of curing (Figure 3).

Curing time (hr)	Initial ρ (g/cm^3)	Travel time (s)	V_s (m/s)	G_{max} (MPa)
1.00	1.60	0.000471	301.81	145.74
1.97	1.60	0.000441	326.53	170.60
2.98	1.60	0.000401	359.55	206.84
4.00	1.60	0.000379	379.45	230.37
5.00	1.60	0.000372	387.62	240.40
6.00	1.60	0.000368	391.84	245.66
7.02	1.60	0.000365	395.06	249.71
8.02	1.60	0.000363	397.24	252.48
9.02	1.60	0.000361	398.89	254.58
10.03	1.60	0.000360	400.56	256.71
11.02	1.60	0.000359	401.67	258.15
11.98	1.60	0.000358	402.80	259.59

Table 1 Summarised values of test.

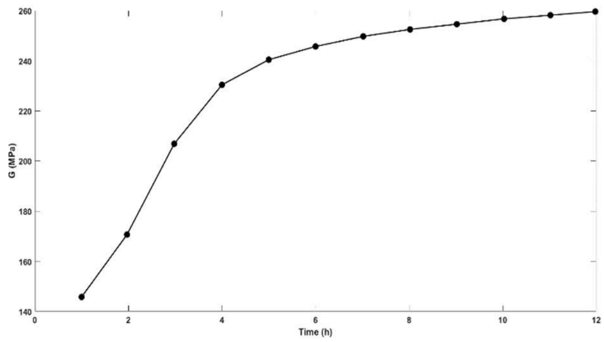

Figure 7 Evolution of G over time.

Conclusions and Future Work

Further work in the effects of different confining pressure during the curing process in the evolution of stiffness is recommended. Monitoring the evolution of artificially cemented samples will provide a valuable tool in the design of geotechnical centrifuge models, where cementation can also occur while samples are subject to stress due to the increase in acceleration. These will allow predicting the evolution of the stiffness of the soil models over time. Further work assessing the stiffness of artificially cemented sand mixed with different amounts of Portland Cement is necessary.

Acknowledgements

This research is funded by the National Council of Science and Technology and the Secretariat of Energy of Mexico.

References

Airey, D., & Mohsin, A. K. M. (2013). Evaluation of Shear Wave Velocity from Bender Elements Using Cross-correlation. *Geotechnical Testing Journal*, *36*(4), 20120125. https://doi.org/10.1520/GTJ20120125

Consoli, N. C., Rotta, G. V., & Prietto, P. D. M. (2002). Influence of curing under stress on the triaxial response of cemented soils. *Géotechnique*, *52*(5), 382–384. https://doi.org/10.1680/geot.52.5.382.38705

Consoli, N. C., Viana da Fonseca, A., Cruz, R. C., & Heineck, K. S. (2009). Fundamental Parameters for the Stiffness and Strength Control of Artificially Cemented Sand. *Journal of Geotechnical and Geoenvironmental Engineering*, *135*(9), 1347–1353. https://doi.org/10.1061/(ASCE)GT.1943-5606.0000008

Dalla Rosa, F., Consoli, N. C., & Baudet, B. A. (2008). An experimental investigation of the behaviour of artificially cemented soil cured under stress. *Géotechnique*, *58*(8), 675–679. https://doi.org/10.1680/geot.2008.58.8.675

Lee, J.-S., & Santamarina, J. C. (2005). Bender Elements: Performance and Signal Interpretation. *Journal of Geotechnical and Geoenvironmental Engineering*, *131*(9), 1063–1070. https://doi.org/10.1061/(ASCE)1090-0241(2005)131:9(1063)

The development of a new micromechanical inter-particle loading apparatus for railway ballast.

C.P.Y. Wong*[1]

*Correspondence: cacin.wong.16@ucl.ac.uk

[1]*Department of Civil, Environmental and Geomatic Engineering, Faculty of Engineering Science, University College London, UK*

Abstract

There is little work in the literature on the micromechanical behaviour of ballast that would be needed for successful DEM modelling. A new 3-axis inter-particle loading apparatus has been developed for testing railway ballast with high accuracy of the loads and displacements. The apparatus has full control of loads or displacements at a contact between two particles three dimensionally. An initial series of tests has shown the ballast to be much softer in behaviour than expected, probably due to the contact behaviour of the particles depending on the local contact geometry more than the overall diameter.

Introduction

The popularity of Discrete Element Modelling (DEM) analyses has increased. This requires real soil particle behaviour as the input parameters. Previous research on particle strength and contact behaviour has focused on natural sand particles (e.g. Senetakis et al., 2013; Nardelli et al., 2017) rather than crushed rocks. Thus, a new inter-particle loading apparatus has been constructed to investigate the contact behaviour of larger particles (e.g. ballast or small rockfill).

Apparatus design

Figure 1 shows a photograph of the new apparatus which consists of 3-axis control, one in the vertical and two in orthogonal horizontal directions. There are linear actuators, load cells and displacement transducers on the loading arms, one in each of the three directions. The load cells are placed between the linear actuators and the particles. The frame has been built to be stiff to prevent deflection under the applied load which would also lead to inaccurate measurements. The top platen is connected to the vertical load cell and the bottom platen is on the sled which is on a 3-point bearing system. Both the plates below and above the bearings are also made of hardened steel to prevent the bearings indenting them.

The measurement of force and displacement can be obtained in all three directions. The loads are measured by high accuracy load cells which have a capacity of 1kN in the vertical direction and 500N in the horizontal direction. The displacements are measured by a new transducer, capacitive non-contact displacement transducers. The authors are not aware of capacitive transducers being used in soil mechanics applications. Therefore, their performance has been investigated in some detail.

Transducer performance and compliance of the apparatus

The sensitivity of the sizes and metals of the target of the capacitive non-contact displacement transducers have been checked and the impact is not significant. The calibration curves for all targets are perfectly linear from contacting to the designed measuring range of 4mm.

The noise resolution is very important to this research to obtain the best quality results, so the stability of the displacement transducers and load cells over a typical test duration has also been checked. For the displacement transducers, the noise is about ±0.01μm, which is also the resolution of the data logger and the drift is around ±0.1μm over 45 minutes. The noise on the load cells is about 0.01N for all load cells while the drift for the vertical and horizontal load cells is around 0.1N and 0.05N respectively.

The compliance of the apparatus was carried out with a single ballast particle with two flat surfaces at both ends and glued to both platens by epoxy resin. The compliance is 0.003μm/N in the vertical system and 0.33μm/N in the horizontal. All of the test data will be corrected for these compliances.

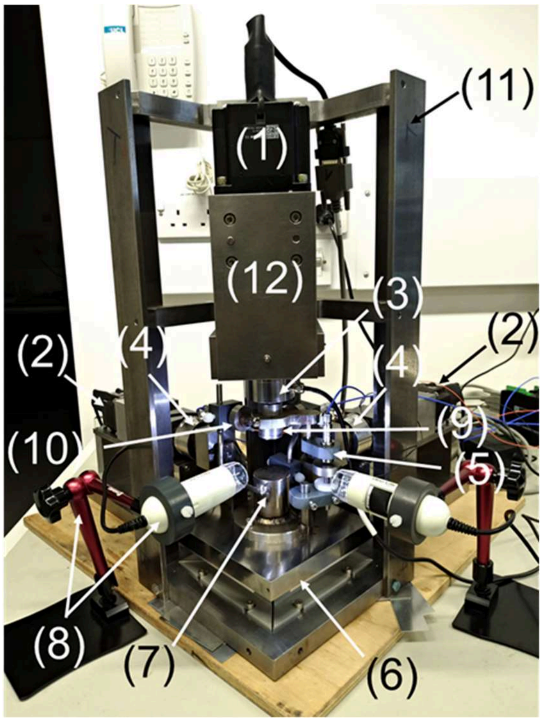

Figure 1. Photograph of the inter-particle loading apparatus: (1) vertical linear actuator, (2) horizontal linear actuators, (3) vertical load cell, (4) horizontal load cells, (5) vertical displacement transducer, (6) sled, (7) bottom platen, (8) digital microscope camera and stand, (9) top platen, (10) horizontal displacement transducer, (11) stainless steel frame (12) front plate.

Results and Discussion

Preliminary tests on both normal and shear loading of ballast (around 30-40mm sized UK granite) have been carried out. The normal loading behaviour of these tests is clearly non-linear and became stiffer as the normal load increased, which agrees with the theory of Hertz (1882). However, it is not, as expected to be, much stiffer than the small size particles (2.36-5mm of quartz sand and decomposed granite) tested by Nardelli & Coop (2018). This indicates that the local contact geometry and surface roughness of the particles are affecting their contact behaviour.

Figure 2 shows a typical shear test over a displacement of 3mm under 100N vertical load. There was a breakage event during the test which was unexpected under the relatively small load. The forces are resolved by deriving the angle of the current particle contact relative to horizontal to obtain the true normal and tangential forces. The values of μ_{mob} were found to vary much more than for simple sedimentary sands (Nardelli et al., 2017).

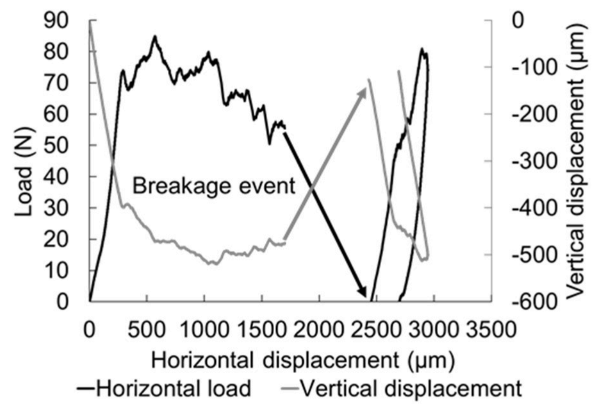

Figure 2. Raw data for shearing test.

Conclusions and Future Work

A new inter-particle loading apparatus has been constructed to investigate the contact behaviour of ballast and small rockfill sized particles. The transducers have high resolution and precision and the compliance of the apparatus is minimised. Less stiff behaviour than expected was found in both normal and shear loading. The contact morphology will need to be quantified carefully to assess its impact on the contact mechanics in the future.

References

Hertz, H. (1882). Über die Berührung fester elastischer Körper. J. Reine und Angewandte Mathematik, 92, 156-171.

Nardelli, V. & Coop, M.R. (2018) The experimental contact behaviour of natural sands: normal and tangential loading. Géotechnique, under review.

Nardelli, V., Coop, M.R., Andrade, J.E. & Paccagnella, F. (2017) An experimental investigation of the micromechanics of Eglin sand. Powder Tech., 312, 166-174.

Senetakis K., Coop M. & Todisco M.C. (2013). The inter-particle coefficient of friction at the contacts of Leighton Buzzard sand quartz minerals. Soils and Foundations, 53(5), 746-755.

The seismic liquefaction of mine tailings

A. Cartwright[1]

Correspondence: a.cartwright.12@ucl.ac.uk

[1]*Department of Civil, Environmental and Geomatic Engineering, Faculty of Engineering Science, University College London, UK*

Abstract

The use of tailings dams as waste mineral deposits are widespread all over the world. The lack of knowledge about the tailings materials, and the poor maintenance of the dams, means that failures of tailings dams continue to occur. The consequences can vary from engineering problems, if the amount of material involved is relatively small, to serious ecological and economic loss.

Tailings deposits are usually soft, loose and permanently saturated. They tend to liquefy during the early phase of major earthquakes, which results in an increased horizontal load on the tailings dam. The cyclic force vibrations from the shaking causes the pore water pressure to build up which reduces the effective stress in the soil. The seismic liquefaction of mine tailings will be investigated through undrained cyclic triaxial tests.

Introduction

Mine tailings are the residual waste materials from mining processes. They are most commonly disposed of by mixing them with water and depositing them into large lagoons retained by dams constructed out of the coarser tailings material (Wei 2017). Tailings dams have a high risk of failure due to liquefaction as a consequence of the sediments loose state and significant water content.

Whilst most disasters involving hydraulic dams have been prevented some years ago, the same has not yet been observed with tailings dams (Soares 2015). The consequences of dam failure can be very severe, through the loss of life, homes, livelihoods and widespread environmental damage from the release of millions of cubic metres of waste.

For example, the 2010 Mw 8.8 megathrust earthquake in Chile caused the liquefaction of the Las Palmas tailings dam. The liquefied tailings flowed 400m downstream, contaminating the area and causing 4 fatalities (Verdugo and González, 2015). It is necessary to understand the earthquake exposure of tailings facilities to try and predict and prevent these catastrophes.

The project will investigate the liquefaction of tailings material under seismic loading. The release of seismic waves from earthquakes cause increased shear stress on tailings dam embankments. This can increase the pore pressure in the saturated tailings and lead to liquefaction. The research will be of an experimental nature, by means of advanced laboratory testing in the Geotechnical Engineering Research Laboratory at UCL. These Laboratory investigations will help develop a clearer understanding of the states of stress and density under which tailings may be susceptible to liquefaction (Carrera 2008). Results from these experiments will allow improved predictions on how the materials will behave in-situ under cyclic loading.

Triaxial tests are commonly used to investigate the collapsibility of a soil. The Critical State framework is generally accepted as a means to identify those states of specific volume and confining stress under which a soil can be susceptible to liquefaction. Those soils in a state that lies above the Critical State Line (CSL) will be considered susceptible to liquefaction, while those soils whose state lies below the CSL will tend to dilate, reducing the likelihood of liquefaction (Carrera 2008).

Methodology

The triggering loading conditions for liquefaction can be investigated through triaxial tests. In these tests, soil specimens are saturated and confined via the difference between the confining pressure (CP), i.e. the surrounding fluid, and the backpressure (BP), i.e. the fluid inside the specimen (Soares 2015). The sample is then saturated and isotropically consolidated before cyclic shearing can take place.

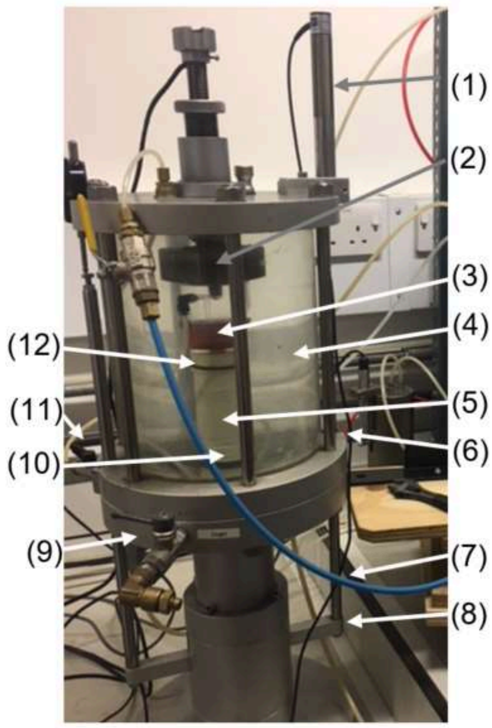

Figure 1: Triaxial apparatus at UCL – (1) displacement transducer, (2) loading piston, (3) suction cap, (4) water filled chamber, (5) latex membrane covering soil sample, (6) CP measurement, (7) tube attaches to piston to allow suction cap connection, (8) loading ram, (9) drainage tap, (10) porous stone, (11) BP measurement, (12) O-ring.

It is suggested by many authors that the CSL of a soil might depend on the sample preparation method due to the different fabrics that different methods create (Carrera 2008). The fabric of a material represents the particles, including size and shape, and associated pores. A variety of preparation methods are to be tested to identify which method or methods can closely simulate the structure and the actual stress-strain response of the tailings being modelled.

The slurry method shall be considered initially. This method ensures reasonably homogenous and reproducible specimens, creating a fabric that is believed to be similar to the one in situ (Murthy et al., 2007). A perspex mould will sit ontop of the split mould so dry tailings can be poured into distilled water or tailings water. The tailings will then be shaken vigorously before being allowed to settle. Following this the specimen is saturated, consolidated and sheared.

Results and future work

Initial tests have been set up in the research laboratory at UCL investigating the liquefaction of tailings through undrained cyclic triaxial tests. Results are not yet available but will be shared during the presentation.

In the laboratory, the study of liquefaction is investigated through two different tests: undrained monotonic tests, to study static liquefaction, and cyclic tests, to study dynamic liquefaction. A comparison will be made between my cyclic loading test data and the framework for static liquefaction from Carrera.

Future work also includes experimenting with sample preparation methods. I plan to develop a method that creates uniform samples that can be replicated consistently.

Mine tailings deposits will be tested from locations all over the world. The results will give important information about the behaviour of these materials and the dam design conditions required for safety.

References

Carrera, A. (2008). Mechanical Behaviour of Stava Tailings. PhD. Politecnico di Torino.

Murthy, T., Loukidis, D., Carraro, J., Prezzi, M. and Salgado, R. (2007). Undrained monotonic response of clean and silty sands. Géotechnique, 57(3), pp.273-288.

Soares, S. (2014). Evaluation of Soil Liquefaction Potential Based on Laboratory Data. PhD. Universidade do Porto.

Verdugo, R. and González, J. (2015). Liquefaction-induced ground damages during the 2010 Chile earthquake. Soil Dynamics and Earthquake Engineering, 79, pp.280-295.

Wei, L. (2017). The Mechanical Behaviour of Tailings. PhD. City University of Hong Kong.

Direct shear and interface shear testing of granular materials using polypropylene counterfaces at low stresses

L.W. de Leeuw*[1], A. Diambra[1] and M.S. Dietz[1]

*Correspondence: lawrence.deleeuw@bristol.ac.uk

[1] *University of Bristol, Department of Civil Engineering, Queen's Building, BS8 1TR, UK*

Abstract

Two sands of varying D_{50} were tested in direct shear and interface shear at low stresses using polypropylene counterfaces. Interface efficiency is generally less than half the direct shear counterpart and interface tests show a modest increase in strength for dense tests. Both direct shear and interface shear tests exhibit an enhanced strength at very low stress and when roughness is normalised to D_{50} the response of sand-polypropylene echoes that of sand-steel.

Introduction

Subsea pipelines are protected from abrasion, impact, or corrosion damage using an external coating. A prevalent coating is a three-layer polypropylene bonded arrangement which gives optimal protection compared to older bitumen or fusion-bonded epoxy technologies.

The geomechanical behaviour of polypropylene coatings in terms of pipeline-soil interaction is poorly constrained. The Joint Industry Partnership SAFEBUCK design guidance for subsea pipelines gives a broad range for the strengths of this interface so better constraining these parameters lends an obvious cost benefit in better understanding the pipeline-soil interaction and reducing overdesign.

Methodology

Two granular materials, Leighton Buzzard 14-25 and Hostun Sand, were selected to explore the effect of D_{50} on the interface response of polypropylene surfaces. A combination of submerged direct shear and surface-over-sand interface tests were carried out at nominal normal stresses of 2.5kPa to 35kPa.

Samples were prepared by the dry deposition pluviation method (Miura et al., 1997) and light compaction to achieve a nominally loose sample of approximate fabrication relatively density of 15%. Dense samples were prepared by pluviation and densification by agitating the shear box frame to encourage compaction to required nominal fabrication density of 70%.

Shear tests were undertaken submerged using a modified winged shear box apparatus (Lings and Dietz, 2004) with one counterface being used for each test sand. Tests were conducted in order of increasing normal stress and loose followed by dense to minimise the effect of surface scour on test results.

Non-contact profilometry using an Alicona InfiniteFocus digital microscope was carried out using focus variation to measure the topography of surfaces before and after testing. The arithmetic mean roughness, R_a, was selected for comparison and normalised against the D_{50} of the test sands to give $R_{norm} = R_a / D_{50}$.

Results and Discussion

Direct shear results are consistent with classical soil mechanics and show stress-dilatant behaviour. Ultimate values for loose and dense tests show good agreement so these are combined to make one data set shown in Figure 8. In both tests for both the peak and ultimate condition there is an enhancement in shear strength as the normal stress decreases.

In contrast, interface tests generally exhibit an elastic, perfectly-plastic type response for both loose and dense samples. Shear stresses increase to a plateau during the early stages and then remain quasi-static through the duration of the test. Interface tests show very little volumetric response, with recorded vertical displacements typically no greater than 0.1mm with a more linear response than is seen in direct shear. In contrast to direct shear where initial density has a negligible impact on the ultimate shear strength, dense interface tests show a slightly higher strength than loose tests, shown in Figure 8.

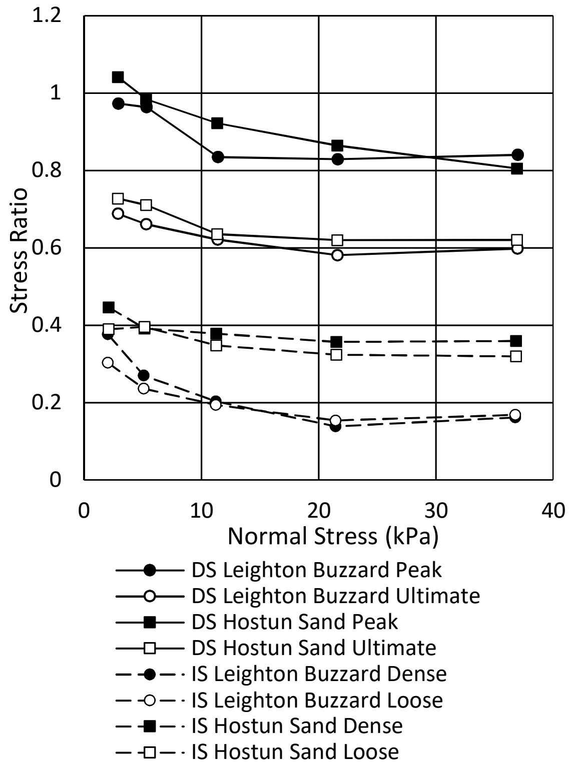

Figure 8 Peak and ultimate stress ratios for direct shear (DS) tests, and dense and loose stress ratios for interface (IS) tests.

It is clear from Figure 8 that the interface efficiency, defined as the ratio between the interfacial shear strength and the direct shear strength, is in the order of 0.33 to 0.36 for Leighton Buzzard and 0.53 to 0.59 for Hostun Sand. The D_{50}, 0.883 and 0.346 respectively, seems to impact the efficiency with the finer grained material mobilising a greater shear strength.

The interface efficiency is governed in part by the effective roughness of the surface, determined by the term R_{norm} to account for effect of grain size. In Figure 9, stress ratio at ~20kPa is plotted against R_{norm} and compared against the trendline which defines the response of sand-steel interfaces at 25kPa after (Dietz and Lings, 2006). Despite the difference in surface type and properties, there is a close alignment between the response of sand-polypropylene and sand-steel.

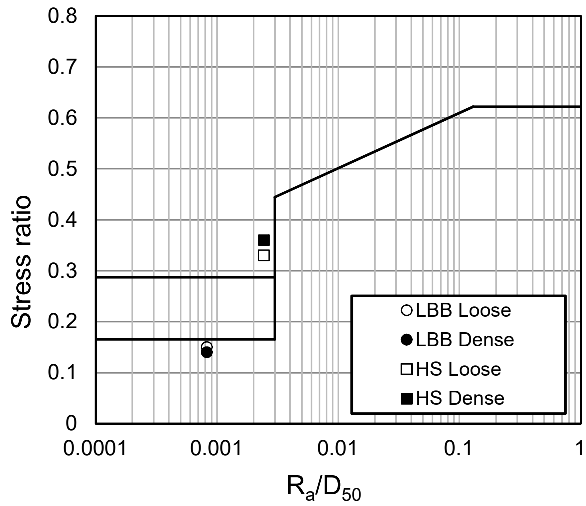

Figure 9 Interface stress ratio for loose and dense tests against normalised roughness at ~20kPa. Black trend lines: (Dietz and Lings, 2006) response of sand-steel interfaces at 25kPa.

Conclusions and Future Work

Dilation and peak-postpeak behaviour is not observed in interface tests and there is a modest strength increase from loose to dense tests. Both direct and interface shear tests show enhanced strengths at very low stresses. Grain size impacts the effective roughness, with smaller D_{50} mobilising greater roughness and greater interface efficiency. It is remarkable to note that the response of sand-polypropylene interfaces appears to echo that of sand-steel.

Future work includes exploring if the remaining portion of the trend line from Figure 9 can be replicated with additional interface variables like temperature, hardness, and roughness.

References

Dietz, M. S. and Lings, M. L. 2006 'Postpeak strength of interfaces in a stress-dilatancy framework', *Journal of Geotechnical and Geoenvironmental Engineering,* 132: 1474-84

Lings, M. L. and Dietz, M. S. 2004 'An improved direct shear apparatus for sand', *Geotechnique,* 54: 245-56

Miura, K., Maeda, K., and Toki, S. 1997 'Method of measurement for the angle of repose of sands', *Soils and Foundations,* 37: 89-96

Compaction Characteristics and Shrinkage Properties of Fibre Reinforced London Clay

J. Wang*[1], A. Sadler[1], P. Hughes[1] and C. Augarde[1]

*Correspondence: jianye.wang@durham.ac.uk

[1]*Department of Engineering, Durham University, South road DH1 3LE, UK*

Abstract

This paper presents an experimental study of changes in the engineering proper-ties of London Clay when reinforced with polypropylene fibres. Standard Proctor tests and linear shrinkage tests were carried out to evaluate changes to optimum moisture content, bearing capacity and shrinkage properties due to the inclusion of fibres. The experimental results indicate that as the fibre inclusion ratio in-creases, both optimum moisture content and maximum dry density of the soil are reduced. Fibre length was also shown to influence maximum dry density but not optimum moisture content. The introduction of fibres also reduced linear shrink-age of the soil by as much as 40% when compared to unreinforced soil.

Introduction

Utilising fibres as reinforcement in fine-grained soils, is a potentially promising method for improving the engineering behaviour of soils. Currently, polypropylene (PP) fibre is the most widely used fibre in laboratory assessments of soil reinforcement. Soganci (2015) studied the effects of polypropylene fibre on compaction and swelling characteristics of an expansive soil. Test results indicated that inclusion of fibre reduced maximum dry density and swell potential. Tang et al. (2012) found that desiccation cracking was significantly reduced and crack resistance improved with fibre inclusion. Here we report on a compaction and linear shrinkage tests carried out on London Clay reinforced with fibres studying the influence of fibre inclusion ratio and fibre length.

Methodology

The soil used in this study is London Clay, with the basic properties shown in Table 1. PP fibres of two different lengths (6mm and 12mm) used in the tests were produced by ADFIL (2018). The physical properties of the fibres are given in Table 2. Fibres were weighed and mixed with the soil in small increments (10% of the total weight) by hand. After fibre/soil mixing, distilled water was added to the mixture until the target moisture content was achieved. The fibre inclusion ratio (ρ) is defined herein as $\rho=W_f/W$, where W_f is the mass of fibre, W is the mass of dry soil. The inclusion ratios of fibre (ρ) in tests were selected as 0.3%, 0.6% and 0.9% for both lengths of fibre. Standard Proctor tests and Linear Shrinkage tests were conducted in accordance with BS-1377, part 4 (1990) and BS 1377, part 2 (1990) respectively.

Property	Value
Specific Gravity	2.72
Liquid Limit (%)	58.2
Plastic Limit (%)	20.9
USCS Classification	CH

Table 1. Basic properties of the London Clay

Property	Value
Tensile Strength (Mpa)	416
Length (mm)	6 & 12
Diameter (μm)	22
Specific gravity	0.91

Table 2. Basic properties of the PP fibre

Results and Discussion

The variation of MDD and OMC with respect to the fibre content is plotted in Figure 1. It can be seen that with the increase of fibre percentage from 0% (i.e. unreinforced soil) to 0.9%, for a given fibre length, the addition of fibre decreases MDD which can be attributed partly to the decrease of the average unit weight of the solids in the soil fibre mixture, and also the fibres preventing efficient particle packing. The OMC also decreases on fibre addition. It can also be concluded that for the same fibre content, soil reinforced with longer fibres tends to have a higher MDD, though this phenomenon becomes less clear when the fibre inclusion ratio increases to 0.9%. This may be due to fibre interweaving. Fibre length is not however seen to have a significant impact on OMC. Figure 2 shows the effects of PP fibre addition on linear shrinkage. It can be seen that linear shrinkage reduces significantly with the increase in PP fibres though the rate of decline decreases as the fibre inclusion ratio increases. When the fibre inclusion is 0.9%, the linear shrinkage percentage is reduced to less than 40% of the value in the unreinforced soil. It is notable that the 6 mm fibre is more effective than the 12mm fibre when the inclusion ratio is relatively low, and there is no obvious difference for the two lengths of fibre when the inclusion ratio increases to above 0.6%. The improvement of the linear shrinkage properties in the reinforced materials is likely due to the development of interaction between fibre surfaces and soil particles, with fibres acting as a frictional and tension resistant element in the mixture to prevent the shrinkage of the sample.

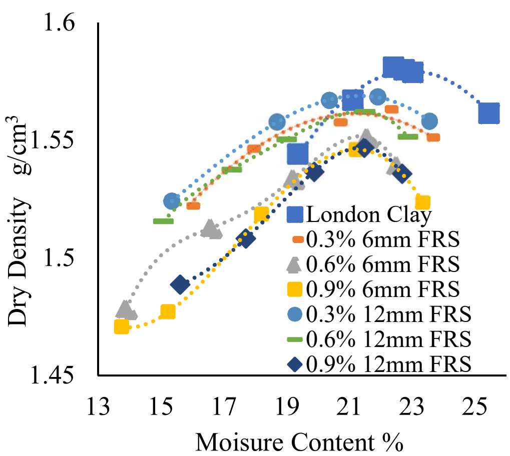

Figure 1. Compaction curves of unreinforced and reinforced soil

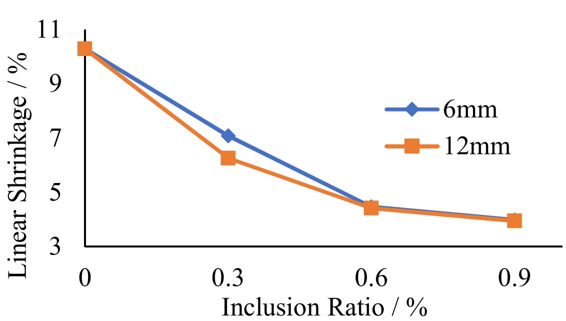

Figure 2. Linear shrinkage of London clay with and without fibres

Conclusions and Future Work

Based on the experimental results presented here, it can be concluded that fibre reinforcement reduces both the MDD and OMC of London Clay. For a given fibre content, longer fibres produce higher MDD but fibre length does not have a clear influence on OMC. In linear shrinkage of reinforced soil is reduced significantly through the addition of fibres and this trend becomes slower as the fibre contents increase. More researches on the shear strength and working mechanism of fibre reinforced clay should be developed.

Acknowledgements

We are thankful to the ADFIL who provided the fibre used in the research.

References

H Soğancı, A.S.: The effect of polypropylene fiber in the stabilization of expansive soils. Int. J. Env, Chem, Eco, Geo and Geophys Eng 9(8), 994-997 (2015).

Tang, C-S.: Desiccation cracking behavior of polypropylene fiber–reinforced clayey soil. Canadian Geotechnical Journal 49(9), 1088-1101 (2012).

ADFIL, Product Data Sheet, http://www.adfil.com/products/micro-synthetic fibres/ monofilament-fibres/ (last accessed 2018/02/28).

British Standards Institution. BS 1377- Part 2 Classification tests, Methods of test for soils for civil engineering purposes. BSI, London (2004).

British Standards Institution. BS 1377- Part 4 Compaction related tests, Method of test for soils for civil engineering purposes, BSI, London (2004)

Thermo-hydro-mechanical characterisation of London clay

S. Chen *[1]

*Correspondence: sihua.chen16@imperial.ac.uk

[1]*Imperial College London, SW7 2AZ, the UK*

Abstract

Thermo-active structures, such as piles, retaining walls and tunnel linings, have been proposed as a possible solution to meeting the sustainability requirements in civil engineering construction and energy production from renewable sources. There are still uncertainties in the design of these structures with respect to soil response under cycles of temperature changes that they impose to the ground. This research is concerned with thermo-hydro-mechanical behaviour of London clay, characterised using temperature-controlled triaxial and isotropic cells developed in the Geotechnics Laboratory at Imperial College. Temperature-based calibrations of instrumentations are performed before tests. Thermally-induced volume changes, pore water pressures, compressibility, strength and stiffness, are investigated in terms of the applied temperature changes in the range of 20 to 40^{o} C.

Introduction

The design of thermo-active structures depends on the thermo-hydro-mechanical behaviour of the surrounding soil under temperature changes imposed by their operation. Abuel-Naga et al. (2007) found that normally consolidated and lightly over-consolidated soft Bangkok clay contracted upon heating, while heavily overconsolidated samples dilated. A range of results for other clays is presented by Hueckel & Baldi (1990) (Pontida clay, Pasquasia clay), Sultan et al. (2002) (Boom clay), Cekerevac & Laloui (2004 (kaolin), and Martinez-Calonge (2017) (London cay), with often contradicting evidence on the temperature effects on the clays' mechanical properties. This research aims to further characterise the behaviour of London clay under heating-cooling cycles.

Methodology

Drained heating tests on samples of reconstituted London clay will be performed in a temperature-controlled triaxial apparatus (Figure 1) developed at Imperial College Geotechnical Laboratory, as presented by Martinez-Calonge (2017). The cell is placed in a computer-controlled 50 kN loading frame. De-aired water inside the stainless steel cell supplies a confining pressure of up to 800 kPa. Three 150 W cartridge heaters are installed in the bottom plate and another three heaters are placed in the top plate, capable of raising the temperature up to 85 °C. Temperature sensors are installed next to each heater and inside the confining fluid to monitor the temperature throughout the tests. Loads and displacements are measured by a submersible load cell and an external linear variable differential transformer (LVDT), respectively.

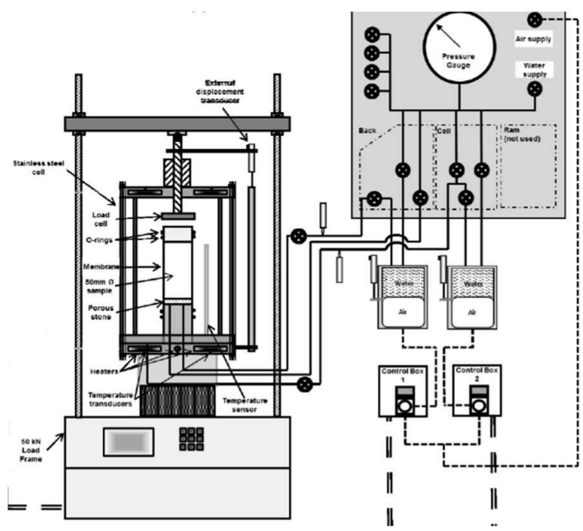

Figure 1. Schematic view of temperature-controlled triaxial apparatus (Martinez-Calonge, 2017)

Undrained heating tests will be performed in a temperature-controlled isotropic cell (Figure 2).

It has the same heating mechanism as the temperature-controlled triaxial cell, except that it does not have a loading frame. Three radial (Ackerley et al., 2016) and two axial LVDTs are placed inside the cell to measure changes in sample dimensions. Pore water pressure is monitored from the back pressure line and also using a mid-height probe.

Figure 2. Temperature-controlled isotropic cell

The TRIAX software (Toll, 1999) is connected to the system to digitally control, monitor and record pressures, load and displacement.

London clay (PI = 45%), taken from a borehole near Victoria and Albert museum at 11-12 m depth, is used in the experimental programme. The clay is ground into dry powder, mixed with water at 1.25 times the water content at liquid limit (Burland, 1990) and consolidated under the effective vertical stress of 200 kPa for three weeks into a 225 mm diameter cake (water content = 22%).

Results and Discussion

Long-term monitoring of the system is performed. Changes in the readings of the instrumentations are more obvious when subjected to first heating-cooling cycles and become less pronounced in the following thermal cycles, due to the warm-up period of the instrumentations. Temperature-based calibrations currently performed will be incorporated in the computer-controlled system to account for the thermal effect.

Conclusions and Future Work

Proceeding from existing work by Martinez-Calonge (2017) on thermo-hydro-mechanical behaviour of London clay, some trial tests have been performed using the temperature-controlled triaxial cell. Local instrumentations are added to the isotropic cell and monitored under elevated temperature.

Tests on London clay will be performed to characterise its thermo-hydro-mechanical behaviour, focusing on thermally-induced volumetric strain, pore water pressure, compressibility, strength and stiffness, to aid the design of thermo-active structures.

Acknowledgements

This research is funded by the Chinese Scholarship Council. Professor Lidija Zdravkovic and Dr Antonio Carraro are acknowledged for supervising the work, and Mr. Steve Ackerley and Mr. Graham Keefe for their technical support with equipment.

References

Abuel-Naga, H. M., Bergado, D. T. & Bouazza, A. (2007a) Thermally induced volume change and excess pore water pressure of soft Bangkok clay. Engineering Geology, 89 (1-2), 144-154.

Ackerley, S. K., Standing, J. R. & Hosseini Kamal, R. (2016) A system for measuring local radial strains in triaxial apparatus. Géotechnique. 66 (6), 515-522.

Burland, J. B. (1990) On the compressibility and shear strength of natural clays. Géotechnique. 40 (3), 329-378.

Cekerevac, C. & Laloui, L. (2004) Experimental study of thermal effects on the mechanical behaviour of a clay. International Journal for Numerical and Analytical Methods in Geomechanics, 28 (3), 209-228.

Hueckel, T. & Baldi, G. (1990) Thermoplasticity of saturated clays: experimental constitutive study. ASCE Journal of Geotechnical and Geoenvironmental Engineering, 116 (12), 1778-1796.

Martinez-Calonge, D. (2017) Experimental investigation of the thermo-mechanical behaviour and thermal properties of London clay. PhD thesis. Imperial College London, United Kingdom.

Sultan, N., Delage, P. & Cui, Y. J. (2002) Temperature effects on the volume change behaviour of Boom clay. Engineering Geology, 64 (2-3), 135-145.

Toll, D. (1999) A Data Acquisition and Control System for Geotechnical Testing. In: Kumar, B. & Topping, B. H. V. (eds.) Computing Developments in Civil and Structural Engineering. Edinburgh pp.237-242.

Effect of salt on liquid limit and plastic limit of kaolin-bentonite mixtures

A. Muththalib*[1] and B. Baduet[1]

*Correspondence: abdulla.muththalib.16@ucl.ac.uk

[1] *Department of Civil, Environmental & Geomatic Engineering, University College London (UK)*

Abstract

Atterberg limits are important in geotechnical engineering as they provide data to decide the stability of soil and if the soil needs to be stabilized prior to any construction work. Like other engineering properties, liquid limit (w_L) and plastic limit (w_P) are affected by pore water composition. Previous research into the effect of pore water chemistry on the behaviour of soil found sodium chloride in bentonite decreases both w_L and w_P significantly, while sodium chloride in kaolin have very little or no effect on w_L and w_P of kaolin. This paper presents new results on the effect of sodium chloride on w_L and w_P of the kaolin-bentonite mixtures. It is shown that w_L and w_P are directly proportional to the percentage of bentonite in the mixture.

Introduction

Effect of pore fluid composition on clay behaviour has been studied by many researchers. (Mitchell, 1961, Di Maio and Onorati, 2000, Di Maio et al., 2004, Pontolillo et al., 2016)

Di Maio et al. (2004) investigated the liquid limits of ponza bentonite, a commercial kaolin, Bisaccia clay and Marino clay and found that the liquid limit decreases with the increase of the concentration of salt solution except in kaolin. When the pore fluid is distilled water, the influence of mineral composition of clay is more significant. It was found that initial void ratio and consolidation increase with the percentage of bentonite and the swelling index increases with the increase of the percentage of smectite. Smectite has high water absorption capacity and hence the smectite fraction has the most influence. The molarity of pore fluid has a direct proportional relationship with smectite content. Previous research also showed that the concentration of pore fluid have opposite effect on the liquid limit of kaolinite and illite than on the liquid limit of bentonite (Anson and Hawkins, 1998).

Di Maio et al. (2004) investigated w_L of kaolin-bentonite mixtures mixed with water and how w_L changes with increasing salt concentration, but no comparison was made of how the w_L and w_P of kaolin-bentonite clay mixtures might change with salt in comparison with kaolin-bentonite mixtures in water.

Methodology

Four clay mixtures are used in this study. They are 100 percent kaolin, 100 percent bentonite, a kaolin-bentonite mixture containing 33.3 percent kaolin and 66.7 percent bentonite and a clay mixture containing 66.7 percent kaolin and 33.3 percent bentonite. De-ionised water and 0.6 Molar concentration (35 grams per litre) of sodium chloride (NaCl) solution were used as pore fluids.

Each clay mixture was mixed with water and NaCl solution. Liquid limit (w_L) tests were carried out using fall cone method according to BS EN ISO 17892-12:2017 and plastic limit (w_P) tests were carried out according to BS EN ISO 17892-12:2017.

Results and Discussion

Liquid and plastic limit tests were carried out to investigate the effect of salt solution as pore fluid on the mixtures of kaolin-bentonite. Liquid limit and plastic limit tests as presented in Figure 1 and Figure 2 show that both properties decrease linearly with the decrease in bentonite content in the kaolin-bentonite clay mixtures, both when mixed with water and when mixed with NaCl solution. The effect of sodium chloride on w_L and w_P of bentonite is significant where w_L decreased from 168 to 110 when mixed with 0.6M NaCl solution and w_P decreased from 59 to 50. The effect of NaCl solution on w_L and w_P of pure kaolin on the other hand is almost negligible. A decrease in w_L and w_P with the decrease in bentonite content in kaolin-bentonite clay mixtures with water as pore fluid was also shown by Di Maio and Fenelli (1994).

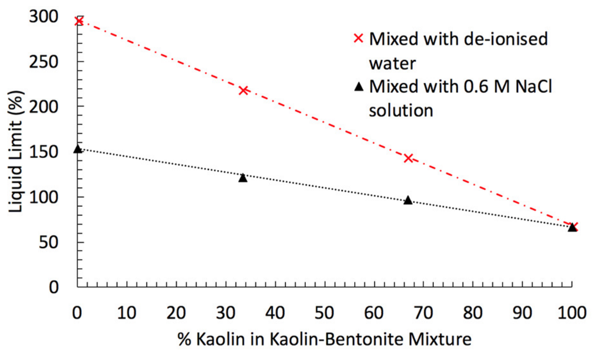

Figure 1: Liquid limits of kaolin-bentonite clay mixtures

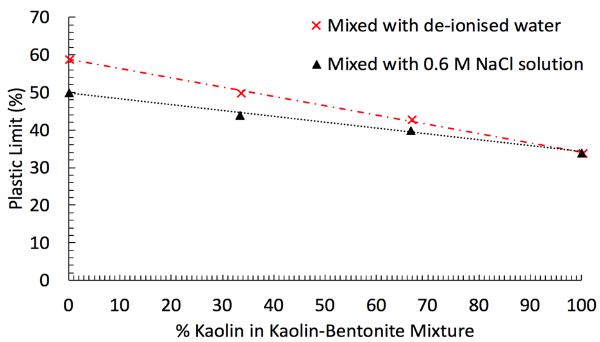

Figure 2: Plastic limits of kaolin-bentonite clay mixtures

Conclusions and Future Work

Sodium Chloride solution was shown to have significant effect on the properties of bentonite while kaolin is not affected. A linear relationship between both w_L and w_P and the percentage of bentonite content of kaolin-bentonite clay mixtures, separately in de-ionised water and 0.6M NaCl solution as pore fluid, was found.

This result suggests that it is important to study the effect of other chemicals in pore fluid such as heavy metal contamination and other salts on the behaviour of soils.

Acknowledgements

This paper is based on initial investigation of the PhD research by A. Muththalib, who is sponsored by Islamic Development Bank (IDB) along with UCL Department of Civil, Environmental & Geomatic Engineering. Special mention of Professor Matthew Coop, who has been providing support and guidance. Also, appreciation to technical staff at Department of Civil, Environmental & Geomatic Engineering for all the assistance.

References

ANSON, R. W. W. & HAWKINS, A. B. 1998. The effect of calcium ions in pore water on the residual shear strength of kaolinite and sodium montmorillonite. *Géotechnique,* 48**,** 787-800.

DI MAIO, C. & FENELLI, G. B. 1994. Residual strength of kaolin and bentonite - the influence of their constituent pore fluid. *Geotechnique,* 44**,** 217-226.

DI MAIO, C. & ONORATI, R. Influences of pore liquid composition on the shear strength of an active clay. VIII International Symposium on landslides, June 2000 2000 Cardiff. 463-468.

DI MAIO, C., SANTOLI, L. & SCHIAVONE, P. 2004. Volume change behaviour of clays: the influence of mineral composition, pore fluid composition and stress state. *Mechanics of Materials,* 36**,** 435-451.

MITCHELL, J. K. 1961. Fundamental aspects of thixotropy in soils. *Transactions of the American Society of Civil Engineers,* 126**,** 1586-1620.

PONTOLILLO, D. M., DE ROSA, J., SCARINGI, G. & DI MAIO, C. 2016. Clay creep and displacements: influence of pore fluid composition. *In:* GOTTARDI, G. & TONNI, L. (eds.) *Vi Italian Conference of Researchers in Geotechnical Engineering, Cnrig2016 - Geotechnical Engineering in Multidisciplinary Research: From Microscale to Regional Scale.* Amsterdam: Elsevier Science Bv.

Re-evaluating interface friction for geotechnical modelling

P. Shepley*[1]

*Correspondence: p.shepley@sheffield.ac.uk

[1]*University of Sheffield, Department of Civil and Structural Engineering, Sir Frederick Mappin Building, Sheffield, S1 3JD, UK*

Abstract

Interface friction is an important aspect in geotechnical physical modelling. This paper is a reinvestigation into interface friction, with a focus on exploring the effect of changing the hardness of the interface material. Three differing materials were tested using two sands under standard and adapted direct shear testing. The initial results suggest that the number of load carrying contacts affects interface friction angle more than the material hardness. The experiment results also indicate the need to re-evaluate the established smooth interface limit for angular materials.

Introduction

Geotechnical engineers face different challenges compared to other engineering disciplines in this age of automation. This is due to the inherent variability of ground conditions and uncertainty in the soil-structure interaction mechanisms which prevent geotechnics from the benefits of mass manufacture and economies of scale available to alternative areas. As a result, most geotechnical projects are functional prototypes with limited structural efficiency.

Efficiencies may be achieved through improved prototyping of the final structure. Small scale physical modelling methods, such as centrifuge modelling, can simulate these structures; directly replicating the physical interactions at soil-structure interfaces. Whilst centrifuge modelling is capable of representing ultimate limit states, the technique struggles to accurately portray serviceability limit states in sands, an area in need of refinement given the increase in serviceability limited problems (e.g. offshore monopiles, urban construction). More investigations into sand shearing behaviour are essential in order to improve physical modelling as a tool for enhancing geotechnical design.

This summary focuses on sand-interface shearing behaviour. Different sands and materials were used to investigate the effect of changing the structural material, as there is often a need to adapt the structure to achieve similitude (e.g. bending stiffness, axial stiffness, etc.) in the physical model. Recent experiments will be reviewed to show that changing materials has negligible effect on interface friction.

Methodology

A series of interface friction tests were conducted using an adapted direct shear test apparatus at the University of Sheffield. The bottom half of the shear box was replaced by a block of material to provide a shearing plane at the centre of the box, with shearing constrained to the interface.

Three materials were used; steel, aluminium and acrylic to reflect a range of material Hardness currently used in physical modelling. Vickers Hardness results using a 5 kg indenter are shown in Figure 1.

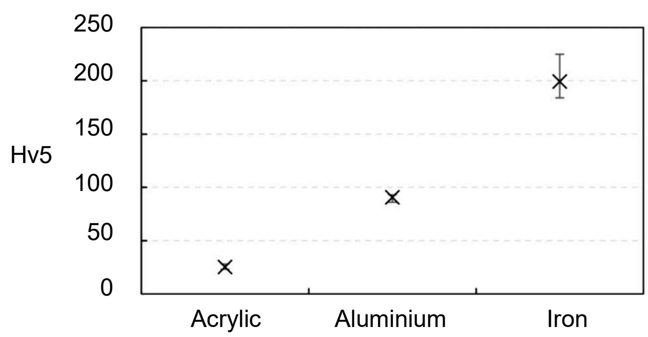

Figure 1. Vickers Hardness for interface materials

The surface profiles of the materials were determined using a TMC surface profilometer.

The roughness is plotted in Figure 2 according to the normalised roughness, R_N,

$$R_N = \frac{R_{max}}{d_{50}} \quad (1)$$

where R_{max} is taken as the difference in minimum and maximum surface profile, over a distance equal to the d_{50} particle size (Kishida & Uesugi 1987). All three surfaces were classified as "smooth" according to the limit $R_N < 0.02$ (Fiovarante 2002).

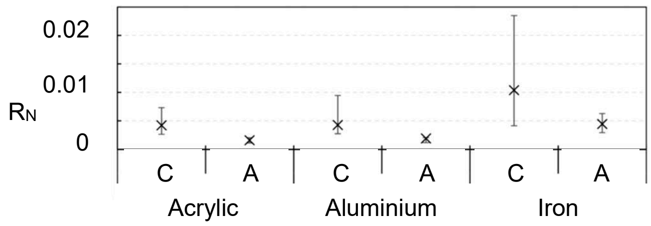

Figure 2. Normalised roughness

Two sands were used during the testing, both Leighton Buzzard sands from David Ball and Associates, Fraction A and Fraction C. The properties of the two sands are given in Table 1. The friction angles are reported from standard direct shear testing using the same apparatus.

Table 1. Sand properties

	Fraction A	Fraction C
d_{50} (mm)	1.50	0.40
ϕ' (°)	36.2	33.0

The sand was air pluviated by hand into the direct shear apparatus. All samples were prepared to a medium density before being sheared at a constant rate of 1.0 mm/min to a maximum displacement of 10 mm. Each sand-interface combination was tested at 6 normal pressures with a range between 60 kPa and 200 kPa.

Results and Discussion

The interface friction angles are reported in Table 2. The results suggest two trends. The first is that the higher interface friction angles reported for the steel interface indicate a rough or transitional friction response, rather than the expected smooth response predicted by Fiovarante (2002) and their R_N limit. There is a need to revisit this limit, in part due to its simplicity, and also its derivation, due to the limit being determined only using spherical particles.

Table 2. Interface friction angles (all given in °)

Material	Fraction A	Fraction C
Acrylic	10.7	8.7
Aluminium	9.0	8.5
Steel	11.8	10.2

The second is that where the normal pressures are carried by a sufficiently large number of contact points (such as for the Fraction C tests), then interfaces may exhibit similar results. However, if the number of contact points reduces, thus localising greater forces, then interface friction may increase. This is suggested by the greater interface friction reported for the Fraction A tests in all materials.

Conclusions and Future Work

1. The results suggest that the $R_N < 0.02$ limit for smooth interface behaviour may be insufficient to properly characterise interface responses. More testing with different sand grain angularities and surface profiles is required.

2. The number of load carrying contacts is a critical factor in determining interface friction. Changing the number of contacts or polishing the steel interface is needed to continue this series of experiments.

Delivering these improvements will enhance confidence in geotechnical physical modelling through a more rigorous interpretation of interface friction.

Acknowledgements

The author wishes to thank William Fletcher, Adam Pearson and Adrian Leyland for their help with conducting the experiment work.

References

Fiovarante V. (2002) On the shaft friction modelling of non-displacement piles in sand. *Soils and Foundations* 42(2), 23-33.

Kishida H. & Uesugi M. (1987) Tests of the interface between sand and steel in the simple shear apparatus. *Géotechnique* 37(1) 45-52.

Model Testing and Industrial Applications

Macro-modelling of anchors for offshore structures

A. Peccin da Silva*[1], A. Diambra[1] and D. Karamitros[1]

*Correspondence: a.peccindasilva@bristol.ac.uk

[1]*University of Bristol, Queen's School of Engineering, BS8 1TR, Bristol, UK*

Abstract

This paper presents a proposed modification of an existing macro-element model for predicting the force-displacement relationship of plate anchors, through the inclusion of a new plastic potential function. Comparison with centrifuge testing results from previous studies is also presented.

Introduction

Studies on novel anchoring systems for offshore structures have increased significantly in the context of renewable energy. Recently, more attention has been given to floating structures, which are becoming popular in deeper waters where the cost of conventional solutions of - jacket piles for wind farms is significantly higher. Furthermore, wave and tidal energy devices are generally floating, requiring an appropriate seabed anchoring .

Few macro-element models for predicting the anchor behaviour have been developed so far. The CASPA model (Cassidy et al. 2012) provides a set of information such as load, displacement and rotation during keying up to peak load. In this context, this paper proposes a modification of CASPA with the aim of improving the prediction of anchor trajectory through the inclusion of a plastic potential function.

Macro-element model

The Chain and SEPLA Plasticity Analysis (CASPA), which was developed for suction-embedded plate anchors (SEPLA) in clayey soils has been adopted as a baseline model. Figure 1 shows the notation for forces, angles and displacements used in CASPA.

CASPA proposes that the combination of loads (vertical, horizontal and moment) is given by a surface in the V-H-M space: the yield surface f, given by Eq. 1.

$$f = \left(\frac{V}{V_{max}}\right)^q - 1 + \left[\left(\frac{|M|}{M_{max}}\right)^m + \left(\frac{|H|}{H_{max}}\right)^n\right]^{\frac{1}{p}} = 0 \quad (1)$$

where m, n, p and q define the surface shape.

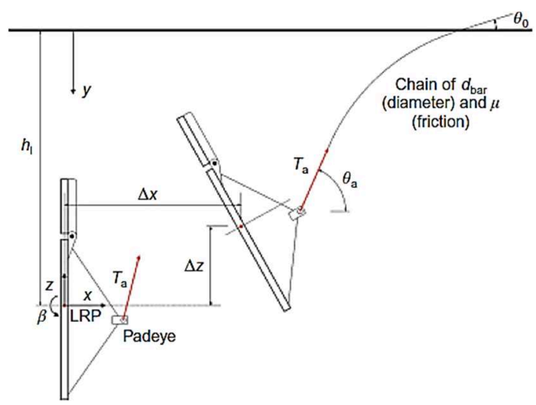

Figure 1. Sign convention adopted in CASPA (Cassidy et al., 2012)

The chain solution by Neubecker and Randolph (1995) is used to relate the angles θ_0 and θ_a, which are the chain angles at the seabed and the pad-eye respectively (Fig.1).

CASPA assumes an associated flow rule, i.e. the direction of the plastic strains is given by the vector normal to the yield surface f.

Initial assessment

To assess the performance of CASPA, comparison of the model results with centrifuge tests from previous studies was carried out. This comparison aimed to verify the effect of distinct load eccentricities (Fig. 2) on the rotational behaviour of the anchors, where "*e*" is the padeye eccentricity normal to the anchor and "*B*" is the height of the anchor. Fig. 2 shows that the rotational behaviour for distinct padeye eccentricities is well captured by CASPA.

The effect of the eccentricity e_p (parallel to the anchor) on the anchor trajectory was also analysed and compared to centrifuge testing results. The outputs from CASPA suggest that for some padeye eccentricities the anchor moves backwards (i.e. in the opposite direction of pulling) and then downwards. However, experimental results with $e_p/B=0.10$ show that CASPA overestimates the movement backwards and that the anchor does not move downwards during keying (Fig. 3).

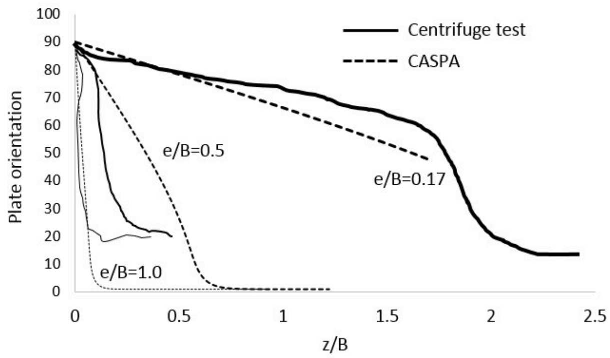

Figure 2. Effect of load eccentricity on the rotational behaviour captured by CASPA and compared to centrifuge tests by O'Loughlin et al. (2006).

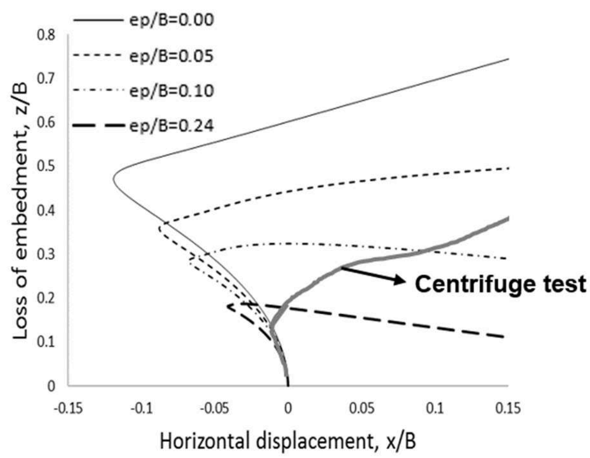

Figure 3. Effect of load eccentricity on anchor trajectory captured by CASPA and compared to centrifuge tests by O'Loughlin et al. (2006).

Proposed improvement

The anchor trajectory can be improved through the inclusion of a plastic potential g, in such a way that the plastic strains are normal to a new surface. A plastic potential similar to that proposed by Nova and Montrasio (1991) was employed (Eq. 2) with γ = 2 and $\chi = \psi$ = 1, and the first results show good agreement with experimental data (Fig. 4).

$$g = \left(\frac{\gamma\, V}{V_{max}}\right)^{q} - 1 + \left[\left(\frac{\chi\,|M|}{M_{max}}\right)^{m} + \left(\frac{\psi\,|H|}{H_{max}}\right)^{n}\right]^{\frac{1}{p}} = 0 \quad (2)$$

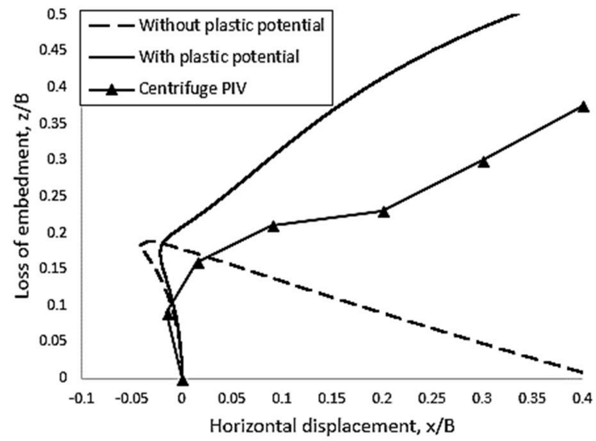

Figure 4. Effect of plastic potential on anchor trajectory and comparison to centrifuge testing.

Fig. 4 shows that the inclusion of a plastic potential improved the prediction of anchor trajectory. Despite the improvement in anchor trajectory, reducing the empiricism of the model under development is necessary, by linking the new parameters γ, χ and ψ to simple laboratory tests.

Conclusions and Future Work

The inclusion of a plastic potential function in the CASPA model improved significantly the prediction of anchor trajectory during keying. Further studies are required to relate the new parameters to simple laboratory data. Future work also includes the extension of this work for cohesionless soils and for accounting of cyclic loading effects.

References

Cassidy, M.J., Gaudin, C. and Randolph, M.F. (2012). A plasticity model to assess the keying of plate anchors. *Géotechnique*, 62(9), pp. 825-836.

Nova, R., Montrasio, L. (1991). Settlements of shallow foundations on sand. *Géotechnique*, 41(2), pp. 243-256.

Neubecker, S.R. and Randolph, M.F. (1995). Profile and frictional capacity of embedded anchor chains. *Journal of Geotechnical Engineering*, 121(11), pp. 797-803.

O'Loughlin, C.D., Lowmass, A., Gaudin, C. and Randolph, M.F. (2006). Physical modelling to assess keying characteristics of plate anchors. In: *Proceedings – 6th ICPMG*. London: Taylor & Francis, pp. 659-665.

Heapey embankment remediation and toolbox methodology

N.F. Griffin*[1]

*Correspondence: Neal.Griffin@uuplc.co.uk

[1] *Graduate Geotechnical Engineer at United Utilities, Warrington, UK*

Abstract

Due to the increasing impacts from climate change, it is predicted that water scarcity will be a significant issue in areas of the UK. It is important that efficient and reliable water resources are safeguarded for the future generations. United Utilities currently manage aging infrastructure using a methodology for performing a risk analysis of piping and internal erosion failure mechanism. At the beginning of 2018 United Utilities completed this methodology (referred to as the Toolbox Methodology internally) on Heapey Embankment after concerns were raised over wet areas on the Embankment. The methodology for the embankment identified an intolerable risks of failure through suffusion of granular embankment material or backwards erosion of the clay core.

Background

Anglezarke Impounding Reservoir is located approximately 3km east of Chorley in Lancashire, England. Heapey Embankment is one of three embankments with a clay core cut off into the in situ Glacial Till foundations. The reservoir was constructed by Thomas Hawksley between 1850 and 1857 as a water supply for Liverpool (United Utilities, 2011).

Heapey Embankment is located in a narrow post glacial overflow drainage valley at the northern end of the reservoir. The embankment is approximately 85m long and 10m high, making it the smallest of the three embankments (Reilly, 2011). A draw off pipe is located in the right of the embankment for compensation flows to White Brook but is now disused.

History of Leakage and Remediation

Heapey Embankment has a history of minor leaks on the downstream face of the embankment, particularly on the right hand of the embankment.

Initially it was believed that the draw off pipe was the source of the leak on the downstream face. The draw off pipe was successfully grouted internally in 1974, however areas of wet ground subsequently appeared on the downstream face.

A significant leak was identified in November 1997 on the right hand downstream mitre following the refilling of the reservoir after a period of dry weather. In 1998 TAM grouting was completed directly above the draw off pipe to remediate the potential leak. Two French Drains were also installed to monitor leakage flows. However following the refilling of the reservoir significant flows were recorded within the French Drains when the reservoir level reached 0.6m below top water level (Reilly, 2011). A second phase of TAM grouting was completed in 1999 in an effort to remediate the high level leakage within the embankment. The grout holes were concentrated in the core along the crest and into the right hand abutment. The reservoir was refilled and the grouting proved to be a success until a leak reappeared in 2002 (Betchel, 1999).

An Aquatrack geophysical survey was completed by Willowstick Technologies in 2005 to detect potential leakage paths (Willowstick Technologies, 2005). As shown in Figure 1, the magnetic survey in the right hand abutment suggests two leakage pathways exist within the embankment.

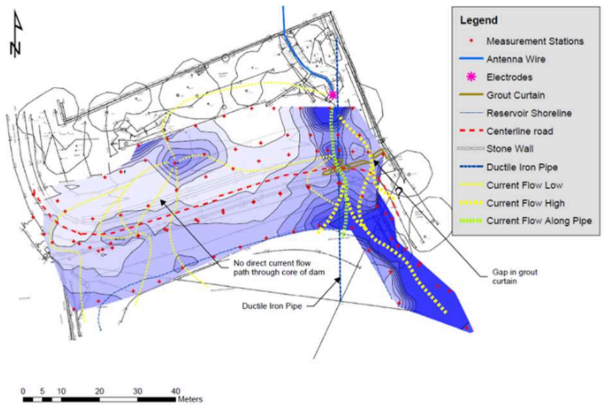

Figure 1 Aquatrack geophysical survey showing potential leakages pathways within the right abutment at Heapey Embankment (Willowstick Technologies, 2005)

In 2008 a Ground temperature survey identified a possible correlation between leakage and reservoir levels. Two temperature probes located in the right hand abutment recorded higher water temperatures than non-percolated ground temperatures. The differing temperatures indicate a possible leak at depths between 3m and 5m below ground level.

As well as the visible wet patches on the downstream side of the embankment, it is evident from the most recent ground temperature survey and geophysical survey that the grouting had limited success in remediating the leak through the embankment.

A weighted filter was installed on the right side of the embankment in 2013 to mitigate risks posed by the high level leakage

Reservoir Toolbox Methodology

Following concerns from the supervising engineer of Anglezarke reservoir over significant wet areas at the embankment toe, Heapey Embankment was subjected to the United Utilities Toolbox Methodology. The Toolbox Methodology assesses the annual probability of failure for individual failure mechanisms of the embankment.

Two mechanisms were identified as "intolerable" by the Toolbox assessment using ground investigation data and historical information detailing the construction of the embankment. The mechanisms were considered "intolerable" due to the potential failure path for suffusion caused by granular material in the right abutment and the potential initiation of backward erosion from a high permeability zone in the clay core of the embankment.

Conclusion

The Toolbox Methodology creates a method to estimate the probabilities of failure of Heapey Embankment and determine the significant risks such as leakage pathways so an appropriate solution can be identified to safeguard reservoir water supply. With increasing impacts from climate change, it is predicted that water scarcity will be a significant issue in areas of the UK. So it is important that efficient and reliable water resources are safeguarded for the future generations. This highlights the need to maintain and remediate our ageing assets and within United Utilities the Toolbox Methodology has been an effective aid to in doing so.

Acknowledgements

The author would like to thank United Utilities and Andy Hughes QCE.

References

Reilly, N (2011) Reservoir Act 1975 Report on the Results of an Inspection and Inspecting Engineer's Certificate under Section 10 (5) – Anglezarke Reservoir

United Utilities (2011) Regional IR Studies Seepage/ Seismic Desk Studies FY07-10, Anglezarke Reservoir

Willowstick Technologies (2005) Aquatrack Geophysical Investigation of Heapey Embankment, Anglezarke Reservoir Dam for United Utilities Water PL

Betchel (1999), Betchel Water Technologies Ltd Heapey Embankment Grouting Phase II Geotechnical Report, Anglezarke Reservoir

Liquefaction-induced lateral spreading at Kamiezu Lake: A case study from the 2016 Kumamoto earthquake sequence

B. Ismael*[1], D. Lombardi[1], S.M. Ahmad[1], J.A. Mendoza Ulloa[1] and S. Bhattacharya[2]

* bashar.ismael@manchester.ac.uk

[1] *School of Mechanical, Aerospace & Civil Engineering, University of Manchester, Manchester, UK*
[2] *Department of Civil and Environmental Engineering, University of Surrey, Guildford, UK.*

Abstract

As a consequence of the 2016 Kumamoto earthquake sequence which hit Japan, several signs of liquefaction-induced failure were apparent including boreholes, differential settlement, tilting of houses and lateral spreading. One purpose of this study is to present liquefaction-induced lateral spreading during the 2016 Kumamoto earthquake at Kamiezu Lake. Moreover, an assessment of liquefaction vulnerability in the visited area is conducted using Eurocode8 and Idriss and Boulanger's (2008) approach. The computed factors of safety are compared with results from a numerical analysis performed in the object-oriented software framework OpenSees. The numerical results confirmed the vulnerability of the aforementioned site to liquefaction, and this finding is in good agreement with the post-earthquake field survey, where extensive ground settlement with localised lateral displacement and cracking had occurred on the embankment of Kamiezu Lake in Kumamoto City. The latter was due to the generation of excess pore water pressure during the shaking, as confirmed by the numerical model.

Introduction

A series of forceful earthquakes struck Japan starting on 14th April 2016 with 6.5 Japan local magnitude (6.2 Mw). The mainshock magnitude was 7.3 Japan local magnitude (7.1 Mw). The foreshock was generated from Hinagu fault located in the southwestern region of Japan at approximately 11 km focal depth, while the main shock was initiated from the Futagawa fault not far from the Hinagu fault at 12 km focal depth.

The ground motion characteristics were obtained from KiK-NET and K-NET operated by the National Research Institute for Earth Science and Disaster Resilience in Japan. The maximum ground motion recorded at KMMH16 station located in Mashiki town (32.7967°N, 130.8199°E) for the mainshock is presented in Figure 1.

Extensive ground settlement with localised lateral displacement and cracking occurred on the embankment of Kamiezu Lake in Kumamoto City.

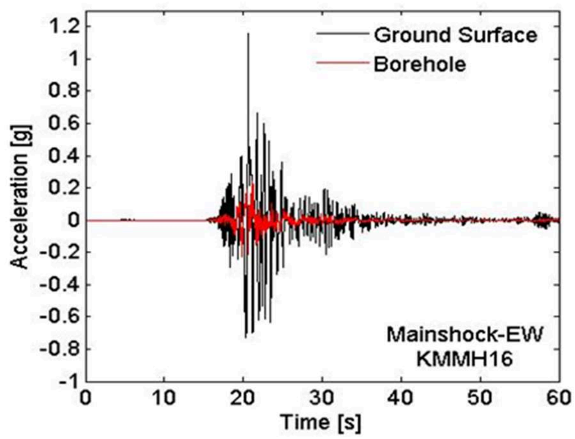

Figure 1: Acceleration time-histories for the main shock.

Usually, man-made riverbanks have shallow slopes downward towards the rivers, if there is no retaining structure put in place. When the sub-layer liquefies and the generated excess pore water pressure (EPWP) is prevented from escaping to the surface (capped by a low permeable/impermeable layer at the surface), the lateral movement occurs for the whole liquefied layer (Figure 2).

Figure 2: Liquefaction-induced lateral spreading at Kamiezu Lake

Analysis and Discussion

The factor of safety is found to be less than 1 up to 15 m depth at Kamiezu Lake, except at the surficial layer where the soil is comprised of non-liquefiable organic soil and clay, as can be seen in Figure 3. The numerical model for a representative borehole located at Kamiezu Lake shows that full liquefaction initiates in the confined zone below 3 m up to 15m, Figure 4. It is suggested that the surficial non-liquefiable layer with limited permeability prevents the dissipation of the generated EPWP, leading the ground to spread laterally, as confirmed in the site investigation near the examined area.

It is worth mentioning that, when the surficial layer liquefies, the confining pressure applied on the lower layer reduces, leading to liquefaction propagation from the top down. Otherwise, if there is a decrease in the density with depth, then liquefaction may occur at a depth below the surface where the soil is loose enough to trigger liquefaction.

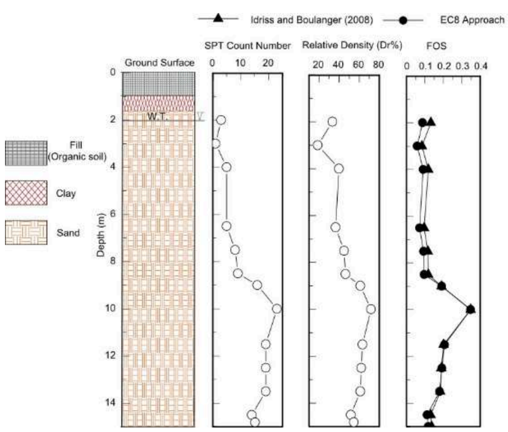

Figure 3: Borehole log, SPT count number and liquefaction assessment.

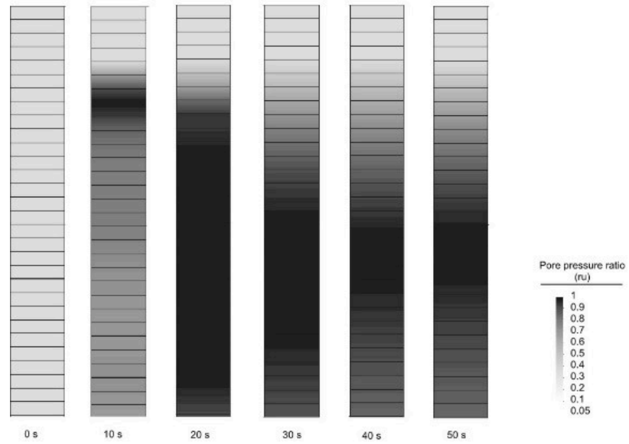

Figure 4: EPWP ratio (r_u) generated at Kamiezu Lake as calculated by OpenSees software.

Conclusions

As a consequence of the 2016 Kumamoto earthquake, extensive ground settlement with localised lateral displacement and cracking occurred on the embankment of Kamiezu Lake. Using two approaches, an assessment of liquefaction vulnerability is conducted. Moreover, to track the enhancement of the EPWP ratio during the ground shaking, a numerical analysis is conducted using OpenSees software. The results show that the different methods yield similar factors of safety, which are consistent with the numerical results and field observations.

References

Idriss, I. M., & Boulanger, R. W. (2008). Soil liquefaction during earthquakes. Earthquake Engineering Research Institute.

EC8, European Committe de Normalisation, C. B. (1998) Eurocode 8: Design of structures for earthquake resistance part 5: Foundations, retaining structures and geotechnical aspects.

Fault Damage Zones: Implications for geotechnical engineering near faulting

T.O. Morgan*[1], R.G. Ghail[1], and J.A. Lawrence[1]

*Correspondence: Tom14@ic.ac.uk

[1]*Geotechnics Section, Department of Civil & Environmental Engineering, Imperial College London, London SW7 2AZ, UK*

Abstract

Faulting not only produces a plane of weakness within the rockmass but can significantly weaken it locally by the development of a damage zone around the fault. The paper aims to highlight to the geotechnical community the potential impact of the fault damage zone by using GSI and Hoek-Brown assessments of the rockmass strength on a case study from Culver, SW England. Both assessments demonstrated that the rockmass within the damage zone is weaker than the un-faulted rock, weakening significantly towards the fault core.

Introduction

Faults are brittle shear planes in the rockmass with macroscopic displacement, be that 0.1 m or 10 km. Whilst strain is localised around the fault plane, the local rockmass is also damaged, producing a high-strain *fault core* of shear zones and disintegrated cohesive cataclasites/breccia (fig. 1, 2-Top), surrounded by a low-strain *brittle damage zone* of extensive jointing (fig. 2-Top) (Choi et al., 2016). The style of the damage zone relates to its generation at the fault tip, fault wall or by the linkage of faults (Kim et al., 2004). The paper focuses on wall damage zones only, to understand and highlight their significance to geotechnical engineering.

Investigation & Methodology

A fault was assessed to demonstrate the mechanical impact of faulting on the rockmass locally and its implications for geotechnics. The chosen fault is located on the Culver cliff line, near Minehead [GR: 9624,4774].

The fault core has a thickness of approximately 1.5 m (fig. 1). The brittle damage zone extends approximately 10m into the host rock.

Two photographs of the fault were assessed using the Geological Strength Index (GSI), one of the fault core (fig. 1) and another taken from ~20 m away. GSI is a rockmass classification technique based on the structure/block size and the surface conditions of discontinuities present (Marinos and Hoek, 2000).

Figure 1. Culver fault core, displaying the central shear zone of gouge surrounded by cataclasite and fault breccia. Yellow notebook approx. 15cm wide.

The differential stress (σ_1-σ_3) at the point of failure was assessed for a hypothetical scenario, where the overburden (σ_v=σ_1) required to induce brittle failure was identified. This was determined by applying empirical parameters determined by the GSI (Hoek and Brown, 1997) to a modified Hoek-Brown criterion (Hoek et al., 1992):

$$(\sigma_1 - \sigma_3) = \sigma_{c_i}\left(m_b \frac{\sigma_3}{\sigma_{c_i}} + s\right)^{\alpha}$$

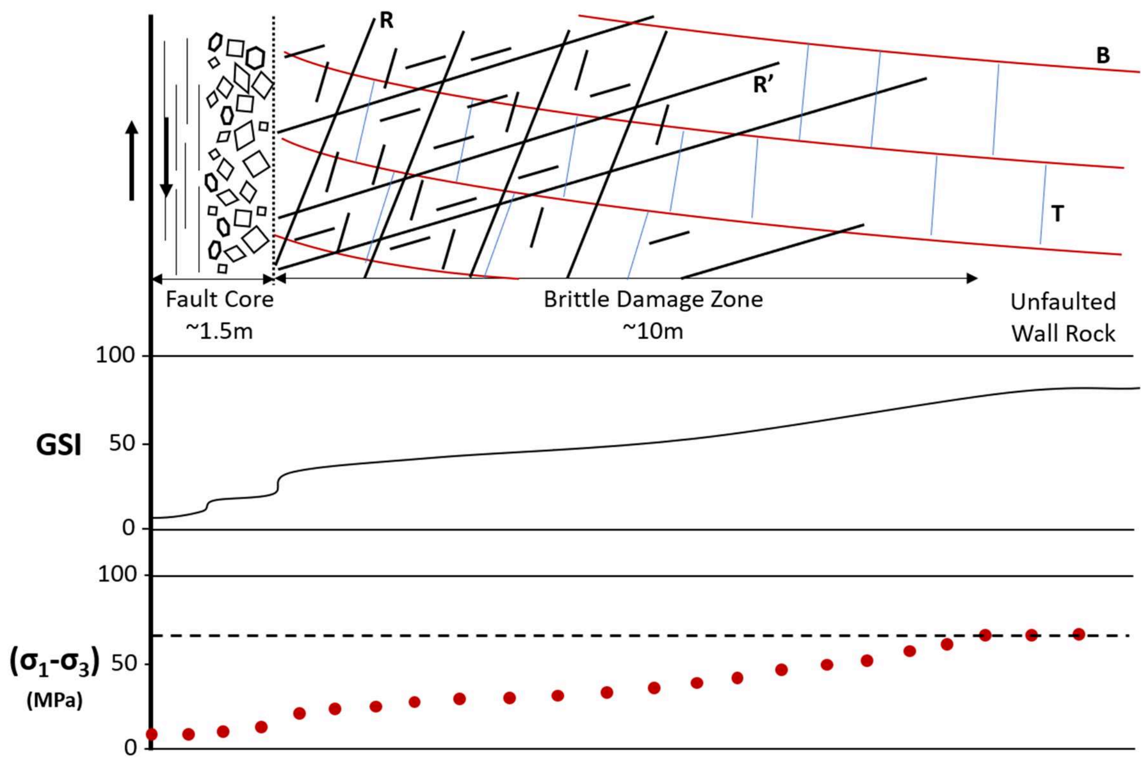

Figure 2. Top: Schematic of the fault core and brittle damage zone. R – Riedel Shear, R' – Antithetic Riedel shear, B – Bedding, T- tensile joint. Middle: Geological Strength Index assessment of fault damage zone. Bottom: Differential stress (σ1-σ3) at failure. Dashed line represents the unfaulted wall rock for comparison.

σ_3 was fixed from initial conditions for a 50m overburden of the Devonian sandstone cliff, ρ=2343 kg/m^3 (Sangha and Dhir, 1972), assuming a coefficient of lateral earth pressure, k=1.5. Intact rock parameters were inferred from Hoek (2007), with σ_{ci}= 150MPa and m_i=17 (used to determine m_b).

Results and Discussion

Both the GSI and numerical assessments indicate that the local rockmass around a fault is mechanically-weakened, with the fault core being most damaged and conditions restoring to 'unfaulted' away from the fault.

It is likely that the numerical assessment overestimates the strength of the fault core and innermost damage zone, as the gouge behaved like a soft soil against a thumb, and the fracture density was higher than can be inferred from the photographs respectively.

Conclusions

Both the GSI and Hoek-Brown assessments of rockmass strength demonstrated that the damage zone is significantly weaker than the unfaulted rock overall. The findings demonstrate that if a fault is encountered on a geotechnical project, an investigation should be undertaken to determine the presence and impact of a damage zone locally.

References

CHOI, J.-H., EDWARDS, P., KO, K. & KIM, Y.-S. 2016. Definition and classification of fault damage zones: A review and a new methodological approach. *Earth-Science Reviews,* 152**,** 70-87.

HOEK, E. 2007. Rock Mass Properties. *Practical Rock Engineering.*

HOEK, E. & BROWN, E. T. 1997. Practical estimates of rock mass strength. *International Journal of Rock Mechanics and Mining Sciences,* 34**,** 1165-1186.

HOEK, E., WOOD, D. & SHAH, S. 1992. A modified Hoek–Brown failure criterion for jointed rock masses. *Rock Characterization: ISRM Symposium, Eurock '92, Chester, UK, 14–17 September 1992.*

KIM, Y.-S., PEACOCK, D. C. P. & SANDERSON, D. J. 2004. Fault damage zones. *Journal of Structural Geology,* 26**,** 503-517.

MARINOS, P. & HOEK, E. 2000. GSI: A Geologically Friendly Tool For Rock Mass Strength Estimation. *ISRM International Symposium.* Melbourne, Australia: International Society for Rock Mechanics and Rock Engineering.

SANGHA, C. M. & DHIR, R. K. 1972. Influence of time on the strength, deformation and fracture properties of a lower devonian sandstone. *International Journal of Rock Mechanics and Mining Sciences & Geomechanics Abstracts,* 9**,** 343-352.

Investigation of loading rate effects for monopile foundations using small-scale model pile tests

K.W. Wu*[1]

*Correspondence: kuenwei.wu@hmc.ox.ac.uk

[1]*Department of Engineering Science, Oxford University, Parks Road, OX1 3PJ, UK*

Abstract

The shear strength of soil can increase when subjected to a transient load, which is recognised as the loading rate effect. For offshore wind turbine structures in Europe, monopiles are typically used. On some occasions, such as the shutdown or start of the wind turbine, transient loading can be induced and acts on both the monopile and surrounding soil. It is possible that if rate effects are considered in the design process, a more economic monopile design may be used. This paper reviews sets out a research project that will explore this problem through experiments.

Introduction

The shutdown, start or yawing of the rotor can cause transient loads to act on a wind turbine structure, which are then transferred to the foundation and surrounding soil (DNV GL, 2016). When the soil is subjected to such loads, the shear strength may increase due to the viscous behaviour of soil, which is recognised as the loading rate effect (Mitchell and Soga, 2005). If the rate effects are considered in the design process, a more economic design may be used due to a material saving.

Many results from element tests, such as triaxial compression tests and cyclic direct simple shear tests (e.g. Matešić and Vucetic, 2003; Watanabe and Kusakabe, 2013), demonstrate that as the loading rate increases, the shear strength of soil increases accordingly. Particularly the results show that the undrained shear strength of clay specimens and the drained shear strength of sand specimens increases with loading rate in monotonic loading tests and high frequency cyclic loading tests. For a saturated sand specimen the pore pressure effects, particularly when there is dilatancy and partial drainage, are much more complicated and so will need careful consideration.

The resistance of the pile foundation may grow with the increase in the loading rate. For example, Brown and Hyde (2008) found that in a series of vertical pile load tests, the pile resistance increased temporarily when the loading rate was rapid. Similarly, it can be expected that when a monopile is subjected to lateral impact loads (e.g. emergency shut down), the lateral capacity may increase due to rate effects.

To investigate the rate effects for monopile foundations a testing rig will be designed for a small-scale monopile to evaluate the interaction between the pile model and the soil. The results may be expressed in non-dimensional groups for future application to the design of a full-scale monopile.

Methodology

In this research project, a small-scale monopile model will be used for 1*g* physical modelling testing in saturated clay and dry sand. In general, an offshore wind turbine is subjected to horizontal wind and wave loads and vertical self-weight loads. The lateral loads can be cyclic loads with varied frequencies. In the Pile Soil Analysis project (known as the PISA project) led by Oxford University and partners from academia and industry, it was found that for the monopile foundation, the ratio of diameter-to-embedment length tends to be smaller than 5. For such a short pile, the base moment and base shear are significant (Byrne *et al.*, 2015). To investigate the resistant forces and moments at different parts of the pile, various combinations of external moments and loads will be applied in the model tests.

The proposed design of the testing rig is shown in Figure 2. In this design, various load combinations can be simulated. The model pile is composed of two parts: the solid round bar and the cylinder. The solid bar can give the vertical load through weight. The ratio of the inner diameter (*D*) of the tub to the outer diameter (*B*) of the pile will be sufficiently large to avoid boundary effects. The linear variable displacement transducers (LVDTs) are used to measure the lateral/vertical displacements at the pile head and the lateral displacement at the ground level. The two actuators are located at different levels to push the pile laterally, and the load cells are connected to the actuators to measure the lateral loads. In this way lateral loads can be applied at different eccentricities and so different magnitudes of moment can be applied to the model pile. The proposed testing program will include: (1) monotonic loading, (2) varied loading rates, (3) varied moments and (4) cyclic loading with various frequencies to simulate realistic conditions.

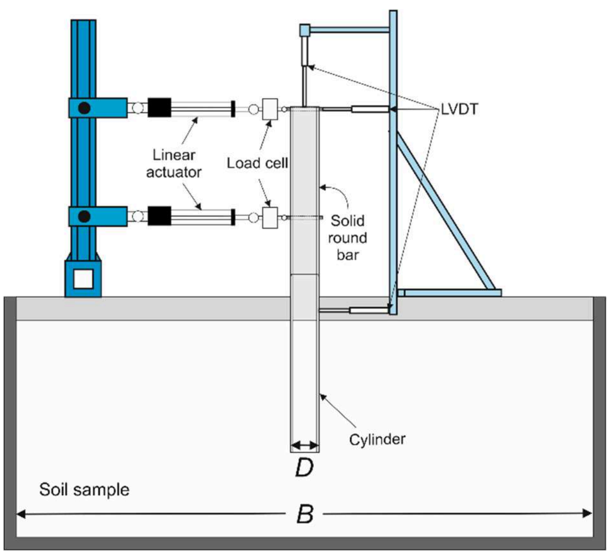

Figure 2. Schematic of the testing rig

Conclusions and Future Work

Recent experimental studies confirm that loading rate effects for pile foundations under axial loading are significant. For a monopile supporting an offshore wind turbine, lateral loads are more critical, and various load conditions should be considered to reflect the real pile behaviour.

In particular the literature indicates that the shear strength of soil increases at fast loading rates; the resistance of the pile foundation may grow as well. This research will focus on laboratory scale pile tests using a new testing rig. The future work will aim to:

1. Investigate the model pile behaviour at different loading rates and frequencies of cyclic loading
2. Investigate the relationship between the loading rate and the pile capacity
3. Develop the non-dimensional parameters for the future design.

Acknowledgements

The Author acknowledges his supervisors (Prof. B.W. Byrne, Prof. G.T. Houlsby) and Ørsted for providing the DPhil studentship at the University of Oxford through the Centre for Doctoral Training in Renewable Energy Marine Structures.

References

Brown, M. J. and Hyde, A. F. L. (2008) ‘Rate effects from pile shaft resistance measurements’, *Canadian Geotechnical Journal*, 45(3), pp. 425–431. doi: 10.1139/T07-115.

Byrne, B. W. *et al.* (2015) ‘New design methods for large diameter piles under lateral loading for offshore wind applications’, *ISFOG III*, pp. 705–710. doi: 10.1201/b18442-96.

DNV GL (2016) *DNVGL-ST-0437 Loads and site conditions for wind turbines*.

Matešić, L. and Vucetic, M. (2003) ‘Strain-Rate Effect on Soil Secant Shear Modulus at Small Cyclic Strains’, *Journal of Geotechnical and Geoenvironmental Engineering*, 129(6), pp. 536–549. doi: 10.1061/(ASCE)1090-0241(2003)129:6(536).

Mitchell, J. K. and Soga, K. (2005) *Fundamentals of Soil Behavior*. New York: John Wiley & Sons, Inc.

Watanabe, K. and Kusakabe, O. (2013) ‘Reappraisal of loading rate effects on sand behavior in view of seismic design for pile foundation’, *Soils and Foundations*. Elsevier, 53(2), pp. 215–231. doi: 10.1016/j.sandf.2013.02.003.

Suitability of monopile and jacket foundations for contemporary offshore wind turbines

A. Abdullahi*[1], Y. Wang[1]

Correspondence: a.abdullahi@surrey.ac.uk

[1]*University of Surrey, Guildford, UK*

Abstract

The increasing popularity of offshore wind turbines (OWTs) as a source of renewable energy has attracted a lot of interests from governments, researchers and industry. The construction of these facilities offshore are even more challenging in terms of designing/choosing suitable foundations to support them. Different foundation types have been specified for different conditions, including various water depth ranges and turbine ratings. This paper presents a global trend of existing OWTs supported on monopile and jacket foundations in relation to these two factors. This trend is properly defined in order to serve as a guide in selecting the appropriate foundation for a particular OWT.

Introduction

The use of wind for electrical energy production requires the construction of wind turbines, which harness this resource and converts it into electrical energy. While it seems easier to place these facilities onshore, certain circumstances make this less attractive, e.g. limited location of suitable plains onshore (Mieloszyk and Ostachowicz, 2017), the fact that wind speeds on oceans are steadier and almost double their amounts on land, (Archer, 2005). Therefore, offshore wind turbines (OWTs) become more popular.

The cost of OWT foundation is normally between 25-34% of the total cost of the wind farm (Bhattacharya, 2017). The choice of support foundation depends on such factors as site conditions (wind, wave, current, sea bed condition, ground profile, water depth etc.), installation, operation and maintenance, decommissioning laws, economics and size/capacity of turbine (Bhattacharya *et al.*, 2012). For the same ground conditions across the sea bed, water depth and turbine size play the most important part in selecting foundation type for an offshore structure (Shi *et al.*, 2014), possible reasons are: the deeper the foundation, the higher the wave loading (Bhattacharya *et al.*, 2012); also, the cost of foundation increases with increase in water depth (Oh *et al.*, 2018), therefore, the decision on choice of foundation depends on the one which can safely support the super structure under prevailing loads and at the minimum cost, hence determining the viability of the wind farm. Water depths can be categorised into three: shallow (0-30m), transitional (30-60m) and deep (60-200m) (Bhattacharya, 2017). In terms of turbine sizes (usually ranging between 0.1 - 9 MW), they also determine the choice of OWT foundation (Eea, 2009), the reason is: with an increase in the size of rotor-nacelle-assembly (RNA) in order to capture more wind, an equally bigger tower size is required to support the RNA, and the reverse is true; this in effect, will also require a foundation capable of safely transmitting the loads to the ground, and on this basis, a choice is made.

Methodology

Based on the above review, the water depths and turbine sizes have been considered vis-à-vis the types of foundations that have been adopted to support the OWTs at their locations. This study undertakes a global survey of existing wind farms housing monopile and jacket supported OWTs constructed between the years 2000 and 2018 to identify the prevailing factors to choose the foundation types for OWTs. These data are obtained from http://www.4coffshore.com/windfarms/. Since the water depths of different OWTs are in a range instead of a single value, the average water depth has been used. Using these data, a graphical plot of turbine sizes against water depths has been made, with the foundation type indicated at their intersection points.

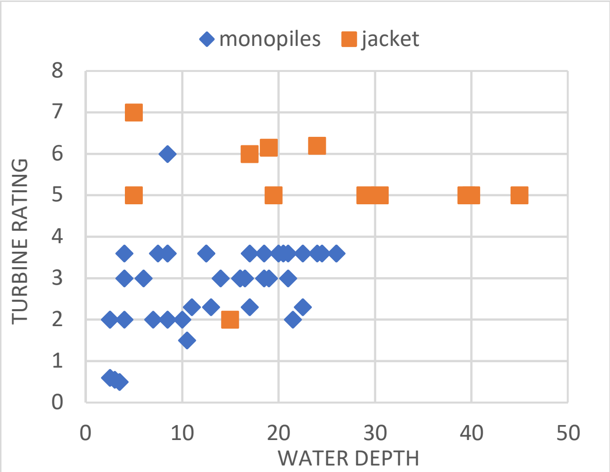

Figure 1. Graphical plot of turbine ratings (in MW) against water depths (in m) for OWTs supported on monopole and jacket foundations between years 2000 and 2018.

Results and Discussion

From Fig. 1, the majority of monopile foundations currently in use, support OWTs at a water depth between 4-26m which agrees with the range specified by (Bhattacharya *et al.*, 2012; Oh *et al.*, 2018); these have a power rating range of 2-3.6 MW. It is also seen from the plot that the jacket foundations supporting OWTs currently in use, are utilised in majority of cases at water depths of 17-45m. This lower limit falls short of (Oh *et al.*, 2018)'s limit by 3m with the upper limit falling well within the limit specified by (Bhattacharya *et al.*, 2012; Oh *et al.*, 2018).; Existing OWTs supported on jacket foundations have a power rating range of 5-7 MW. From the foregoing, it is clear that turbine rating has more influence on the choice of a foundation to support an OWT than the water depth at its location. This is obvious from the figure, as OWTs having power ratings of 5 MW and above are all supported on jacket foundations except one (which is an outlier) while turbine ratings below 5 MW are supported on monopiles except one (another outlier). On the other hand, OWTs located at average water depths exceeding 26m are all supported on jacket foundations while those below are supported on monopiles in majority of the cases. This loss of generality in the case of water depth as a factor in the selection of foundation type would place the turbine rating above it in this regard.

Conclusions and Future Work

A graph of existing OWTs supported on monopile and jacket foundations with relation to turbine ratings and average water depths has been plotted. This has led to the emergence of a trend/ranges for basing decisions regarding choices between the two foundation types. First, the choice of foundation types for the OWTs with 5 MW or higher ratings was overwhelmingly jacket, while for those with 4 MW or lower ratings, monopiles were selected. Second, all the OWTs with the monopiles are within the shallow water zone, while those with jackets cover both shallow and transitional water zones.

Acknowledgement

PTDF Nigeria is duly acknowledged

References

Archer, C. L. (2005) 'Evaluation of global wind power', *Journal of Geophysical Research*, 110(D12), p. D12110..

Bhattacharya, S. *et al.* (2012) 'Soil–Structure Interactions for Offshore Wind Turbines', *Engineering & Technology Reference*, 1(1), pp. 1–16.

Bhattacharya, S. (2017) *Civil Engineering Aspects of a Wind Farm and Wind Turbine Structures*, *Wind Energy Engineering*. Elsevier Inc.

Damgaard, M. *et al.* (2013) 'Cross-wind modal properties of offshore wind turbines identified by full scale testing', *Journal of Wind Engineering and Industrial Aerodynamics*. Elsevier, 116, pp. 94–108.

Eea (2009) *Europe's onshore and offshore wind energy potential*, *EEA Technical report*. doi: 10.2800/11373.

Mieloszyk, M. and Ostachowicz, W. (2017) 'An application of Structural Health Monitoring system based on FBG sensors to offshore wind turbine support structure model', *Marine Structures*, 51, pp. 65–86.

Oh, K. Y. *et al.* (2018) 'A review of foundations of offshore wind energy convertors: Current status and future perspectives', *Renewable and Sustainable Energy Reviews*. Elsevier Ltd, 88(May), pp. 16–36.

Shi, W. *et al.* (2014) 'Feasibility study of offshore wind turbine substructures for southwest offshore wind farm project in Korea', *Renewable Energy*. Elsevier Ltd, 74(2015), pp. 406–413.

Wymore, M. L. *et al.* (2015) 'A survey of health monitoring systems for wind turbines', *Renewable and Sustainable Energy Reviews*. Elsevier Ltd, 52(1069283)

Dynamic design effects of foundation configuration of jacket supported offshore wind turbines

S. Jalbi[1,2]

*Correspondence: m.jalbi@surrey.ac.uk

[1] *University of Surrey, Guildford, United Kingdom*
[2] *Robert Bird Group, London, United Kingdom*

Abstract

To support large wind turbines in deeper waters (30m-60m) jacket structures mounted on multiple caissons are currently being considered. Offshore wind turbines (OWT's) are effectively a slender column supporting a heavy rotating mass and are subjected to cyclic & dynamic loads. Dynamic performance plays an important role in the overall design of the system and is dictated by two limit states: Fatigue Limit State (FLS), and overall deformation in Serviceability Limit State (SLS). If the forcing frequency of the rotor (so called 1P) or the blade shadowing frequency (2P/3P) are in close proximity to the natural frequency of the system, resonance may occur affecting the fatigue design life. This presentation aims to suggest that designers should engineer the configuration of the jacket and choose a symmetrical arrangement of the foundation such that two natural frequency peaks are prevented. Practical examples considering different arrangement of symmetric and asymmetric jacket foundations are considered to show that a symmetrical configuration results in a better performance over the service life of the structure.

Introduction

Jackets or seabed frames supported on multiple shallow foundations are currently being installed to support offshore wind turbines in deep waters ranging between 23m and 60m, see for example Borkum Riffgrund 1 (Germany, water depth 23 to 29m), Alpha Ventus Offshore (Germany, water depth 28 to 30m), Aberdeen Offshore wind farm (Scotland, water depth 20 to 30m). For offshore wind turbines, rocking modes of vibration have been observed in small scale tests for jacket/seabed frame supported on shallow foundations, see (Bhattacharya, et al., 2011), (Bhattacharya, et al., 2013). Moreover, the scaled tests also showed that symmetric foundations resulted in a single peak when performing a snap-back test, whilst asymmetric foundations have two closely spaced peaks, where the ratio of the frequency peaks ranges between 1.2 and 1.5. This might have severe implications on the dynamic performance and the fatigue life of the structure as will be discussed in the conclusion section of this paper.

Methodology

In order compute the natural frequency, a simplified structural model is adopted. Effectively, the jacket and wind turbine towers are an Euler-Bernoulli beam and the foundations are replaced with a set of linear springs See Figure 1.

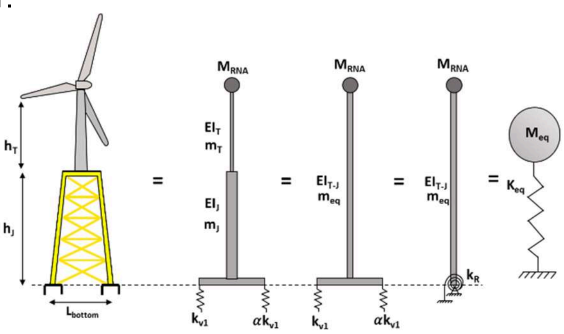

Figure 3: Mechanical iddealization of the system

Finally a single degree of freedom system is obtained. This method can be used for 3 or 4 legged jackets of both symmetric and asymmetric arrangements. In the next section, this method will be used to compute the stiffness of both these types of foundations. A detailed form of the derivations is shown in (Jalbi & Bhattacharya, 2018)

Results and Discussion

The stiffness terms derived for the arrangements shown in Figure 2 are summarized in Table 1. Ac is representative of the area of the jacket chords and k denotes the stiffness of the foundation springs

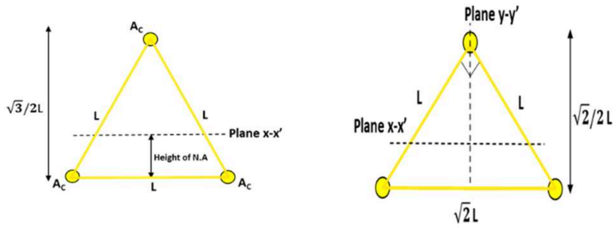

Figure 4: Symmetric and Asymmetric foundation arrangements

Table 1:Summary of results

Plane of vibration	Jacket Stiffness	Foundation Stiffness
Plane x-x'(Asymmetric)	$\frac{A_C L^2}{3}$	$\frac{k_v L^2}{3}$
Plane y-y' (Asymmetric)	$A_C L^2$	$k_v L^2$
Planes-x'/y-y' (Symmetric)	$\frac{A_C L^2}{2}$	$\frac{k_v L^2}{2}$

As shown in Table 1, for an asymmetric arrangement both the jacket and foundation stiffness values are different for the planes x-x' and y-y', which results in two closely spaced natural frequencies of the soil-structure system. This is why the snap-back test results on the scaled tests showed 2 peaks rather than one even after a large number of loading cycles. Moreover, the scaled tests showed that the peak frequency ratios ranged between 1.2 and 1.5. For the presented analytical method this can also be estimated as the frequency of a system in its simplest form is a function of:

$$f_0 = \frac{1}{2\pi}\sqrt{\frac{K}{M}}$$

Assuming that the accelerating mass is the same for x-x' and y-y', the ratio of the roots of the stiffness values should be indicative of the analytical frequency ratios. It may be noted that this result is in close proximity to the 1.2-1.5 shown in the scaled tests.

$$r = \sqrt{\frac{A_C L^2}{\frac{A_C L^2}{3}}} = \sqrt{\frac{kL^2}{\frac{kL^2}{3}}} = 1.73$$

Conclusion

Offshore wind turbines are dynamically sensitive structures that are subjected to a wide band of forcing frequencies, namely the rotor frequency (1P), blade shadowing frequency (3P), wind, and wave. Typically, to achieve an economic design in terms of structural stability and the use of the optimum amount of materials, the natural frequency is typically targeted to be between the 1P and 3P frequency or what is generally known as “Soft-Stiff” region. It is evident that the target natural frequencies of the system must be fitted in a very tight range to avoid resonance which might induce fatigue and lower the overall economic service life of the structure or potentially increase maintenance and operation costs. For asymmetric arrangements, it would prove more difficult to fit two natural frequencies rather than one in the tight frequency band, which makes jackets supported on asymmetric foundations more prone to early fatigue damage due to resonance

References

Bhattacharya, S., Cox, J. A., Lombardi, D. & Muir Wood, D., 2011. Dynamics of offshore wind turbines supported on two foundations. *Geotechnical Engineering,* pp. 159-169.

Bhattacharya, S. et al., 2013. Observed dynamic soil-structure interaction in scale testing of offshore wind turbine foundations. *Soil Dynamics and Earthquake Engineering,* pp. 47-60.

Jalbi, S. & Bhattacharya, S., 2018. Closed form solution for first natural frequency of offshore wind turbine jackets supported on multiple foundations incorporating soil-structure interaction. *Soil Dynamics and Earthquake Engineering* .

Centrifuge modelling of screw piles for offshore wind energy

C. Davidson*[1]

*Correspondence: csdavidson@dundee.ac.uk

[1]*School of Science and Engineering, University of Dundee, UK*

Abstract

Screw piles have been proposed as a possible new foundation solution for jacket supported offshore wind turbines. Screw piles are able to both develop greater axial load capacities and offer quieter installation than driven tubular piles. However, the geometric upscaling of current small-scale onshore screw pile designs to meet the loads of the offshore environment is beyond existing experience and design methods. The project is investigating installation requirements and behaviour of screw piles under axial loads using centrifuge modelling to develop screw piles for offshore wind energy systems.

Introduction

Screw piles, consisting of one or more large diameter (typically 150 - 400mm) helical plates welded to a low diameter (typically 64 – 200mm) tubular shaft are installed by applying simultaneous vertical and rotational force. Onshore, screw piles are often used as foundations for gantries and guy wires. For use offshore, such screw piles would need to be upscaled substantially, leading to greater installation requirements and uncertainty over their performance.

The findings of a centrifuge testing programme which investigated the behaviour of three screw pile designs during installation and load testing are reported.

Methodology

Using published methods (Perko, 2009, Das and Shukla, 2013), several screw piles were designed to investigate the geometries required to meet the expected in-service loads. The design loads of 32.31MN in compression and 24.23MN in tension were defined by an 8MW wind turbine on a four-legged steel jacket in 80m of water, with single screw piles at each corner in very-dense sand experiencing environmental loads with a 1% exceedance level. Initially, single and double-helix screw pile designs (fig. 1a & b) were devised to compare the axial capacities and installation requirements. The design process highlighted that tensile capacity was critical and required relatively deep embedment of the uppermost helix. In the double helix case, this resulted in the lowermost helix being placed at a depth beyond that required to generate the necessary compressive capacity. Thus, the geometry of the screw pile was optimised by reducing the core and lower helix diameters (fig. 1c) to better suit the design loads, while maintaining torsional and lateral resistance. As the core contributes most to the total installation loads (Al-Baghdadi, 2018), reducing the core diameter results in decreased installation requirements.

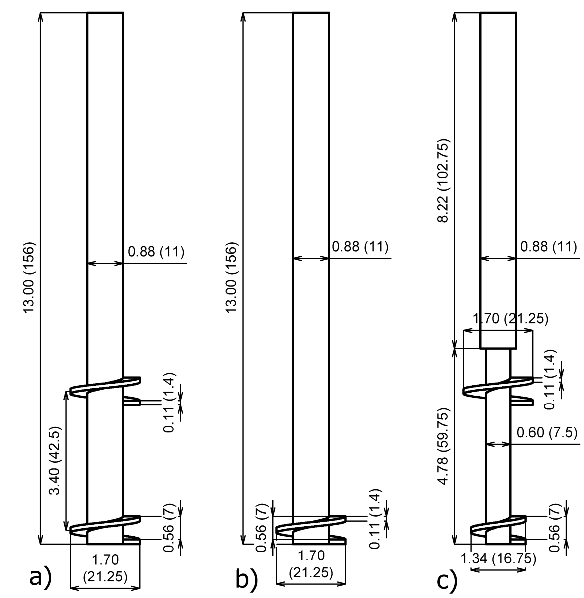

Figure 5. Prototype scale (in metres) screw pile designs used in centrifuge testing (model scale dimensions in millimetres in parenthesis).

1/80th scale model screw piles were created from each of the three designs for testing in the centrifuge at 48g to give the equivalent saturated stress field in the 84% relative density dry sand bed used (Li et al., 2010). Monotonic compression and tensile tests were conducted along with a Cone Penetration Test (CPT) to gather cone resistance (q_c) data.

Results and Discussion

The centrifuge test results demonstrate that the installation requirements are significant in very-dense sand and may require the development of new installation technology. The optimised design reduced the torque and installation force by 17 and 34% respectively. However, the torque prediction method employed, based on q_c data, un-conservatively under-predicted the measured torque values. A revised torque prediction method developed by Davidson et al. (2018) enhanced predictions greatly. The axial compressive and tensile capacities (at a displacement of 10% of the helix diameter) measured in the centrifuge tests underperformed with respect to the design loads (fig. 2), indicating that the design methods used for onshore screw pile designs may not be suitable for the large-scale screw piles needed for offshore wind energy foundations. Early analysis of the design methods suggest that the uplift breakout factors calculated using a shallow wedge mechanism with an angle equal to the dilation angle of the soil, measured from vertical, give a closer match to the measured data than the breakout factors defined by a 45° wedge in Perko (2009), Das and Shukla (2013).

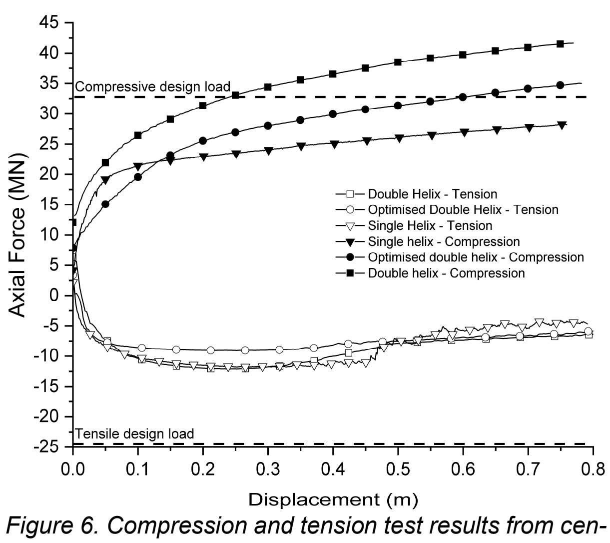

Figure 6. Compression and tension test results from centrifuge tests of model piles.

Evaluation of the single and double-helix designs shows that they have similar tensile capacity (fig. 2) and that the single helix design is more efficient in terms of tensile loading and installation requirements. The optimised design under-performs in both axial loading directions (fig. 2) and is not considered beneficial over the single-helix design.

Conclusions and Future Work

Screw piles have been proposed as alternative foundations for offshore wind energy systems due to their enhanced capacity and quiet installation. Centrifuge tests of screw piles designed for a jacket supported wind turbine in deep water indicate that substantial installation torque and vertical force are required. Furthermore, measured axial capacities were lower than predicted suggesting that design methods for relatively small onshore screw piles may not be suitable for upscaled designs. Initial studies have shown improved predictions are possible by revising the failure mechanisms. Research is ongoing, with tests being conducted in lower relative densities and equipment being modified to allow cyclic loading and testing of pile groups.

Acknowledgements

This work is part of an EPSRC (EP/N006054/1) and industry funded project in partnership with Durham University and the University of Southampton.

References

Al-Baghdadi, T. 2018. *Screw piles as offshore foundations : Numerical and physical modelling.* PhD, University of Dundee.

Das, B. M. & Shukla, S. K. 2013. *Earth anchors*, J. Ross Publishing.

Davidson, C., Al-Baghdadi, T. A., Brown, M., Brennan, A., Knappett, J., Augarde, C., Coombs, W., Wang, L., Richards, D., Blake, A. & Ball, J. 2018. A modified CPT based installation torque prediction for large screw piles in sand. *CPT'18.* Delft, Netherlands: manuscript accepted.

Li, Z., Haigh, S. K. & Bolton, M. D. 2010. Centrifuge modelling of mono-pile under cyclic lateral loads. *Physical Modelling in Geotechnics*, 965-970.

Perko, H. A. 2009. *Helical piles: a practical guide to design and installation,* Hoboken, New Jersey, John Wiley & Sons.

Grouting in Chelburn Valley – Improvements to aging assets

J.A. Richardson[1*]

*Correspondence: Jennifer.richardson@uuplc.co.uk

[1] *Graduate Geotechnical Engineer at United Utilities, Warrington, UK*

Abstract

Upper Chelburn Impounding Reservoir is situated within Chelburn Valley, located approximately 2km north of Littleborough in Rochdale, England. Upper Chelburn is formed by two embankments with the northern embankment having a history of leakage issues which has resulted in a number of remediation works. In 2013 United Utilities undertook an internal erosion assessment for the dam which identified an intolerable risk of failure by contact erosion between the embankment and the cohesionless soil foundation. In response, permeation grouting remedial works was completed in 2017, targeting this cohesionless soil foundation zone. With the future risk of Climate Change leading to more extreme weather events there is a need more than ever to protect and remediate these assets; especially those which are aging and have a history of issues.

Background

Upper Chelburn Impounding Reservoir is situated within Chelburn Valley, located approximately 2km north of Littleborough in Rochdale, England. The reservoir is formed by two embankments with the north embankment being the main embankment containing the draw-off and overflow facilities.

Both embankments are homogenous without a clay core of cut-off into the foundation. The north embankment is the main embankment which is approximately 160m long and 16.5m high. It was constructed between 1799 and 1801 to provide compensation flow to the Rochdale Canal Network, and this remains its function. It is founded on old landslide deposits within a glacial overflow channel, resulting in Glacial Till containing many sandstone boulders and this was later scoured by fast flowing water leaving boulders and some clay (Rowe, 1981).

History of Grouting

It is reported that the northern embankment has always suffered from leakage issues, in particular the right hand abutment and beneath the spillway channel (Reilly, 2007) considered to be associated with the boulder zone (Rowe, 1981).

Following new draw off syphon works in 1994 there was leakage reported around the outside of the overflow structure after first filling. This resulted in nine grout holes to a depth of approximately 5.0m below ground level at the southern end of the new overflow. Approximately 500 litres of grout was recorded for each grout hole and also loss of flush during drilling which indicates the voided nature of the embankment.

In 2001 a ground temperature measurement investigation was conducted for leak detection which confirmed leakage around the right hand abutment or beneath the spillway (MWH, 2003). As a result of this, further grouting work was completed in this area in 2002 across a 35.0m section along the crest and right abutment. Loss of flush whilst drilling and high grout takes of up to 21,800 litres for a single 18-19m depth grout hole supported that the embankment is highly voided.

A Willowstick survey was conducted in 2007 to identify seepage pathways through Chelburn northern embankment. This identified notable seepage pathways through coarse granular glacial material beneath the embankment (Willowstick Technologies, 2007).

As a result of these issues, United Utilities carried out a routine assessment of the risk of piping and internal erosion failure for the dam using a revised approach to the Risk Analysis for

Dam Safety guidance document (United States Bureau of Reclamation, 2008). This identified an intolerable risk (greater than 1:10,000) of failure by contact erosion between the embankment and the cohesionless soil foundation.

With the future risk of Climate Change leading to more extreme weather events there is a need more than ever to protect and remediate these assets; especially those which are aging and have a history of issues.

Remedial Works 2017

During Asset Management Period (AMP) 6 United Utilities has committed to OFWAT to address reservoir safety risks with a probability of failure risk greater than intolerable. In response, permeation grouting remedial works was undertaken between May and August 2017 on the north embankment, targeting the zone between the embankment and cohesionless soil foundation.

Ascending stage permeation grouting was conducted in two offset rows along the dam crest, connecting to the 2002 remedial works. These two rows were 1.0m apart, with a 1.5m spacing of the grout holes within rows. To ensure this, grout holes were drilled into this zone and continued at least 0.5m into the underlying competent glacial clay material.

The zone between the embankment and cohesionless soil foundation was on average 2.9m thick but this varied between approximately 1.0 and 7.0m across the dam. Due to the need to extend the grouted zone into competent material, grout holes extended to a maximum depths of around 31.5m below ground level which was the right hand extent (overflow side) of the area to be grouted. A total of 286,947 litres of grout was used with grout takes of up to approximately 6440 litres for a 17.2m borehole.

Falling head permeability tests were conducted in-situ prior to the grouting works in order to provide a baseline dataset for this target zone. This is to allow direct comparison of the permeability in these locations following the grouting works. These permeability tests will be submitted as part of the Validation Report and this will confirm the success of the project; however, permeability results for post-grouting are said to be two orders of magnitude less than the pre-grout boreholes.

Acknowledgements

The author wishes to thank Mott MacDonald Bentley as the Principal Contractor for the works

References

MWH (2003) United Utilities Upper Chelburn IR Geotechnical Works 02/03 – Geotechnical Report on Grouting Works

Reilly, N (2007) Reservoir Act 1975 Report on the Results of an Inspection and Inspecting Engineer’s Certificate under Section 10 (5) – Upper Chelburn Reservoir

Rowe, P (1981) North West Water Authority – Pennine Division, Upper Chelburn Dam. Site Investigation, Report to G.H. Hill and Sons

United States Bureau of Reclamation (2008) A Unified Method for Estimating Probabilities of Failure of Embankment Dams by Internal Erosion and Piping - Draft Guidance Document

Willowstick Technologies (2007) Aquatrack Geophysical Investigation of Upper Chelburn Reservoir Dam for United Utilities Water PLC

Strain and strain rate effects on rocking response of footings subjected to machine vibrations

E. Katsiveli*[1]

* Correspondence: e.katsiveli@bristol.ac.uk

[1] *Department of Civil Engineering, University of Bristol, Bristol, UK*

Abstract

This study investigates shear strain rate effect on the stiffness of rigid surface foundations subjected to rocking oscillations for different strain amplitudes and excitation frequencies. A numerical methodology is developed based on the implementation of the modified hyperbolic (MH) model into the explicit finite difference code FLAC while taking into consideration shear modulus degradation and hysteretic damping increase effects for the foundation subsoil.

Introduction

The design of machine foundations requires evaluation of the dynamic impedance function (stiffness and damping) of the footing-subsoil system to an externally applied load. Solutions are available in the literature for the elastic case (e.g., Gazetas 1991; Mylonakis et al. 2006a; NIST 2012). However, as the vibration amplitude increases, soil shear modulus decreases in a nonlinear fashion and can be modelled for fine grained soils of different plasticity (Vardanega & Bolton 2013, 2014). In this case, shear modulus degradation becomes sensitive to strain rate effects. The simulations of this study allow the extent of non-linearity and its variation with frequency, geometry, material characteristics and loading amplitude to be quantified (Katsiveli et al, 2018).

Problem Description

The configuration examined is illustrated in Figure 1 as a weightless strip footing of half-width *B*, resting on a clay stratum of thickness *H*, density ρ, shear wave velocity V_s, shear modulus $G = \rho V_s^2$, damping ratio ξ, and Poisson's ratio v.

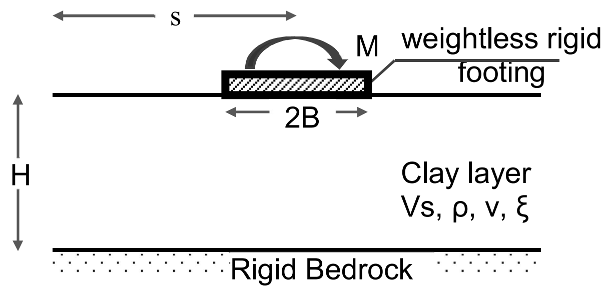

Figure 1. Problem description: footing resting on clay

The footing is subjected to rocking oscillations of amplitude θ, induced by a concentrated harmonic moment *M.* Both the footing and the bedrock underlying the soil layer are assumed to be perfectly rigid, while the soil is modelled as a nonlinear material according to MH model.

Numerical Analysis Methodology

The secant shear modulus reduction curve is according to MH model described as:

$$G_s/G_{max} = [1 + (\gamma/\gamma_r)^{\alpha}]^{-1} \quad (1)$$

Where α is the curvature coefficient while γ_r is a pseudo-reference shear strain which is equal to the level of shear strain for which G_s/G_{max}= 0.5.

Vardanega and Bolton (2013) produced expressions for the γ_r linked to plasticity index (Ip). For the static adjustment (STA) the strain rates 10^{-6}/s, and the parameters α and γ_r were given in equation (2):

$$\alpha=0.736\ , \quad \gamma_r=2.2(I_p/1000) \quad (2)$$

while for the dynamic adjustment (PSSR) were expressed as in equation (3):

$$\alpha=0.943, \quad \gamma_r=3.7(I_p/1000) \quad (3)$$

which correspond to a strain rate of 10^{-2}/s.

Numerical analyses have been conducted for static and dynamic loads. In the case of static loads STA and PSSR conditions are examined while for dynamic loads additionally shear strain rate (SSR) effects are investigated by interpolating MH model parameters between the values given in Equations. (2) and (3).

Results and Discussion

In Fig. 2, static values of normalised non-linear rocking stiffness $K_{rx}/K_{rx,elastic}$ are plotted versus the rocking angle θ normalised by γ_r. Stiffness degradation might be stronger for the case of pseudo-shear strain rate parameters, beyond $\theta = 10^{-4}$ and $\theta/\gamma_r = 10^{-1}$. The effect of model parameters is also evident. The increase in stiffness due to PSSR effects does not exceed 10%. Results for SSR effects on nonlinear dynamic footing stiffness $\overline{K}_{rx}$ are provided in Fig. 4. Since the model is formulated in terms of absolute strain rate (measured in units of 1/Time), use of dimen-sionless frequency α_0 is not possible. For small rocking amplitudes, the curves exhibit patterns analogous to those observed for STA and PSSR conditions in Fig. 3. For the $\theta_{max} = 10^{-3}$, however, a different pattern is observed, with the nonlinear rocking stiffness increasing with frequency.

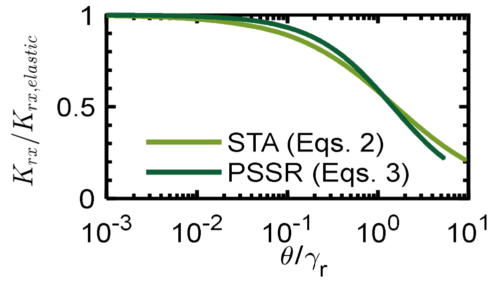

Figure 2. Normalised nonlinear static rocking stiffness over linear counterpart versus normalised rocking angle.

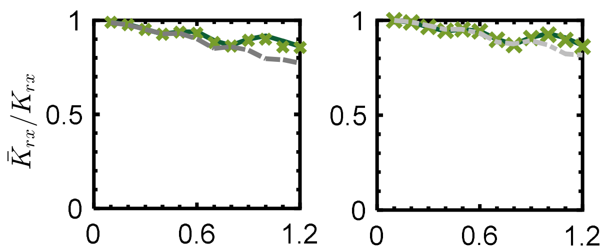

Dimensionless frequency, α_0

Figure 3. Normalised nonlinear dynamic rocking stiffness over linear counterpart versus dimensionless frequency.

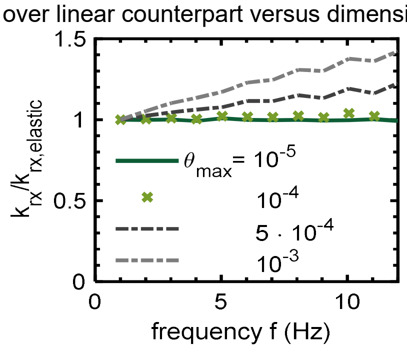

Figure 4. Normalised nonlinear over linear stiffness modifier versus absolute frequency.

Conclusions and Future work

For rocking amplitudes $\theta_{max} = 10^{-5}$ and 10^{-4}, $\overline{K}_{rx}$ is fluctuating past $\alpha_0 = 0.4$. For $\theta_{max} = 10^{-3}$ the values are dropping. This suggests that nonlinearity mainly affects K_{rx}. Regarding SSR effects, an increase in $\overline{K}_{rx}$ is observed with increasing frequency for the largest rocking amplitude, $\theta_{max} = 10^{-3}$. The causes of this behaviour are related to stress-induced inhomogeneity in the soil mass, as shear strain rate varies for point to point in proportion to strain. SSR effects are becoming evident from very low frequencies for rocking amplitudes larger than $\theta_{max} = 10^{-4}$ and they are increasingly more significant with increasing frequency. For rocking amplitudes equal or under $\theta_{max} = 10^{-4}$, nonlinearity and SSR effects have negligible impact on dynamic stiffness.

Future work is focused on the vertical and swaying mode of oscillations where shear strain rate is expected to influence the stiffness in a similar trend.

Acknowledgements

The author would like to thank Prof. George Mylonakis, Dr. Dimitris Karamitros and Dr. Paul Vardanega for their support and guidance, and acknowledges the financial support which has been provided through the EPRSC DTP studentship.

References

Gazetas, G. (1991) 'Foundation Vibrations', in Fang, H.-Y. (ed.) *Foundation Engineering Handbook*. 2nd edn. Boston, MA: Springer US, pp. 890–902.

Katsiveli, E, Karamitros, D, Vardanega, P & Mylonakis, G 2018, Strain and strain rate effects on the rocking response of footing subjected to machine vibrations. in *Proceedings of the 16th European Conference on Earthquake Engineering.* Springer, 16ECEE, Greece

Mylonakis, G., Nikolaou, S. and Gazetas, G. (2006) 'Footings under seismic loading: Analysis and design issues with emphasis on bridge foundations', *SDEE*

NIST (2012) *Soil-structure interaction for building structures*. NIST GCR 12-917-21.

Vardanega, P. J. and Bolton, M. D. (2013) 'Stiffness of Clays and Silts: Normalizing Shear Modulus and Shear Strain', *Journal of Geotechnical and Geoenvironmental Engineering*, 139(9), pp. 1575–1589.

Vardanega, P. J. and Bolton, M. D. (2014) 'Stiffness of Clays and Silts: Modeling Considerations', *Journal of Geotechnical and Geoenvironmental Engineering*

A method to evaluate the accuracy of velocity models used in the positioning of microseismic events

J. Whittaker*[1], R. Sandford[1], H R. Thomas[1] and P. Brabham[1]

* Correspondence: whittakerj4@cardiff.ac.uk

[1] *Cardiff University, UK*

Abstract

This paper details a method to quantitatively determine the accuracy of a velocity model used to position passive microseismic events detected during hydraulic fracturing operations. The method uses the arrival times from perforated shots combined with forward modelling of the arrival times by a 3D ray tracer. By using the double-difference times an objective function is calculated resulting in a single root-mean-squared (RMS) error for a source. This method was then applied to an industrial case study to inform a decision between choosing between two different starting velocity models as part of a larger investigation. This approach indicated a preference for one velocity model, and this model will now be used in the next part of the investigation. The advantage of this method is that there is now an efficient means to evaluate the accuracy of a velocity model which will assist in the optimisation of velocity models and accurate positioning of microseismic events.

Introduction

Microseismic monitoring has been utilised in the production of shale gas wells for over 20 years. In order to determine the extent of hydraulic fracture operations and make informed decisions for the next stage of the production program, the positions and origin times of each microseismic event have to be determined. Without a velocity model event position and origin time cannot be determined. Velocity models are generated from the sonic logs, vertical seismic profiles (VSPs), seismic reflection surveys or geological models. To position the events accurately a method was developed to quantitatively assess the competency of these velocity models.

Methodology

The method presented in this paper uses the arrival times at each station from the perforation shots in combination with forward modelling of the travel times. Perforated shots are small charges fired through the casing to enable hydrocarbons to flow through the casing and up the well bore. The first stage of the method is to identify the arrival times from these perforated shots at each station. While the shot times are sometimes recorded the accuracy of this measurement is a key concern, so the double-differencing method of hypocentre relocation (Waldhauser, 2000) was utilised which uses the arrival times referenced to another station to circumvent the origin times. The arrival times at each station are subtracted from a reference time from the station with the shortest source-receiver distance. These are the single difference values.

The travel times between source and stations are then forward modelled using a 3D ray tracer (Sambridge and Kennett 1990). The single difference values are then calculated for these forward modelled arrival times using the previous reference time. The double -differencing values are then the difference between these two sets of values. The objective function by Jiang et al (2016) is finally used to calculate a single RMS error value for each perforated shot, with a value of zero indicating the velocity model correctly predicted the arrival time for that particular shot.

Industrial Case Study

A dataset of microseismic readings recorded during a 26 stage hydraulic fracture operation on a horizontal well bore was provided by an industrial contact. The microseismic events were recorded onto a 96 station surface array where each station contained upwards of 7 geophones. The dataset has been processed twice and two different velocity models produced both based on the sonic log (Fig 1).

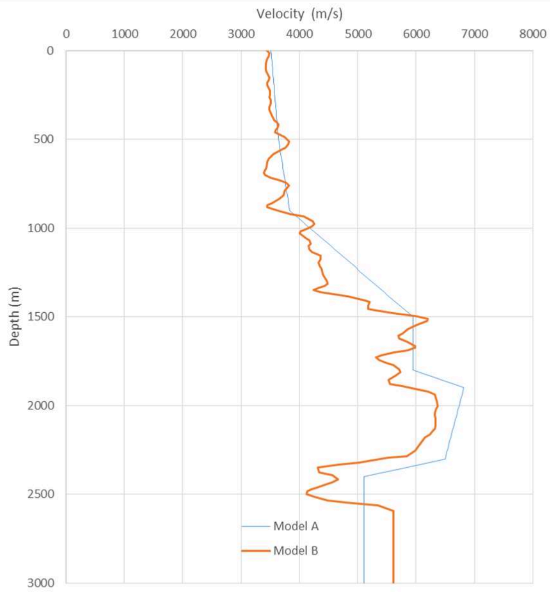

Figure 1 : Velocity models provided in the dataset. Both velocity model are based on the sonic well log. Where model B has a shorter length smoother applied than model A. Model A has a 6.5% bulk shift applied.

As part of a larger investigation of this dataset this method was applied in order to determine which of the two velocity models would be used as the starting point for an optimisation stage.

Given that the source-receiver distances were greater than 7 km ray refractions and the signal to noise ratio were a problem. To improve the signal to noise ratio all geophone traces at each station were stacked together to form a single trace, after trace by trace corrections were applied. To solve the issue of ray path refractions, the 3D ray tracer has been designed to handle ray refractions. Of the 79 perforated shots fired, 66 had clear perforated shot arrivals that could be identified. Of this total in 42 of these shots the RMS error was lower for Model A than for Model B. This is reflected in the distribution plot showing a preference for Model A as shown in fig 2.

The geographical distributions also showed an overall preference for Model A, although the shots closest to the well bore heel indicated a preference for Model B. This is due to the 6.5% bulk velocity shift applied to Model A to garner a more reliable fit at all perforated shots at the cost of a consistent fit next to the well bore heel. Given this evidence Model A will be used as the starting point in the next stage of investigation for this dataset.

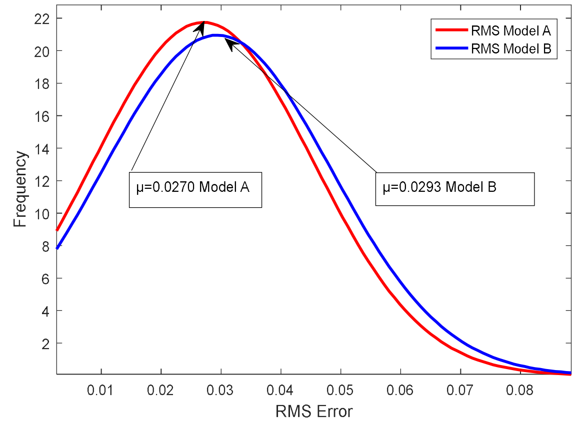

Figure 2 : A distribution plot showing the differences in RMS error for two different velocity models compared to observed arrival times from the perforated shots.

Conclusions and Future Work

This method when applied to an industrial case study allowed a decision to be made, backed up with quantitative evidence, to use one velocity model over another. Without such a method this would not be have been possible.

The next step of investigation for this project involves optimisation of the velocity model. This method will be crucial in this regard as the RMS error provides a measure of the competency of the velocity model and with the correct optimisation principals an improved velocity model can now be easily attained.

Acknowledgements

The work described in this paper has been carried out as part of the FLEXIS project, funded by the Welsh European Funding Office. This funding is gratefully acknowledged.

References

Jiang, H.Y., Chen, Z.B., Zeng, X.X., Lv, H. and Liu, X., 2016. Velocity calibration for microseismic event location using surface data. Petroleum Science, 13(2), pp.225-236.

Sambridge, M.S. and Kennett, B.L.N., 1990. Boundary value ray tracing in a heterogeneous medium: a simple and versatile algorithm. Geophysical Journal International, 101(1), pp.157-168.

Waldhauser, F. and Ellsworth, W.L., 2000. A double-difference earthquake location algorithm: Method and application to the northern Hayward fault, California. Bulletin of the Seismological Society of America, 90(6), pp.1353-1368.

Predicting pile settlement in London Clay

J.J. Crispin*[1]

* Correspondence: j.crispin@bristol.ac.uk

[1] *University of Bristol, Bristol, UK*

Abstract

This paper presents some preliminary work comparing the accuracy of two models at predicting pile settlement in London Clay. Both methods are suitable for hand or spreadsheet calculation and are compared against previously published test results from a site in Wembley.

Introduction

Pile settlement prediction methods that are suitable for hand or spreadsheet calculation are useful to engineers as they allow rapid estimates of foundation performance at the early stages of design. In this paper two such methods are discussed, and their predictions compared with previously published load tests.

Winkler Model

Winkler/load transfer models (e.g. Mylonakis and Gazetas, 1998) are commonly used for settlement prediction and, with careful selection of the Winkler modulus, provide similar results to more rigorous continuum analyses. Closed-form solutions (e.g. Crispin et al. 2018) are available for piles embedded in inhomogeneous, linearly elastic soils. These have been extended to a linear elastic-perfectly plastic soil model by assuming a yielded zone propagates down the pile. The applied load and resulting settlement can be calculated for a set of yielded lengths to generate a full load settlement curve.

Nonlinear Soil Model

Vardanega et al. (2012) proposed a simple analytical method that allows soil nonlinearity to be considered without resorting to numerical analysis. It employs the power-law constitutive model that was developed by Vardanega and Bolton (2011a) using a database of soil tests in clays. Vardanega et al. (2018) modified the method to better account for the base settlement, particularly for under-reamed piles.

Analysis

Predictions using both models have been compared for the load test results reported by Whitaker and Cooke (1966). 11 concrete bored piles (5 straight-shafted and 6 under-reamed) embedded in London Clay were successfully tested at a site in Wembley (1 additional test recorded no settlement).

An undrained shear strength profile was interpreted by the authors based on triaxial test data from 38mm samples. Patel (1992) showed that these samples overestimated the fissured strength of the London clay by a factor of about 1.3. Therefore, an undrained strength profile reduced by this factor and the α-method (Skempton, 1959) have been employed to predict the skin friction at yield and the pile ultimate capacity, P_u.

Vardanega and Bolton (2011b) obtained deformation parameters for London Clay by analysing 15 high-quality triaxial tests. These have been related to a Winkler modulus using the concentric cylinder model (Randolph and Wroth, 1978). A bilinear model was employed for the pile base spring by estimating the mobilised shear strength when the shaft resistance was exhausted and calculating a secant shear modulus to failure.

To illustrate the predictions of the two methods, Figure 1 shows example load-settlement curves for two of the piles: Pile K, a straight-shafted pile ($D_b = D_s$) and Pile P, an under-reamed pile ($D_b \approx 2 \cdot D_s$). Both methods show good agreement with the experimental results for Pile K. However, for Pile P, Vardanega et al. (2012, 2018) over predicts settlements and is only valid up to a Factor of Safety of around 2.6. This is due to lack of a base resistance model in the method and the conservative assumption that no resistance is mobilised until the shaft resistance is exhausted.

The predicted and measured settlements using both methods for all 11 piles are shown in Figure 2 for pile head settlement, *w*, less than 1% of the base diameter, D_b.

Conclusions and Future Work

Two methods for predicting pile settlement have been compared using the classical measurements from Whitaker and Cooke (1966). Vardanega et al. (2012, 2018), while simpler to employ, gives more conservative predictions than Crispin et al. (2018) and is unable to model the base resistance, although most piles are designed with a working load within the applicable range.

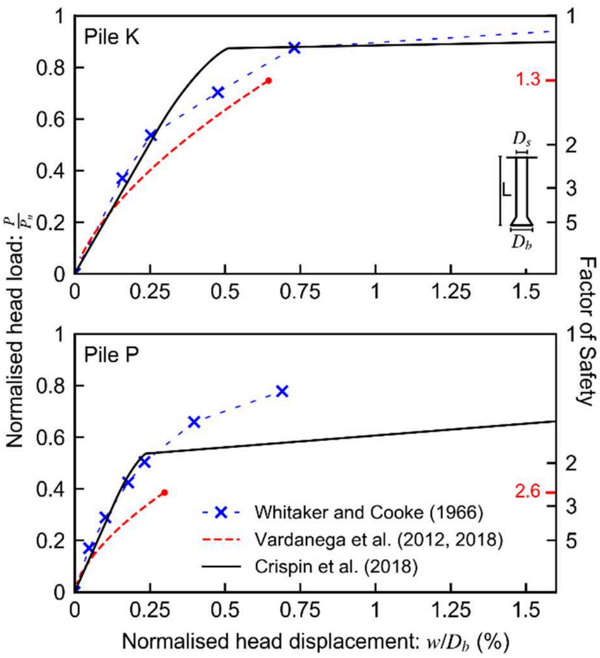

Figure 1. Comparison of the predicted load-settlement curves against the experimental results ($w<1.6\%\cdot D_b$).

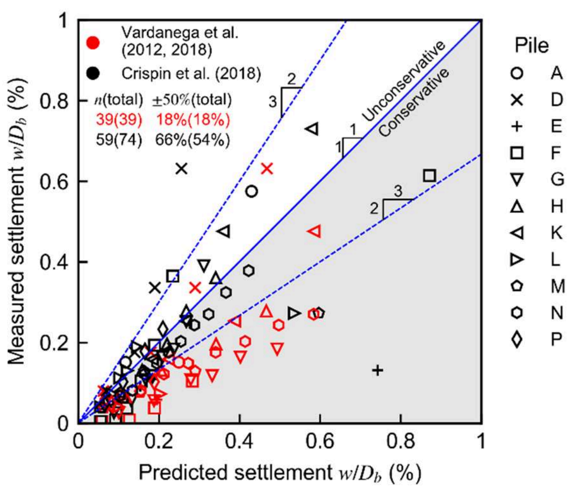

Figure 2. Predicted vs. measured pile head settlements ($w<1\%\cdot D_b$).

Crispin et al. (2018) showed good agreement with the test results, however, the method gives very conservative predictions ($w>>1\%\cdot D_b$) after the shaft resistance is exhausted.

Further work is presented in Voyagaki et al. (2018) where the methods discussed here are compared using the much larger dataset of pile test results in London Clay reported in Patel (1992).

Acknowledgements

The author would like to thank Prof. George Mylonakis, Dr. Paul Vardanega and Dr. Elia Voyagaki for their support and guidance in the preparation of this manuscript.

References

Crispin, J.J., Leahy, C.P. and Mylonakis, G. (2018). Winkler Model for Axially-Loaded Piles in Inhomogeneous Soil, *under review*.

Mylonakis, G. and Gazetas, G. (1998). Settlement and additional internal forces of grouped piles in layered soils. *Géotechnique*,48(1): 55-72.

Patel, D. (1992). Interpretation of pile tests in London Clay. In: *Piling: European practice and worldwide trends*. London: Thomas Telford. 100-110.

Randolph, M.F. and Wroth, C.P. (1978). Analysis of deformation of vertically loaded piles. *Journal Geotechnical Engineering, ASCE*, 104(12): 1465-1488.

Skempton, A.W. (1959). Cast in-situ bored piles in London Clay. *Géotechnique*, 9(4): 153-173.

Vardanega, P.J. and Bolton, M.D. (2011a). Strength mobilization in clays and silts. *Canadian Geotechnical Journal*, 48(10): 1485-1503.

Vardanega P.J. and Bolton M.D. (2011b). Predicting Shear Strength Mobilisation of London Clay. In: Proceedings 15th ECSMGE: Geotechnics of Hard Soils – Weak Rocks, (A. Anagnostopoulos et al. (eds)). Athens, Greece. Vol. 1: 487-492.

Vardanega, P.J., Williamson, M.G. and Bolton, M.D. (2012). Bored pile design in stiff clay II: mechanisms and uncertainty. *Proceedings of the Institution of Civil Engineers - Geotechnical Engineering*, 165(4), 233-246.

Vardanega, P.J., Crispin, J.J., Gilder, C.E.L., Voyagaki, E., Shepheard, C.J. and Holcombe, E.A. (2018). Geodatabases to improve geotechnical design and modelling. *ce/papers*, 2(2-3): 401-406.

Voyagaki E., Crispin J.J., Gilder C.E.L., Nowak P., O'Riordan N., Patel D. and Vardanega P.J. (2018). Analytical approaches to predict pile settlement in London Clay, *under review*.

Whitaker, T. and Cooke, R.W. (1966). An investigation of the shaft and base resistance of large bored piles in London Clay. In: Large Bored Piles. Institution of Civil Engineers, London, UK: 7-

Numerical Modelling

Contact models to simulate clay particle interaction

S. Bandera*[1], C. O'Sullivan[1], S. Angioletti-Uberti[2] and P. Tangney[2]

*Correspondence: s.bandera17@imperial.ac.uk

[1]*Department of Civil and Environmental Engineering, Imperial College London,* London, UK
[2] *Department of Materials, Imperial College London,* London, UK

Abstract

The behaviour of clay is influenced by its structure, defined as the combination of the effects of fabric and inter-particle forces. The importance of structure has been highlighted in several experimental studies. Particle-scale simulations of clay have the potential to explain structure effects in a fundamental way. Due to the difficulty in characterising the elementary units and the inter-particle interactions, which are highly affected by the pore fluid chemistry, use of particle-scale simulations has been limited. In order to model the behaviour of clayey materials, a deep understanding of the forces that control the particle interactions is required. For this reason, this contribution compares two published models to describe the interaction between clay particles.

Introduction

Inter-particle forces between clay particles can be divided into two main categories (e.g. Pedrotti and Tarantino, 2017): contact and non-contact forces. The first refer to interactions transferred from one particle to another through contact, whereas non-contact forces, also called electro-chemical forces, consist of electrostatic forces associated with the electrical double layer (E_{Edl}) and the van der Waals attraction (E_{vdw}). The electro-chemical forces are usually described by the well-known DLVO (Derjaguin-Landau-Vervey-Overbeek) model (Gupta et al., 2011). These forces have been considered to dominate the interaction between clay particles by several authors in the literature. For this reason, only electro-chemical forces are examined in this paper.

In a recent contribution, Ebrahimi et al. (2014) simulated the interaction between clay particles with the Gay-Berne (GB) potential. The GB potential defines the interaction of two rigid, aspherical and ellipsoidal particles (Everaers and Ejtehadi, 2003) including the contribution of both the attractive and repulsive energies. It is an extension of the Lennard-Jones potential that is often used in molecular dynamics simulations of colloids. The GB potential is implemented in the highly optimised open source molecular dynamics software LAMMPS (Plimpton, 1995). This paper explores whether the GB potential can capture the shape of the interaction energy-surface separation relationship predicted by the DLVO theory.

Methodology

Various interpretations of the DLVO theory exist in the literature. The expression of the total interaction energy, $E_T\ [J/m^2]$, between two particles used by Gupta et al. (2011) is given by:

$$E_T = E_{vdw} + E_{Edl} \quad (1)$$

where the van der Waals attraction (E_{vdw}) is defined as:

$$E_{vdw} = \frac{A_H}{12\pi}[h^{-2} + (h + \delta_1 + \delta_2)^{-2} - (h + \delta_1)^{-2} - (h + \delta_2)^{-2}] \quad (2)$$

$A_H\ [J]$ is the Hamaker constant for the interaction between the interacting faces, $h\ [nm]$ is distance between the interacting faces, and $\delta_1\ [nm]$ and $\delta_2\ [nm]$ are the thicknesses of the interaction surfaces.

E_{Edl} is the double layer repulsive energy (Eq. 3):

$$E_{Edl} = \frac{2\psi^2 \varepsilon_r \epsilon_0 \kappa}{\exp(\kappa h) + 1} \quad (3)$$

where $\psi\ [mV]$ is the surface potential (pH- dependent), ε_r is the relative permittivity, $\epsilon_0\ [F/m]$ is the permittivity of free space and $\kappa\ [nm^{-1}]$ is the thickness of the double layer (dependent on the concentration of ions in the solution).

The analytical form of the GB potential (Everaers and Ejtehadi, 2003) is given by the following equation:

$$U_{GB} = 4\epsilon\left[\left(\frac{\sigma}{h_{12} + \sigma}\right)^{12} - \left(\frac{\sigma}{h_{12} + \sigma}\right)^{6}\right] \times \eta \times \chi \quad (4)$$

where $\epsilon\ [kcal/mol]$ is the energy scale, $\sigma\ [nm]$ is the atomic interaction radius, $h_{12}\ [nm]$ approximates the inter-particle distance and is related to the particle size and orientation, η and χ, dimensionless quantities, refer to the shape and to the energy anisotropy, respectively.

The DLVO model proposed by Gupta et al. (2011) and the GB potential were implemented in Matlab. The implementations were checked against the results published by Gupta et al. (2011) and Ebrahimi et al. (2014), respectively. All the parameters used to reproduce the work of Gupta et al. (2011) are summarised in Table 1. The GB parameters were determined by tuning as discussed below.

Table 1. Parameters used to compute the energy with the DLVO model at pH=8, 1 mM KCl solution (Gupta et al., 2011 & Gupta, 2011)

A_H $[J]$	3.90×10^{-20}	$\varepsilon[-]$	78
$\delta_1 = \delta_2$ $[nm]$	11.2	ϵ_0 $[F/m]$	8.854×10^{-12}
ψ $[mV]$	-55.32	κ^{-1} $[nm]$	9.6

Two kaolinite particles of diameter $D = 600\ nm$ and thickness $\delta_1 = \delta_2 = 11.2\ nm$ (Figure 1) were considered to compare the models. The face to face interaction considers two alumina surfaces.

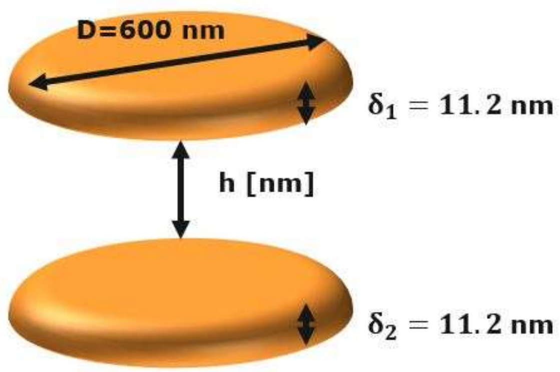

Figure 1. Schematic representation of the particles (h=surface-to-surface distance)

Results and Discussion

The direct comparison of the energies of the models considered was obtained tuning the parameters σ and ϵ describing the GB potential. Considering a 1 mM KCl electrolyte solution with pH=8, the values, $\sigma = 470$ nm and $\epsilon = 2.38$ kcal/mol, provided the best match of the two curves. The results obtained (Figure 2) show that the GB potential captures the shape (repulsion at short range and attraction at long-range) of the energy computed with the DLVO model, indicating that it is well suited to model this type of clay. These results suggest that it is possible to optimise the GB potential parameters to capture the effects of different types of pore fluid chemistry (pH and ion concentrations) according to the DLVO model predictions.

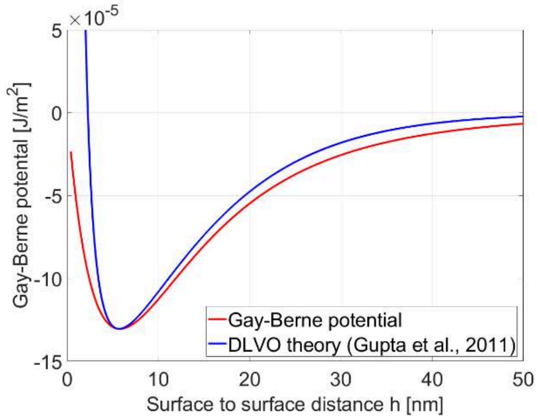

Figure 2. Comparison between DLVO and GB

Conclusions and Future Work

The study presented here is a preliminary comparison between one DLVO model (Gupta et al., 2011) and the GB potential. The objective is to extend this comparison to other DLVO models presented in literature, in order to confirm its applicability in modelling clays. An optimization algorithm that allows a more rigorous comparison between these two models is needed. Following these preliminary studies, LAMMPS will be used to simulate element tests.

Acknowledgements

This research is funded by The Leverhulme Trust.

References

Ebrahimi, D., Whittle, A.J. & Pellenq, R.J.-M., 2014. Mesoscale properties of clay aggregates from potential of mean force representation of interactions between nanoplatelets. *The Journal of Chemical Physics*, 140, p.154309

Everaers, R. & Ejtehadi, M.R., 2003. Interaction potentials for soft and hard ellipsoids. *Physical Review*, 67, p. 041710

Gupta, V., 2011. *Surface charge features of kaolinite particles and their interactions*. PhD thesis. The University of Utah.

Gupta, V., Hampton, M.A., Stokes, J.R., Nguyen, A.V. and Miller J.D., 2011. Particle interactions in kaolinite suspensions and corresponding aggregate structures. *Journal of Colloid and Interface Science*, 359, pp. 95-103

Pedrotti, M. & Tarantino, A., 2017. An experimental investigation into the micromechanics of non-active clays. *Géotechnique*

Plimpton, S., 1995. Fast Parallel Algorithms for short-range Molecular Dynamics. *Journal of Computational Physics*, 117, pp. 1-19

Modelling of stone columns using the Discrete Element Method: an initial calibration study

P. Shukla*[1], R. Fuentes[2], and Y.P. Cheng[1]

*Correspondence: palak.shukla@ucl.ac.uk

[1] *Department of Civil, Environmental & Geomatic Engineering, UCL, London, UK*
[2] *School of Civil Engineering, University of Leeds, Leeds, UK*

Abstract

Stone columns are widely used as an efficient and sustainable ground improvement technique. Numerous experimental and continuum based studies have been carried out since the early 1970s, increasing the understanding about the behaviour of stone columns and their capabilities. However, these numerical studies consider a stone column as a continuum rather than the arrangement of particles that it is. The use of the Discrete Element Method (DEM) allows for the particle level behaviour of a stone column material to be investigated. In this study an initial calibration of the clay soil surrounding a stone column has been modelled in one-dimensional compression.

Introduction

Experimental and numerical based studies have been carried out by numerous researchers to investigate the behaviour and design parameters of stone columns. However, the numerical studies consider a stone column as a continuum. Modelling a stone column using Discrete Element Method (DEM) provides the opportunity to investigate the particle level behaviour of the stone column material. Research into stone columns using DEM is still relatively unexplored.

The work presented in this paper illustrates that it is possible to model the compression behaviour of the clay soil that surrounds a stone column using DEM, developing on the earlier study by Shukla and Fuentes (2017). The experimental study conducted by Black (2007) has been used to calibrate the DEM model simulations.

Methodology

The DEM model simulations were performed using PFC2D (Itasca, 2014). The one dimensional compression on kaolin conducted by Black (2007) was used to calibrate the DEM model.The earlier study used ball particles to model the clay, the DEM model gave a good response for the unreinforced clay behaviour, but the sample void ratios were very small, and the response elastic. Thereby, it was clear that an improved methodology had to be applied, to give a value of C_c within an acceptable range and to have a soil model that exhibits plasticity.

There are a few studies available on modelling clay using DEM, most of these consist of complex DEM systems which model the forces that influence clay behaviour. The methodology presented by Bock *et al* (2006) (Figure 2) uses PFC to produce a 2D model. The clay platelet is surrounded by four layers of balls which have bonding applied, the green balls are the free water which can be modified to simulate drained loading.

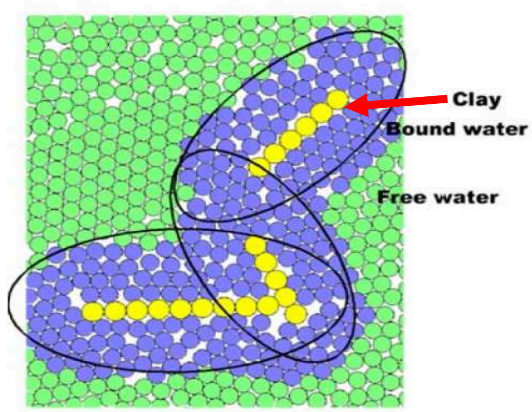

Figure 2. Opalinus clay DEM model (Bock *et al 2006)*

Using the properties given in Table 1, a one-dimensional loading test was carried out. A clay platelet was modelled using a five-particle clump and the water using ball particles; two layers of balls were defined as bound water and the rest of the balls as free water. The size of the clump and ball particles was chosen to be in the mm size range to reduce the number of particles within the simulation.

In this initial model, the two layers of 'bound' water had no bonding applied within the DEM model. As the sample was loaded, whenever the sum of the total contact force of the free water exceeded a 1% tolerance from the initial value, the free balls were shrunk by 0.01% of their current radius. This method was applied to simulate drained loading, giving a void ratio reduction and a reasonable C_c value.

Table 1. Model input parameters

Parameter	Value
Initial sample dimensions (mm)	154x104
Stiffness ratio: pebble/ball-ball contacts, k_{ratio}	1.5
Elastic modulus-clump and bound water (GPa)	0.6
Number of clumps	65
Pebble particle size (mm), D_p	1.12
Particle friction coefficient (clump), μ_c	0.5
Density (clump and balls) (kg/m^3),	500
Elastic modulus-free water (GPa)	6
Number of ball particles (bound)	1103
Number of ball particles (free)	1274
Ball particle size (mm), D	1.0-1.5
μ_f (free water balls)	0.0
μ_{bw} (bound water balls)	0.5

Results and Discussion

Figure 3 shows the generated sample with the clumps in black and the bound water layers in darker blue and the free water as light blue. As the sample underwent 1D loading and unloading, the C_c and C_s obtained were 1.46 and 0.20 respectively (Figure 4).

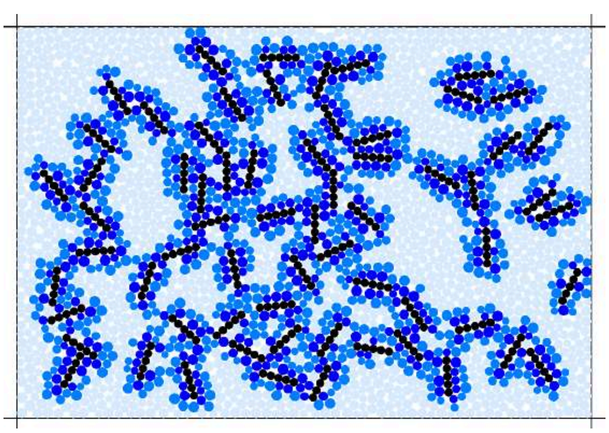

Figure 3. 1D compression DEM model

The value obtained for C_c from the test was too high, indicating that the void ratio had undergone too much of a reduction. However, the value of C_s was found to be within an acceptable range.

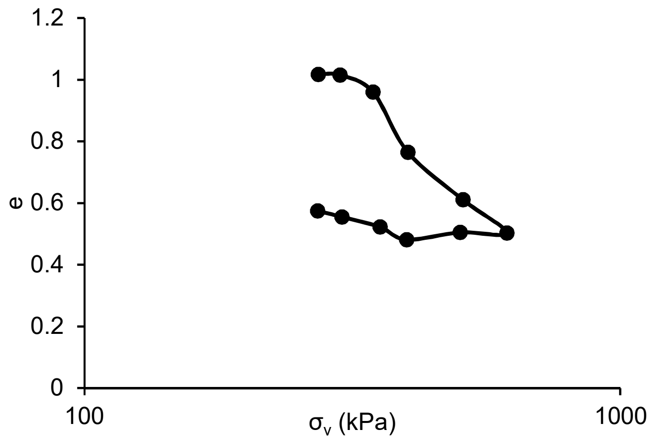

Figure 4. One dimensional loading and unloading.

Conclusions and Future Work

The DEM model that was developed found some agreement with the experimental study, but further work needs to be carried out. The next stage of the study will involve applying various bond strengths between the inner layer of balls and the clump, and a lower bond strength between the outer and inner layer balls to obtain better agreement with the C_c value.

Acknowledgements

The authors wish to thank Prof M Coop and Mr S Emam at Itasca for their help and contributions towards this study.

References

Black J.A. (2007). The settlement performance of a footing supported on soft clay reinforced with vibrated stone columns. *Queen's University of Belfast, Northern Ireland*.

Bock H, Blümling, P. & Konietzky, H. (2006). Study of the micro-mechanical behaviour of the Opalinus Clay: an example of co-operation across the ground engineering disciplines. *Bulletin of Engineering Geology and the Environment*, *65*(2), 195-207.

Itasca, (2014), PFC (Particle Flow Code) Version 5.0. Itasca Consulting Group Inc. Minneapolis, United States.

Suction-enhanced geotechnical design through Capillary Barrier Systems

R. Scarfone*[1,2], M. Lloret-Cabot[1], and S.J. Wheeler[1]

*Correspondence: Riccardo.Scarfone@glasgow.ac.uk

[1]*University of Glasgow, Glasgow, UK,* [2] *LimitState Ltd, Sheffield, UK*

Abstract

Capillary barrier systems (CBSs) can be potentially applied to maintain suction in the underlying soil, with consequent gains in the strength of the soil. The effect of hydraulic constitutive modelling of the materials of CBSs was shown to be significant in the prediction of the failure of the CBS (water breakthrough). Moreover, multi-layered CBSs were shown to have better performances than single CBSs in certain conditions. Applications of CBSs will be analysed (e.g. slope stability and retaining walls).

Introduction

Suction s (negative pore-water pressure) occurs under unsaturated and saturated conditions and can impart significant strength gains to soil. This effect is generally neglected in geotechnical design because pore-water pressure may become zero or even positive after a heavy rainfall event. Nevertheless, if one could find a way to keep high suction values in the ground even during rain and predict the minimum value of suction expected over the design life, geotechnical design could take into account the effect of suction.

Capillary barrier systems (CBSs) are geotechnical structures made of two layers of soil, a finer-grained layer (F.L.) overlying a coarser-grained layer (C.L.), placed over the ground with the aim of avoiding or reducing percolation of rain-water into the underlying soil [Stormont and Anderson, 1999]. Under unsaturated conditions, the C.L. will typically be at much lower degree of saturation S_l than the F.L., because of differences in the water retention behaviour. As a consequence, the hydraulic conductivity K of the C.L. will typically be much lower than the F.L., even though the C.L. has the higher value of conductivity under saturated conditions. Hence, prior to significant water breakthrough to the C.L., it is this C.L. that acts as the low permeability barrier, whereas the infiltrating rainwater is stored in the F.L. This water can be removed from the F.L. through evapotranspiration and/or lateral drainage if the CBS is sloped. However, as infiltrating rainwater is stored in the finer layer, the suction at the interface between the layers decreases. If this suction at the interface decreases down to the "bulk water-continuity value" of the C.L. (BWC), at which the hydraulic conductivity of the C.L. increases significantly, the C.L. becomes conductive and breakthrough of water from the F.L. into the C.L. occurs, making the CBS fail.

The C.L. is typically at low degree of saturation. Conventional hydraulic constitutive models (e.g. Van Genuchten-Mualem (VG-M) [Van Genuchten, 1980]) provide a poor description of the hydraulic behaviour of unsaturated soils at low degree of saturation. A new hydraulic conductivity model is proposed, where the M model is modified introducing a cutoff at the bulk water-continuity value (modM), where the bulk water filling the pores becomes continuous. For suction higher than this value, bulk water is discontinuous and water can flow only within thin liquid films surrounding the grains, whose contribution is represented by a straight line in a log-log plot of K against s (LF) (see Figure 1b). A comparison between these models in terms of the hydraulic behaviour of a CBS at breakthrough has been carried out.

The effect of the use of multi-layered CBSs, made of the alternation of different coarser and finer layers, on the water storage capacity (WSC), defined as the maximum amount of water which can be stored in the CBS before breakthrough occurs, has been studied numerically.

Methodology

Numerical simulations of one-dimensional hydraulic infiltration tests on CBSs were carried out by means of CODE_BRIGHT, a FEM code. In the first set of analyses, a single CBS was analysed with the hydraulic conductivity of the C.L. modelled with the models M and modM+LF (see Figure 1). In the second set of analyses, multi-layered CBSs were analysed varying both the total thickness of the CBS excluding the lowest C.L. (t_{tot}) and the layering factor, which is the number of pairs of finer and coarser layers present in the CBS.

Results and Discussion

Figure 1 shows the results obtained using different constitutive models for the hydraulic conductivity of the coarser layer. Using the conventional M model, the water velocity across the interface increases gradually over time whereas, using the modM+LF model this velocity increases almost instantaneously at breakthrough, in agreement with what has been observed experimentally [Stormont and Anderson, 1999]. Similarly, the suction profile at breakthrough observed in experiments [Stormont and Morris, 1998] is better predicted in the F.L. using the modM+LF model.

Figure 2 shows the ratio between the WSC of a multi-layered CBS and the WSC of the corresponding single CBS (WSC_{SCB}) varying the layering factor, for given materials and infiltration rate. In certain conditions (e.g. high thickness t_{tot}) the WSC of CBSs may be improved significantly by layering.

Conclusions and Future Work

A new constitutive model describing effectively the hydraulic behaviour of unsaturated coarse soils is proposed. When applied in the study of CBSs, it is able to represent the phenomenon of water breakthrough better than conventional hydraulic constitutive models.

The use of multi-layered CBSs may lead to a substantial increase of the WSC in certain conditions, according to numerical results. In the future, this is intended to be shown also experimentally.

The ability of CBSs to maintain suction high in the underlying soil in the long term will be studied numerically, for different weather conditions, materials and geometries of the problem. Moreover, the potential gain given by the application of CBSs to slope stabilization problems and to the design of retaining walls will be analysed numerically.

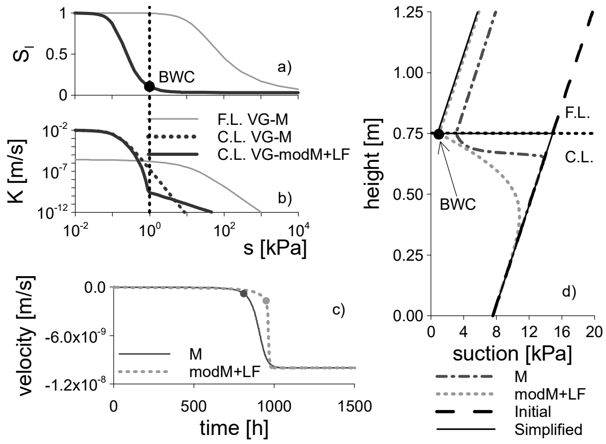

Figure 1. Comparison between the results obtained using different constitutive models for the C.L.: a) water retention curves, b) hydraulic conductivity curves, c) time history of the velocity at the interface, d) suction profiles at breakthrough

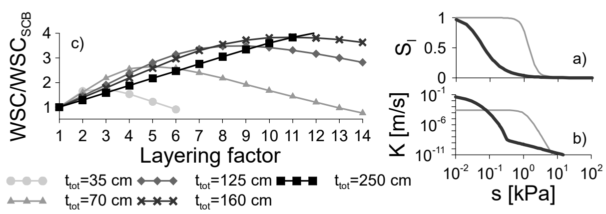

Figure 2. Multi-layered CBS: a) water retention curves, b) hydraulic conductivity curves, c) WSC curves against layering factor

Acknowledgements

The authors wish to acknowledge the support of the European Commission via the Marie Skłodowska-Curie Innovative Training Networks (ITN-ETN) project TERRE 'Training Engineers and Researchers to Rethink geotechnical Engineering for a low carbon future' (H2020-MSCA-ITN-2015-675762).

References

Stormont, J.C., & Anderson, C.E. 1999. “Capillary Barrier Effect from Underlying Coarser Soil Layer.” Journal of Geotechnical and Geoenvironmental Engineering 125 (8): 641–48.

Stormont, J.C., & Morris, C.E. 1998. “Method to Estimate Water Storage Capacity of Capillary Barriers.” Journal of Geotechnical and Geoenvironmental Engineering 124 (4): 297–302.

Van Genuchten, M.T. 1980. “A Closed-Form Equation for Predicting the Hydraulic Conductivity of Unsaturated Soils.” Soil Science Society of America Journal 44 (5): 892–98.

Finite element analysis of buried concrete thrust block providing lateral support to raking props

G. di Marzo*[1] and R.M. Singh[2]

*Correspondence: guido.dimarzo@a2-studio.com

[1] A-Squared Studio Engineers Ltd. (1 Westminster Bridge Rd, London, SE1 7XW, United Kingdom),
[2] University of Surrey (Guildford, Surrey, GU2 7XH, United Kingdom)

Abstract

Installing a series of temporary raking props supported by embedded concrete thrust block represents an effective solution to reduce displacements and stresses within an excavation retaining system. Ultimate inclined resistance of firm clay adjacent to the thrust block under different prop load inclination was assessed using Finite Element Method (FEM) for two different block geometries: triangular and rectangular. Results showed a positive correlation between the ultimate soil resistance and increased verticality of the prop line of thrust for both geometries. Triangular thrust block performed in a similar fashion as the rectangular geometry when the prop angle (to the horizontal) was increased. This study enabled a better understanding of thrust block failure mode including: bearing, sliding, overturning and combined bearing-sliding.

Introduction

Thrust blocks are embedded in the ground to balance the lateral prop load with the passive resistance of the soil. The block is normally cast-in-situ prior to the excavation is finalized. Surrounding soil should remain undisturbed during any operation as to generate full passive earth pressure. Failure of this mass concrete structure could cause sudden collapse of the overall retaining system. There is a limited published data on thrust blocks behaviour and the current design methods are often too conservative. Yet extensive research is available on bearing capacity and passive earth resistance of buried structures subjected to inclined loading.

Goodey et al. (2004) and Cabrera et al. (2006) investigated behaviour of thrust blocks subjected to equivalent prop loading by small scale testing within a high gravity centrifuge environment. Results from both studies highlighted that the load transfer into the soil is highly affected by the angle of inclination as well as thrust block geometry and the measured response of the thrust block exhibits a similar general behaviour to vertically loaded foundations with an initial elastic response followed by a plastic response.

The objective of this study is to determine behaviour of thrust block subjected to different prop angles as well as to compare performance of two different geometries namely, triangular and rectangular.

Methodology

A series of analyses on thrust block under varying load angle and geometry were carried out by the aid of the Finite Element Method (FEM) based commercial software Plaxis-3D. Three-dimensional modelling was preferred as to quantify passive, bearing and shear resistance developed at each face of the thrust block.

Table 1 indicates the angle of inclination range selected as to represent the raking prop action. The angle α was varied between 19° and 45° in accordance to a typical industry practice. For each angle a different triangular geometry was proposed as to provide normality condition between the imposed load line of thrust and the bearing side. Conversely, the rectangular section (i.e. Kier typical thrust block sizes) was not varied in any loading condition. The prop action Q magnitude was set equal to 1000kN as to bring the soil to failure and evaluate the thrust block ultimate bearing capacity.

Figure 1 shows the geometries considered including the load application point.

Table 1. Thrust block geometries and sizes

Geometry	B = L (m)	D (m)	α (°)
Rectangular	1.6	1	19, 32, 45
Triangular (i)	1	0.74	19
Triangular (ii)	1	0.62	32
Triangular (iii)	1	0.5	45

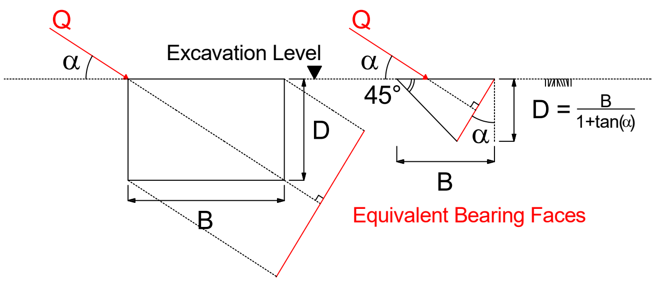

Figure 1. Problem definition

The generated mesh was composed by 10-noded quadratic tetrahedral for all elements. Local mesh and remote boundaries location were implemented as a function of the thrust block geometry and load angle. The concrete thrust block was modelled as a linear elastic non-porous rigid body with interfaces at each face. The soil was modelled as elasto-plastic material, obeying the Mohr-Coulomb plasticity model, with undrained short-term behaviour (i.e. temporary work conditions). Table 2 presents the material parameters adopted for FEM analysis.

Table 2. Material parameters

Material	γ (kN/m^3)	C_u (kPa)	E' [E_u] (MPa)	v' [v_u] (-)
Firm Clay	20	50	[37.5]	[0.495]
C32/40	24	-	32800	0.150

The analysis, once the initial stresses were defined, followed with applying the load specified incrementally in dynamic implicit steps. The analysis was terminated when excessive distortion of the soil was occurring as this would correspond to the ultimate soil resistance.

Results and Discussion

Different results of ultimate soil resistance are assessed in combination with observed failure mechanisms for each analysis differing in geometry/load angle. Figure 2 displays the equivalent ultimate bearing resistance vs. displacement curves associated to each geometry/load angle. The equivalent bearing face for both geometries is shown in Figure 1 (i.e. line of thrust acting normally at bearing face mid-point). The curves show a similar trend with elastic deformations followed by plastic deformation and with the ultimate load soil resistance increasing in respect to α. This confirms the tendency indicated by Cabrera et al. (2006). The triangular geometry performs comparably to the rectangular block.

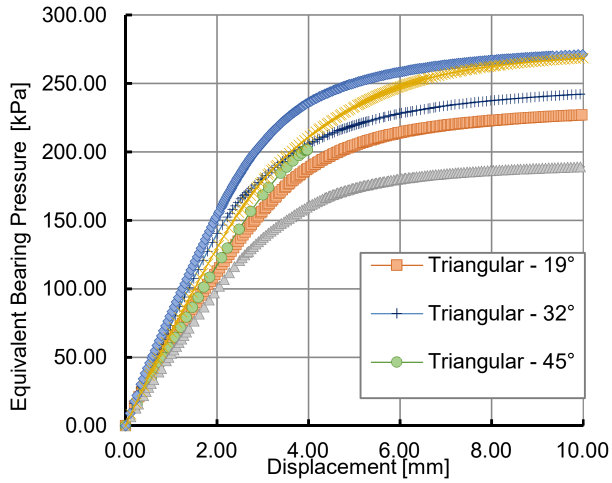

Figure 2. Bearing pressure vs. displacement

Conclusions

It has been evaluated that there is a positive correlation between the ultimate soil resistance and the increase in prop angle. The triangular geometry represents a more economical solution as it occupies a reduced volume and analogous size to a tractor loader bucket. It enables effective load transfer through the bearing side and greater passive resistance area generation.

Acknowledgements

This research was conducted with the support of A-Squared Studio Ltd. and MGF Ltd.

References

Brinch Hansen, J., (1970). A revised and extended formula for bearing capacity. Bull. Danish Geotechnical Institute.

Goodey, R.J, McNamara, A.M. & Taylor, R.N. (2005). The effectiveness of buried mass concrete thrust blocks as a means of lateral support for excavations. Proceedings of the 16th International Conference on Soil Mechanics and Geotechnical Engineering.

Cabrera, M., Taylor, R.N. and McNamara, A.M. (2006). Inclined load capacity of buried mass concrete thrust blocks. Geotech. Eng. Research Centre. City University, London, UK.

Potts, D.M. & Zdravkovic, L. (2011). Finite Element Analysis in Geotechnical engineering: Theory and application. London, UK: Thomas Telford.

Numerical analysis of Double-O-Tube shield tunnelling

D. Zhou *[1]

*Correspondence: ding.zhou16@imperial.ac.uk

[1] *Department of Civil and Environmental Engineering, Imperial College London*

Abstract

This project focuses on the numerical study of Double-O-Tube (DOT) shield tunnelling. A numerical model of an engineering case in Shanghai, with the corresponding ground profile constitutive modelling, has been developed in the finite element software ICFEP (Imperial College Finite Element Program). Considering the geological environment of Shanghai, a critical state based constitutive framework, using an extended Modified Cam Clay (MCC) model, has been employed for describing the non-linear small strain behaviour and the failure conditions of the soils in the ground profile. The parameters for the constitutive model are based on the hydro-mechanical characterisation of soils from laboratory and field testing data. The resulting ground response and the lining forces are then assessed and discussed.

Introduction

Double-O-Tube shield tunnelling (DOT) is a new tunnelling technology developed for metro transportation systems, aiming at improving the efficiency of tunnel construction and usage of underground space with its unique geometrical shape (Fig. 1). This technology firstly appeared in Japan in 1989 and there have been 6 engineering cases to date on the Shanghai metro system.

Shanghai is located on the coastal plain of the Yangtze River Delta in south-eastern China. The Quaternary strata thickness of the Shanghai area reaches to 280m-300m (SGEAEB 2002), with high groundwater table. Significant research has been carried out on the single circular tunnels in this area but less attention has been paid to DOT.

Some unique problems such as the rolling of DOT machine have been observed and discussed by some researchers. A number of useful comparisons between DOT and single circular tunnels have also been presented. However, there is a lack of research focus on the systematic numerical analysis of DOT tunnels constructed in the Shanghai area. The hydro-mechanical behaviour of the soil and the development of lining forces during the tunnelling process have not been properly assessed to date.

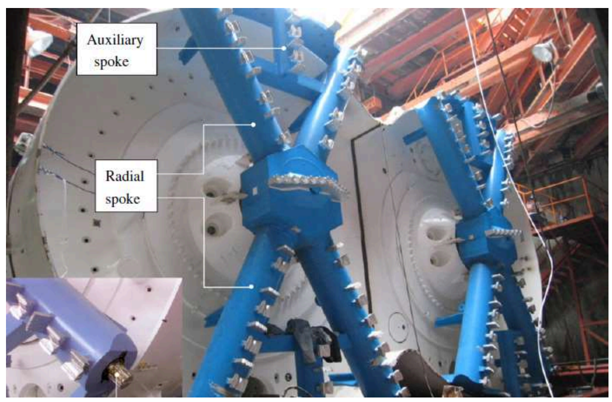

Figure 1 the DOT machine (Fang et al. 2012)

Methodology

An extended MCC model (Roscoe & Burland, 1968; Potts & Zdravkovic, 1999), incorporating the Imperial College Generalised Small Strain Stiffness model (IC3GS; Taborda & Zdravkovic, 2012), is employed for simulating the behaviour of the Shanghai clay. The soil mechanical parameters are obtained from the laboratory and field testing of the Shanghai soils. The segmental DOT concrete lining is modelled with elastic beam elements in the preliminary study. This will be followed with the modelling of the concrete material using an elasto-plastic concrete model (Schutz et al., 2011) and full consideration of the lining thickness. The database of information for this research, including the parameters of the Shanghai clay, the ground conditions and details of DOT lining, is built through literature survey.

The process of numerical simulation is carried out using the finite element software ICFEP (Potts & Zdravkovic, 1999), in which the excavation and construction sequences of tunnelling are simulated over a number of increments (analysis steps). The analyses are hydro-mechanically coupled, accounting for appropriate hydraulic boundary conditions and enabling both short and long term ground movements and lining forces to be assessed.

The accuracy of the modelling is verified against the available field monitoring data. The study will involve detailed comparison between DOT, single and twin circular tunnels constructions in the same ground conditions.

Results and Discussion

The preliminary analysis results have demonstrated the suitability of the MCC model to accurately describe the undrained shear strength and small strain properties of the Shanghai clay.

The surface settlements of the DOT tunnelling in short term broadly match the monitoring data. Larger bending moments in the segments placed in the top and bottom middle positions are observed after the construction simulation, and the similar results have also been obtained by other researchers who conducted numerical modelling.

Conclusions and Future Work

The DOT technology seems efficient but has not been widely spread as yet. The engineering properties of the ground strata in Shanghai, especially the high ground water table and weak soft clay layers, make it a challenging environment for tunnelling. The settlement control and the lining forces in DOT should be specifically paid attention to.

Further research will be carried out on modelling the DOT lining with thickness by using the concrete model (Schutz et al., 2011) in ICFEP. The comparison between DOT with single circular tunnel and the usual twin-tunnelling will be made. Furthermore, the problems such as the rolling of DOT machine during construction and the leakage of lining will also be investigated. As for the longitudinal settlement profile and longitudinal stiffness of the lining during constructions, 3D analysis will be conducted.

Acknowledgements

The research is fully funded by China Scholarship Council (CSC) and their financial support is greatly appreciated. Professor Lidija Zdravkovic is highly acknowledged for her supervision and guidance during the research. Many thanks are given to those colleagues working with ICFEP in the Geotechnics research group at Imperial College for their help and useful suggestions.

References

Fang, Y., Kao, C. and Shiu, Y. (2012). Double-O-Tube shield tunneling for Taoyuan International Airport Access MRT. Tunnelling and Underground Space Technology, 30, pp.233-245.

Potts, D.M. & Zdravkovic, L, (1999) “Finite element analysis in geotechnical engineering: theory”, London: Thomas Telford.

Roscoe, K.H. & Burland, J. (1968). On the generalised stress-strain behaviour of 'wet' clay. J Eng Plast. 553-609.

Schutz, R. (2010). Numerical Modelling of Shotcrete for Tunnelling. Ph.D. Imperial College London.

Schütz, R., Potts, D. and Zdravkovic, L. (2011). Advanced constitutive modelling of shotcrete: Model formulation and calibration. Computers and Geotechnics, 38(6), pp.834-845.

Shanghai Geological Environmental Atlas Editorial Board (SGEAEB). (2002). Shanghai Geological Environmental Atlas (SGEA). Geology Press, Beijing

Taborda, D. (2011). Development of constitutive models for application in soil dynamics. Ph.D. Imperial College London.

Taborda, D.M.G. & Zdravkovic, L. (2012) Application of a Hill-Climbing Technique to the Formulation of a New Cyclic Nonlinear Elastic Constitutive Model. Computers and Geotechnics, 43, pp.80-91.

Single element tests of normally consolidated and overconsolidated clays under drained and undrained triaxial compression in ABAQUS

M.H. Sohawon*[1], R.N. Taylor[1] and S.E. Stallebrass[1]

*Correspondence: hashmi.sohawon@city.ac.uk

[1] *Affiliation: City, University of London, Northampton Square, London EC1V 0HB, UK*

Abstract

In soil design involving small strain stiffness, closed form solutions are derived using several assumptions; typically the soil is assumed to behave as an elastic material or in an elastic-perfectly plastic manner. These techniques do not take into account strain hardening or softening when a soil yields. Therefore, such analytical solutions fail to capture the real soil behaviour and tend to be very over-conservative. With the finite element method, more realistic soil responses can be predicted by using advanced constitutive soil models. In particular, this paper presents and discusses the use of the Modified Cam Clay Model (MCC) on the finite element package ABAQUS to predict the stiffness and volumetric responses of soils in triaxial compression.

Introduction

The motivation of this research is to make accurate predictions of ground movements induced by underground constructions. *(Taylor, 1998)* To do so, advanced constitutive soil models must be used such as the 3-surface kinematic hardening (3-SKH) model. The ultimate goal of this research project is to implement the 3-SKH model in ABAQUS. The aforementioned model is not available in any other geotechnical package for 3D analyses thus greatly increasing the need for such computational capabilities. *(Stallebrass & Atkinson, 1991)* The 3-SKH model is unique as it takes into account the recent stress history of the soil which affects the stiffness response of the soil to loading and hence deformation.

Methodology

In order to be in a strong position to judge the outputs from ABAQUS, an independent method of verification had to be implemented. Two MCC codes were consequently written on MATLAB for a single soil element to predict the stiffness and volumetric responses of the soil if the analysis was drained and the stiffness and pore-water pressure responses of the soil if the loading was undrained. The first MATLAB code adopted a stress controlled approach whereas the second MATLAB code used a strain controlled method. To run the code and obtain a solution, the user had to input the initial axial and radial stresses (σ_a and σ_r), the initial pore-water pressure (u), initial size of the yield locus (p'_{0y}), Poisson's ratio (μ), Γ, M, λ and κ, the total number of increments (n) and the stress increment or strain increment.

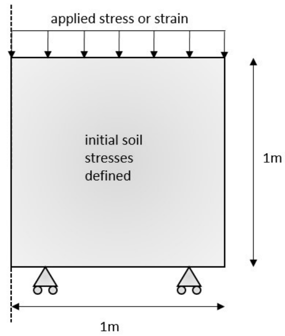

In the FE analyses, a 2D axisymmetrical single element with radius of 1m and height of 1m was set up in ABAQUS with boundary condition as shown in *Figure 1*.

Figure 1: Single element model in Abaqus which is a second order quadratic element with 8 nodes and uses a reduced integration scheme solver.

Four simulations were carried out to the analyse clay samples whose initial stress states are either wet of critical or dry of critical (overconsolidated). The clay properties are shown in *Table 1*. Since pore water pressure changes were not a required output in the drained analyses, the element could be defined as general stress while ensuring that external forces are applied to balance the initial internal stresses in the geo-static step. The clay properties are shown in *Table 1*.

Table 1. Summary of Parameters in the Single Element Drained and Undrained Analyses

Parameters	***Wet of Critical***	***Dry of Critical***
λ	0.25	0.2
κ	0.05	0.07
Γ	3.38	3.16
μ	0.3	0.3
M	0.94	0.94
e_0	1.15	1.05
p'_i (kPa)	200	100
p'_{0y} (kPa)	250	844
γ_w (kN/m^3)	10	10
k (m/s)	1E-9	1E-9

Results and Discussion

Only two sets of results have been presented in this paper. In the finite element simulations, a vertical displacement boundary condition was applied to the top of the clay to load the sample. The results of the wet of critical sample which was loaded in a drained manner are shown in *Figures 2 and 3*.

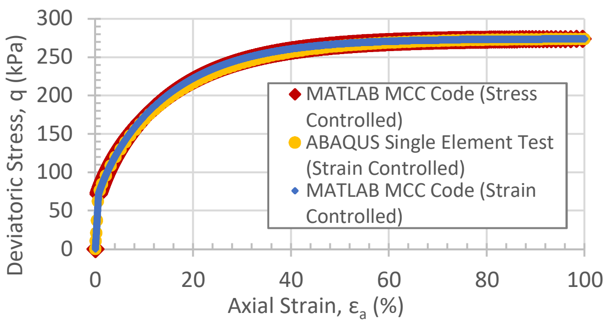

Figure 2: Drained Analysis (Wet of Critical)

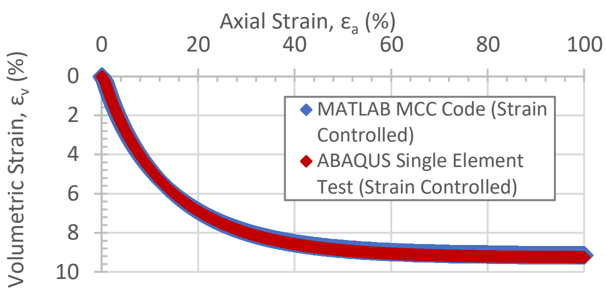

Figure 3: Drained Analysis (Wet of Critical)

The response predicted by ABAQUS matches exactly with the theoretical predictions from the MATLAB codes. In *Figure 2*, the stress-strain relationship is linear followed by strain softening as the clay yields. The deviatoric stress then reaches a plateau at critical state. *Figure 3* depicts a completely contractant and ductile volumetric behaviour upon straining which is expected when a sample is sheared from an initial condition lying above the CSL in the volumetric (v-lnp') space.

The results of the dry of critical sample which was loaded in an undrained manner are shown in *Figures 4 and 5*. Once again, the results from the MCC code and those on ABAQUS are in good agreement with each other. Since the clay is overconsolidated, a dilatant behaviour where the soil swells is observed in *Figure 5* while the deviatoric stress reaches a peak and then reduces to a constant value at critical state in *Figure 4*.

It must be noted that during undrained shearing, the zero volume change condition during deformation is achieved in ABAQUS by using a pore fluid/stress element in a coupled consolidation soil analysis. The latter leads to the development of excess pore-water pressures as the soil is sheared. With a very low permeability and using very small time steps (rapid loading), the short term strength of the clay is invoked in the software.

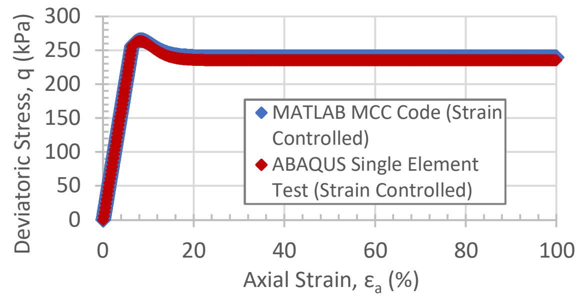

Figure 4: Undrained Analysis (Dry of Critical)

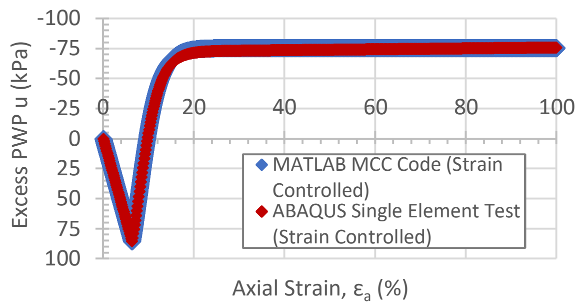

Figure 5: Undrained Analysis (Dry of Critical)

Conclusions and Future Works

This study concludes that the MCC model (Clay Plasticity) implemented in ABAQUS is reliable. The latter may be used with confidence to simulate more complex foundation designs. The next steps of this research is to repeat the above process and validate a 3-SKH UMAT routine on ABAQUS with a MATLAB code that predicts the stiffness and volumetric responses of a single element according to the 3-SKH model. Moreover, there are numerous centrifuge tests; from tunnels to retaining walls, that have been carried out at City, University of London and they will be back analysed using FE to investigate how MCC and 3SKH compare when predicting ground movements.

References

Stallebrass, S.E. and Atkinson, J.H., (1991). *A model for recent stress history and non-linearity in the stress-strain behaviour of overconsolidated soil.* Proceedings of the 7th IACMAG, Cairns, 555-60

Taylor, R.N. (1998). *Modelling of Tunnel behaviour.* Journal of Geotechnical Engineering, 131(3), pp. 127–132.

Validation of 3D Finite Element models of pipelines crossing active faults via analytical and experimental methods

H.E. Demirci*[1]

*Correspondence: h.demirci@surrey.ac.uk

[1] *University of Surrey, Guildford, UK*

Abstract

Buried pipelines are subjected to permanent ground deformations (PGDs) caused by earthquakes such as fault, landslide, lateral spreading and seismic settlement. Buried pipelines are mostly designed considering strain based performance criteria including tensile failure, local buckling and ovalisation. Hence, estimation of maximum pipeline strains under PGDs is essential to design earthquake-resistant pipelines. Maximum tensile and compressive strains in pipelines are often predicted via analytical methods and Finite Element (FE) based numerical analysis. The analytical methods are useful for preliminary design of buried pipelines crossing PGD zones. However, FE analysis should be performed for the final design of such pipelines. The reliability of FE models needs to be ensured by verifying their results via analytical and experimental methods. In this study, a FE model of a pipeline crossing a strike-slip fault is validated via analytical method proposed by Sarvanis and Karamanos (2017) and FE models of pipelines crossing reverse faults and landslides are validated via small scale model tests. The FE results confirm its capability of capturing the response of pipelines crossing PGD zones.

Introduction

Buried pipelines crossing permanent ground deformation (PGD) zones experienced severe damage during past earthquakes. The pipeline damage had significant effects on world industry, economy and society. Therefore, to understand pipelines response to PGDs is essential to mitigate the effects of PGDs on buried pipelines. The pipeline behaviour for such problems is analysed via using analytical methods or Finite Element (FE) based numerical methods. Analytical models of pipelines crossing strike-slip and normal faults were proposed by several researchers over the past four decades (e.g. Karamitros et al., 2007). All these methods are for pipelines under tension and bending forces and they have several limitations which are summarised in Demirci et al.'s study (2017). Despite their limitations, the analytical models are very time-efficient compared to FE analysis and quite practical for preliminary design of pipelines crossing strike-slip and normal faults. FE models were used by several researchers for the evaluation of parameters affecting the behaviour of pipelines crossing PGD zones, the verification and refinement of the analytical methodologies and the assessment of pipeline performance based on performance criteria such as local buckling, tensile rupture and ovalization (e.g. Vazouras et al., 2010). Large-scale and centrifuge tests were performed to investigate response of buried pipelines to ground faulting (e.g. O'Rourke and Bonneau, 2007; Ha et al., 2008). The verification of analytical and numerical models, the evaluation of soil springs in ASCE (1984) and the assessment of parameters affecting pipeline response to faulting were in the scope of these studies. In this paper, the validation of developed 3D FE models of pipelines crossing reverse, strike-slip fault and landslides are given.

Methodology

The 3D FE models of pipelines crossing reverse faults and landslides are validated via small-scale model test results. The detailed description of small-scale models and their working principles are given in Demirci et al. (2017). The details of 3D FE model of pipeline crossing a reverse fault is given in Demirci et al. (2018). Therefore, an extra information about numerical models and experimental setups will not be provided in this paper. Furthermore, the 3D FE model of pipelines crossing strike-slip with 20° fault crossing angle is validated via analytical method proposed by Sarvanis and Karamanos (2017).

Results and Discussion

Figure 1 shows distribution of normalised pipe bending strains along the pipeline for both experimental and 3D FE models of the pipeline crossing reverse faults. Fault displacements in both tests and models are 6.6 and 10.6 times of pipe diameter.

The distribution of longitudinal pipe strain for 3D FE model and experiment of the pipeline crossing the landslide zone is shown in Figure 2. The maximum ground movement (δ) is 80mm for this problem.

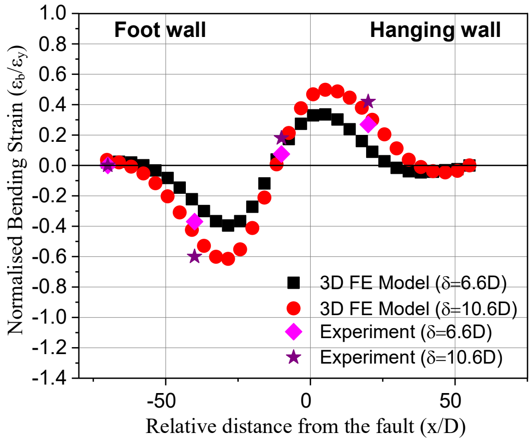

Figure 1. Plots of normalised pipe bending strains (ε_b/ ε_y) vs relative distance from fault (x/D) (Reverse faults)

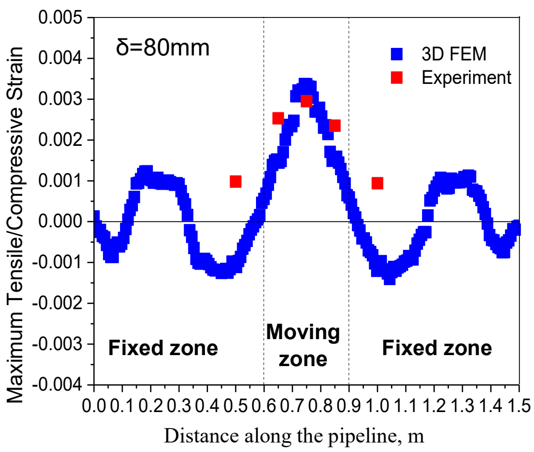

Figure 2. The distribution of longitudinal pipe strains for 3D FE Model and experiment (landslide model)

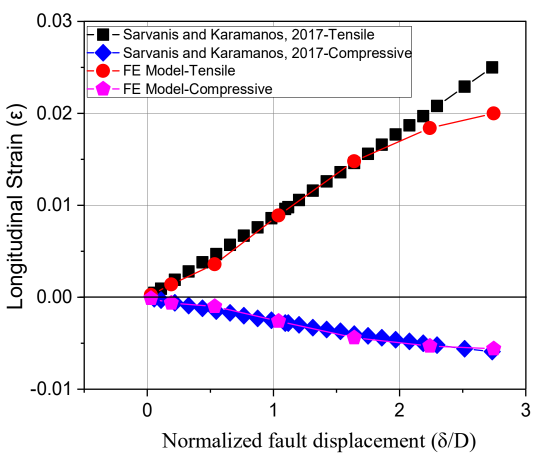

Figure 3. Validation of the proposed 3D FE model for pipelines crossing strike-slip faults via analytical methods

Figure 3 demonstrates variation of maximum tensile and compressive pipe strains with normalised fault displacement for analytical and numerical models.

Conclusions and Future Work

This paper focuses on the validation of 3D FE models via small-scale model tests and the analytical method. Good agreement was achieved and the 3D FE models are considered as a reliable tool to effectively capture pipeline response to PGDs.

Acknowledgements

The authors wish to thank Turkish Government (Republic of Turkey Ministry of National Education) for funding this research.

References

ASCE (1984). Guidelines for the Seismic Design of Oil and Gas Pipeline Systems, Committee on Gas and Liquid Fuel Lifelines, American Society of Civil Engineers, Reston, VA.

Demirci H.E., Bhattacharya, S., Singh, R.M. (2017). A review of the behaviour of buried continuous pipelines crossing faults. 3rd International Soil-Structure Interaction Symposium, Izmir, Turkey.

Demirci H.E., Bhattacharya, S., Karamitros, D.K., Alexander, N., Singh, R.M., Mahoney, W., Draper, F. (2017). Scale model of buried pipelines crossing faults. 4th International Earthquake Engineering and Seismology Conference, Eskisehir, Turkey.

Demirci, H.E., Bhattacharya, S., Karamitros, D.K., Alexander, N. (2018). Experimental and numerical modelling of buried pipelines crossing reverse faults. Soil Dynamics and Earthquake Engineering - accepted

Ha D, Abdoun TH, O'Rourke MJ, Symans M, O'Rourke TD, Palmer MC and Stewart HE (2008). "Centrifuge Modeling of Earthquake Effects on Buried High-density Polyethylene (HDPE) Pipelines Crossing Fault Zones," ASCE J Geotechnical and Geoenvironmental Engineering, 134: 1501–1515.

Karamitros, D.K., Bouckovalas, G.D. and Kouretzis, G.P. (2007). "Stress Analysis of Buried Steel Pipelines at Strike-Slip Fault Crossings", Soil Dynamics and Earthquake Engineering, ASCE, 27(3), 200-211.

O'Rourke, T.D. and Bonneau, A. (2007). "Lifeline performance under extreme loading during earthquakes." Earthquake Geotechnical Engineering, K.D. Pitilakis, Ed., Springer, Dordrecht, Netherlands: 407-432.

Sarvanis GC, Karamanos SA (2017). Analytical model for the strain analysis of continuous buried pipelines in geohazard areas. Engineering Structures, 152:57-69.

Vazouras P, Karamanos SA, and Doulakis P (2010). Finite element analysis of buried steel pipelines under strike-slip fault displacements. Soil Dyn. Earthqu. Eng. 30:11, 1361-1376.

Investigation into the use of screw piles in clay for off-shore wind turbine foundations

Y.U. Sharif*[1],

Correspondence: Y.U.Sharif@Dundee.ac.uk

[1] *School of Science and Engineering, University of Dundee, UK.*

Abstract

Large diameter helical plated screw piles used alongside jacket structures may become a more practical alternative to current foundation options for use in deep waters for offshore wind turbine foundations. The current uses of these foundations have produced screw piles with relatively small diameter helical plates which benefit from large axial resistance and low noise pollution during installation. To optimise the foundation geometry for use offshore as a wind turbine foundation 2D and 3D FE simulations will be conducted. The outcome of these simulations will used to design a series of centrifuge tests that include in flight installation and load testing. Initial results from the simulations show that an H/D of 2 is the optimum depth for installation.

Introduction

The next iteration of offshore wind farm installation in the UK is to take place within Round III, in which the wind turbines are to be installed in deeper water (up to 70m) further off the coast of the UK. The traditional forms of foundations that have been used for offshore wind turbines (OWT) usually consists of a steel monopile (maximum diameter of 6m) which is driven into the sea bed. These foundations are typically only installed in water depths less than 30m in depth (Siems & Scharff, 2013). Once the water depth increases above 30m, the monopile no longer appears to be a feasible option in both economic and structural sense. Structures such as tri-piles or jackets start to become more ideal in the deeper water depths, where higher wind speeds would result in larger production of electricity, as they are able to spread the load over multiple smaller foundations than a single pile.

Therefore, any subsequent foundations that are to be used with these systems (tri-pile or jacket) would be required to be designed to deal with the V-H-M loading regime that is to be generated over the 20 year life span of the structure.

One option that has been considered for use is the screw pile due to its relatively low noise levels during installation in conjunction with its lower cost from a reduction in material and time required.

Screw piles have been used for a substantial period of time with the first recorded use being in 1836 for ship moorings and lighthouse foundations (Perko, 2009). Current uses of the foundation are usually for relatively low loads with most of the loads being vertical in nature and therefore consist of small diameter helical blades. To be able to use this foundation option in offshore applications the screw pile must be scaled accordingly and the geometry of the screw pile must be assessed and optimised for its new use.

This study aims to start to assess the optimum geometric properties of the screw pile for use in clay. It will look into the effects of embedment depth and how this effects the vertical capacity and the failure mechanism that is induced. Using this data an optimized screw pile for this purpose can be created.

Numerical modelling

For the numerical analysis of the screw piles the Finite element software “Plaxis 2D 2017” was used with an axisymmetric model. The model consisted of a screw pile with a 1m diameter flight and a 0.3m diameter shaft, embedded into various depths of a normally consolidated clay. The depths that have been investigated are normalized into a H/D ratio, which represents the embedment depth from the top of the plate to the mudline (H), over the diameter of the screw pile flange (D).

The purpose of the FEM was to establish if it was possible to use this form of analysis to assess the uplift capacity of the screw piles and how depth of installation affects the mechanism of failure. This can then be used aid in the creation in an optimised geometry for centrifuge testing. The centrifuge testing would also be used as a validation method for the FEM analysis.

The soil model that was chosen for use in the analysis was Modified Cam Clay, with the properties for a London clay as the soil to be tested, the properties that were inserted can be seen in Table 1.

Table 1.- Plaxis modified cam clay input parameters

London clay property	Value
Saturated Unit weight γ	17 kN/m^3
$e_{initial}$	0.70
λ	0.16
κ	0.0624
M	0.89
v	0.3
R_{inter}	0.7

Results and Discussion

The results of the FEM show that there are two mechanistic failure modes that occur creating a "shallow" and "deep" failure mechanism similar to the effect seen in plate anchors. In which the shallow mechanism is a wedge of cylinder which propagates to the surface of the soil, and the deep failure mechanism is a flow around mechanism which is localised around the flight of the screw pile. Examples of these mechanisms can be seen in work such as (Merifield, 2001) which assess embedded plates in clay soils.

From the output of the analysis it is possible to back calculate a breakout factor for the helical piles which shows the cross over from a shallow to a deep failure mechanism at a H/D of 2. Figure 1 shows the comparison of the relationship of H/D to breakout factor (Nc) of the screw piles and circular plate anchors.

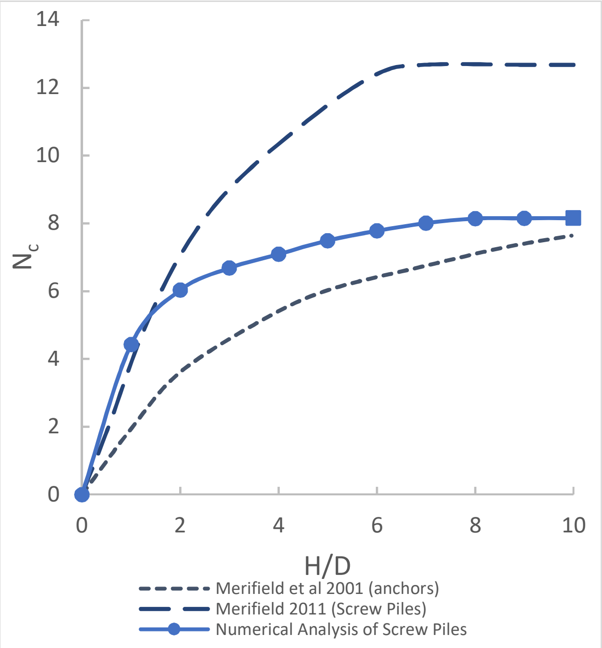

Figure 1: Breakout factor Nc variation with embedment depth ratio

Conclusions

From Figure 1 it can be seen that the breakout factor Nc is similar but slightly higher than to those seen in plates and that numerical models can be used to assess the capacity of these forms of foundation. Thus, making the assessment of an optimised geometry much easier than physical model.

The results also show that a H/D of 2 is the transition point from a shallow to deep failure mechanism which is relatively low value meaning that the foundations can be installed to much lower depths and still achieve the resistance seen in traditional foundation options. The difference that is seen between the various analysis is due to the influence of the shaft which is debatable, and which has been ignored in this study due to influence of the shaft being an unknown quantity.

Future Work

To further the research into the use of screw piles and to validate the numerical models that will be used in future, centrifuge testing will be completed with various geometries of model screw piles using the installation and loading system developed by (Albaghdadi, et al., 2016). The project will use both centrifuge modelling and numerical analysis, both finite element and discrete element modelling to determine the optimum geometry for the screw pile in terms of installation torque required and loading for various regimes of forces.

Acknowledgements

This is a 4-year research project funded by Engineering and Physical |Sciences Research Council (EPSRC) along with an Industrial sponsorship with Roger Bullivant Limited.

References

Albaghdadi, T., Brown, M. J. & Knappett, J., 2016. *Development of an inflight centrifuge screw pile installation and loading system.* Nantes, France, European Conference on Physical Modelling Geotechnics Eurofuge 2016.

Merifield, R. S., 2001. Stability of plate anchors in undrained clay. *Geotechnique,* 51(2), pp. 141-153.

Merifield, R. S., 2011. Ultimate Uplift Capacity of Multiple Helical Type Anchors in Clay. *Journal of Geotechnical and Geoenvironmental Engineering,* 137(7), pp. 704-716.

Perko, H. A., 2009. *Helical piles, A practical guide to design and Installation.* Hoboken(New Jersey): John Wiler & Sons, Inc.

Siems, M. & Scharff, R., 2013. *Monopile foundations for offshore wind turbines - solutions for further depths,* s.l.: Steel construction 6.

Numerical investigation on the performance of geothermal energy contiguous flight auger (CFA) pile

A. Kawuwa Sani[1]; R.M. Singh[1] and I. Cavarretta[1]

*Correspondence: a.sani@surrey.ac.uk

[1]*Department of Civil and Environmental Engineering, Faculty of Engineering and Physical Sciences, University of Surrey, Guildford, GU2 7XH, UK.*

Abstract

The practice of fitting energy loops in pile foundation elements dualizes the role of the pile for load support and in meeting the energy requirement of the superstructure. Water based solution is circulated through the energy loops to extract or reject heat in to the ground during space heating or cooling process. However, the smaller the shank spacing between the inlet and outlet loops leg the lower the energy output of the system. This study investigates via numerical means the effect of shank spacing on the thermal performance of a contiguous flight auger (CFA) pile. Shank spacing was found to be significant in maximising the energy output of a geothermal energy CFA pile.

Introduction

Geothermal energy pile (GEP) system is an innovative technology that connects the pile foundation element and the heat pump unit to harness energy from the ground and achieve building heating/cooling demand. The system operates by circulating water-based solution within high-density polyethylene (HDPE) or energy loops, embedded in the concrete pile, and connected to the heat pump. Inside the pile, the HDPE loops are attached to the pile reinforcement cage in rotary bored piles or at the centre of the pile in contiguous flight auger piles (CFA). Thus, the close proximity of the inlet and outlet loops leg in the CFA piles results in thermal interaction in comparison to the case with the loops at the edges (Sani *et al.*, 2018). This study investigates the thermal performance of a geothermal energy CFA pile, with a focus on how the distance between the loops affects the GEP system performance.

Methodology

Model properties

A 2D finite element modelling and analyses of the energy pile were carried out in COMPASS (COde for Modelling PArtially Saturated Soils). The pile geometry shown in Figure 1 comprises pile cross-section with a dimeter of 600 mm and two pipes installed to represent the inlet and outlet legs of a single U-loop. The modelled pipes have an outer and an inner diameter of 32 and 28 mm, respectively. The pipe location was varied during the analyses i.e. at the edge, at equal shank spacing, and at the pile centre attached to a 40 mm steel for rigidity. In addition, the pile is embedded in a soil domain which spans out to a radial distance of 5 m from the centre of the pile. A large domain was chosen to ensure thermal processes are allowed to be fully implemented.

The pile and HDPE pipes were discretised using triangular mesh elements with sizes of 10 and 1 mm respectively. Also, a triangular mesh of 20 mm size was applied at the pile surface and the elements size increases to 500 mm at the far field boundary in the soil.

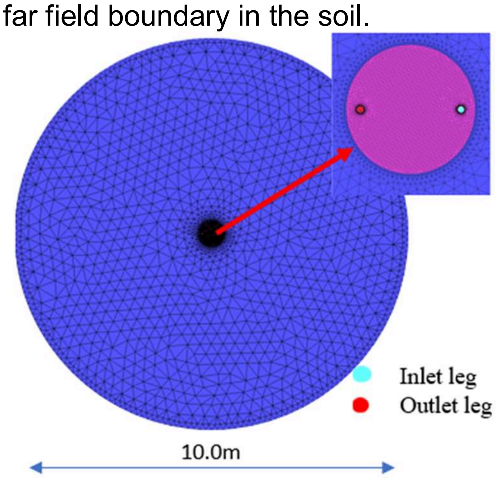

Figure 2 Geometry of a geothermal energy CFA pile with 1–loop

Initial and Boundary conditions

An initial temperature of 13.4°C was applied on the pile and soil model. Also, constant temperature of 308.15 K (35°C) and 303.15 K (30°C) were applied to the internal surface of the inlet and outlet leg of the HDPE pipes respectively, representing summer mode of operation or achieving building cooling. In addition, a fixed temperature of 286.55 K (13.4°C) was applied at the outer surface of the soil domain. The parameters such as saturated hydraulic conductivity *(K_{sat})*, soil saturation *(S_r)*, thermal conductivity *(λ)*, specific heat capacity, *(C_p)*, density *(ρ_d)* and porosity *(n)* are given in Table 1.

Table 1 Materials properties (adopted from Loveridge, 2012; The-metal-store, 2018)

Parameter	Clay	Concrete	HDPE	Steel
K_{sat} *(m/s)*	5.8×10^{-11}	–	–	–
S_r *(%)*	100	–	–	–
λ (W/m K)	1.5	1.5	0.385	43
C_p *(J/Kg K)*	1820	1050	1465	47
ρ_d *(Kg/m³)*	1968	2210	1100	7801
n	0.37	0.1	–	–

Simulation

Transient numerical analyses were carried out by applying continuous temperature at the HDPE pipe surfaces for 180 days. This operation represents the summer mode.

Results and Discussion

The model was validated via the use of analytical equation for determining GEP resistance proposed by (Loveridge and Powrie, 2014). The analytical results and that of COMPASS showed very good agreement and do not vary by more than 0.3%.

Figure 2 shows the results of maximum temperature observed at the pile centre at the end of the heating period (180 days). A maximum temperature of about 32°C, was observed at the centre of the pile when the loop was placed at the pile centre. The temperature magnitude decreases to about 29 and 27°C as the shank spacing between the inlet and outlet loop leg increases. The drop in temperature is due to lesser heat interaction between the legs of the loops. Thus, the loop legs should be kept apart to maximise the energy output of the system. Furthermore, Figure 3 presents the radial temperature distribution for the 3 cases. Higher energy was exchanged between the pile and soil when the loops are installed at the edge, with the amount decreasing with the decrease in shank spacing between the loops. Hence, it is advised that greater shank spacing should always be maintained to maximise the system performance.

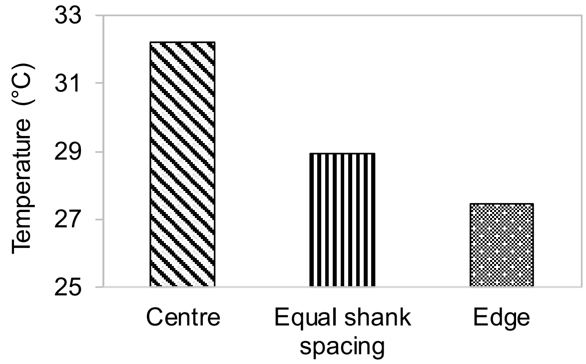

Figure 3 Temperature at the pile centre for the 3 cases

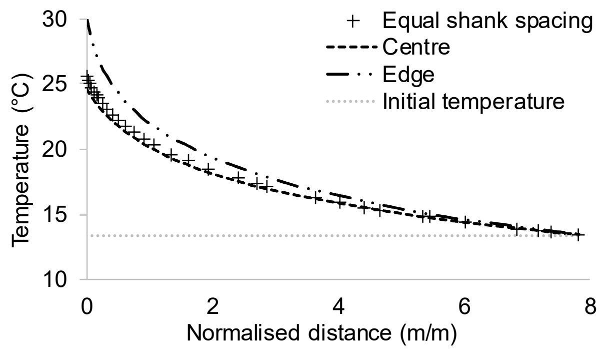

Figure 4 Radial temperature distribution for the 3 cases

Conclusions

This paper highlights the important role of shank spacing in maximising the energy output and the longevity of the system.

References

Loveridge, F. (2012) 'The Thermal Performance of Foundation Piles used as Heat Exchangers in Ground Energy Systems', p. 206.

Loveridge, F. and Powrie, W. (2014) '2D thermal resistance of pile heat exchangers', *Geothermics*. CNR-Istituto di Geoscienze e Georisorse, 50, pp. 122–135.

Sani, A. K., Singh, R. M., Hollanda, C. De, Tsuha, C., Cavarretta, I. and Sani, A. K. (2018) 'Acta Geotechnica Pipe-pipe thermal interaction in a pile heat exchanger', *Acta Geotechnica*.

The-metal-store (2018) *Stainless steel round bar.* https://www.themetalstore.co.uk/products/stainless-steel-304-round-bar-2m.

Analysis of geothermal energy utilisation in underground

O. Ogunleye[1] and R.M. Singh[1]

*Correspondence: o.ogunleye@surrey.ac.uk

[1]*Department of Civil and Environmental Engineering, Faculty of Engineering and Physical Sciences, University of Surrey, Guildford, GU2 7XH, UK.*

Abstract

In order to meet the increasing energy demand for space heating and cooling, it is imperative to provide a sustainable way of generating the required energy and design efficient systems. Due to recent technological advancements, geothermal energy has been successfully harnessed for space heating/cooling and hot water. The widely used system to harness shallow geothermal energy is a Ground Source Heat Pump (GSHP), this is due to its higher efficiency compared to electrical resistance heating. This study focuses on the use of underground tunnel components and GSHP as a means to extract shallow geothermal energy, the underground tunnels used for this purpose are also known as energy tunnels. A 3D numerical model was developed to simulate the conjugate transient heat transfer in energy tunnel in order to understand the effect of the tunnel air temperature, intermittent operation, fluid flow rate and ground's thermal conductivity conditions on the efficiency of the energy tunnel. The results from this study shows that the aforementioned factors affects the thermal efficiency and a strategic selection of these parameters is important to achieving an efficient system whilst allowing the ground to recover and stop any adverse effect on the surrounding or the thermo-active structure.

Introduction

Due to the steady increase in the global usage of ground source heat pump systems, (Figure 1) engineers are constantly looking for new ways to improve their economic viability and sustainability. Recently, existing and new underground structures are now being used as part of the geothermal system, the concept of using existing underground structures in harnessing geothermal energy for space heating and cooling is beginning to attract considerable interest. In energy tunnel (Figure 2), the tunnel linings are equipped with absorber pipes which are then connected to a heat pump in order to exchange heat with the ground and surrounding buildings. The thermal energy extracted or ejected is used to provide heating/cooling and hot water to nearby buildings. Energy tunnel provides a sustainable and renewable solution to the growing energy crisis as a carefully designed energy tunnel could operate at a relatively low cost to conventional fossil fuel based heating systems. Most underground tunnels are situated at depth where the ground temperature is relatively constant all year round (10-14°C), energy tunnel takes advantage of this condition. The exploitation of geothermal energy in this way is relatively new compared to other thermos-active ground structures e.g. energy piles. It is therefore imperative for engineers to understand the site conditions and the tunnel's behaviour under induced thermal stress in order to maximise its potential.

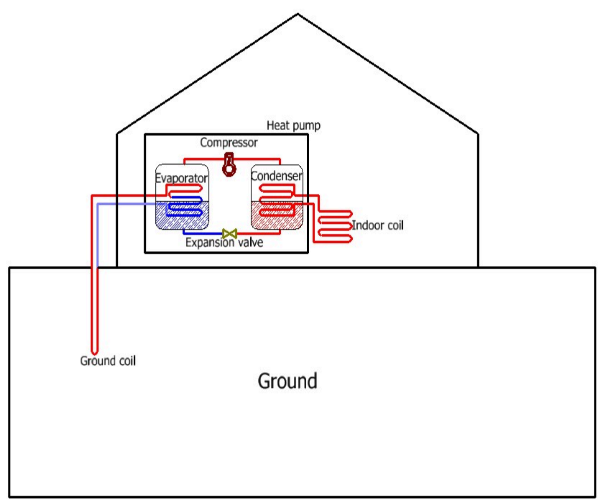

Figure 1. Schematic of a GSHP

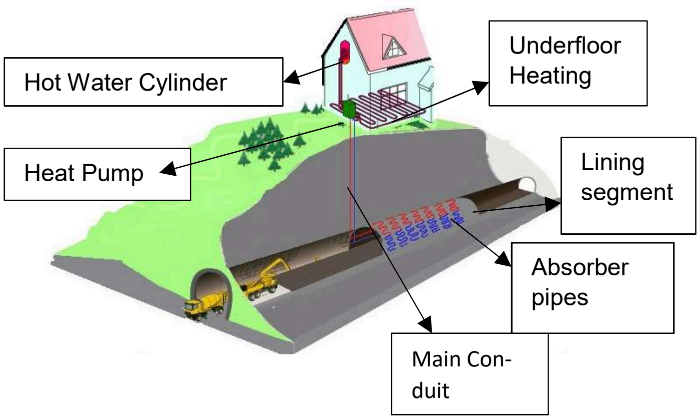

Figure 2. Schematic of an energy tunnel.

Methodology

In this study, a 3D FE model was developed using ABAQUS in order to simulate the conjugate heat transfer in energy tunnel. The effect of the tunnel air temperature, intermittent operation, fluid flow rate and ground's thermal conductivity on the extractable heat inside the tunnel were investigated. The model was validated using data measured from Linchang underground tunnel (equipped with absorber pipes) in China. The tunnel geometry, conditions and material properties from the experimental test performed in Linchang tunnel (Zhang et al., 2013), are presented in Tables 1 & 2 below:

Table 1. Test data for Linchang Tunnel

Parameter	Value
Inner diameter of the tunnel	11.40 m
Thickness of the secondary Lining	400 mm
Thickness of surrounding rock	600 mm
Pipe spacing	1 m
Pipe Length	50 m
Absorber pipe outer diameter and wall thickness	25 mm, 2.3 mm
Heat transfer coefficient inside the tunnel	15 W/m^{2}K
Inlet temperature	20°C
Tunnel air temperature	10°C
Surrounding rock temperature	5.6°C

Table 2. Thermophysical properties

	Thermal conductivity (W/m K)	Density (kg/m^3)	Specific heat (J/kg K)
Circulating fluid	0.56	1000	4200
Concrete lining	1.85	2400	970
Surrounding rock	3.22	2544	1293

Results and Discussion

The temperature contour plot of the result after 90 days of simulating the heat extraction process is shown in Figure 3. The preliminary result from this study shows that running the system intermittently increases the thermal output. Increasing the fluid flow rate also increases the extractable heat and finally as the thermal conductivity of the ground increases the thermal output increases. The temperature profile of the air inside the tunnel also affects the heat exchange rate and it is important to include this when estimating the geothermal potential of an energy tunnel

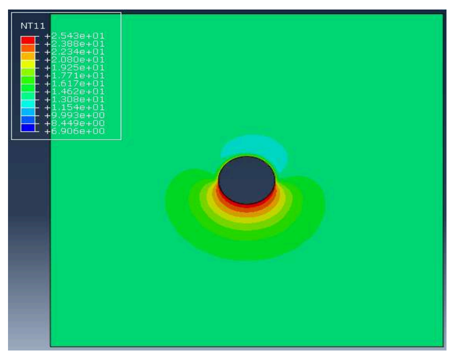

Figure 3. 2-D view of the model result.

Conclusions.

The results from this study shows that the tunnel air temperature, intermittent operation, fluid flow rate and ground's thermal conductivity affects the thermal efficiency and a strategic selection of these parameters is important to achieving an efficient system whilst allowing the ground to recover and stop any adverse effect on the surrounding or the thermo-active structure

References

ZHANG, G. Z., XIA, C. C., SUN, M., ZOU, Y. C. & XIAO, S. G. 2013. A new model and analytical solution for the heat conduction of tunnel lining ground heat exchangers. Cold Regions Science and Technology, 88, 59-66.

List of participants and affiliations

Arup
B. Simpson

A-Squared Studio Engineers Ltd
G. di Marzo

University of Bath
L. Tong

University of Bristol
J.J. Crispin
L.W. de Leeuw
E. Ibraim
E. Katsiveli
A. Peccin da Silva

University of Cambridge
Malcolm Bolton

Cardiff University
R. Rees
J. Whittaker

City, University of London
M.H. Sohawon
G. Tanghetti

University College London
A. Cartwright
S. Lopez-Querol
A Muththalib
Z.L. Ren
P. Shukla
C.P.Y. Wong

COWI
H. Wood

University of Dundee
C. Davidson
Y.U. Sharif

Durham University
J Wang

University of Glasgow
R. Scarfone

Imperial College London
S. Bandare
S. Chen
T.O. Morgan
C. O'Sullivan
D. Zhou

University of Loughborough
T. Biller

University of Manchester
J.A. Mendoza Ulloa
B. Ismael

University of Oxford
K.W. Wu

University of Sheffield
P. Shepley

Sir Robert McAlpine
G. Prakhya

University of Surrey
H.A. Abba
A. Abdullahi
H.E. Demirci
S. Jalbi
P. Mohanty
G. Nikitas
E. Nyebe
I.O. Olawoore
O. Ogunleye
R. Rele
A.K. Sani
R.I. Woods

Tony Gee and Partners LLP
George Marketos

United Utilities Ltd
J.A. Richardson
N.F. Griffin

University of Waterloo, Canada
D. Basu